UNIVERSITY OF CATANIA
Department of Mathematics and Computer Science

International Doctorate Course in Apllied Mathematics
XXV Cycle

POPUZIN VITALY

METHODS OF FAST FOURIER TRANSFORM IN DIFFRACTION PROBLEMS OF ELASTIC AND ACOUSTIC WAVES WITH APPLICATIONS TO CRACK MECHANICS

PhD Thesis

COORDINATOR
Prof. Giovanni Russo

SCIENTIFIC SUPERVISOR
Prof. Antonio Scalia

Final Exam – 2013

Thanks

I am very grateful to Prof. Antonia Scalia **(University of Catania, Italy)** and Prof. Mezhlum A. Sumbatyan **(Southern Federal University, Russia)** for their assistance, guidance and advice in writing this thesis.

Contents

List of Figures

List of Tables

0.1 Introduction

One of the main reasons of the falling out of the high-duty constructions is the appearance of defects (such as flaws, cavities, etc.) as a result of their continuous exploitation. These defects results in the strength loss of the construction material and, in the extreme case, can cause their partial or complete destruction. Quite a number of scientific works are dedicated to the crack theory, but in actual practice the simple engineering solutions, which enable to identify the appearance of the defects on its early stage and carry out their evaluation, are used more often.

Non-destructive testing of materials represents common tool of detection of such types of defects. In the early fifties of the 20th century, in addition to the surface sensing, the x-ray method was developed, which is based on the radioactive isotopes. Afterwards, the ultrasonic approach was evolved. It uses frequencies with short wave-length, which, thanks to their high velocity of propagation in metals and high frequency of oscillations, permits to recognize small-size defects. Nowadays, ultrasound non-destructive testing is one of the most efficient and frequently used methods of strength evaluation of modern materials.

It is based on probing items by generating high-frequency (also known as ultrasound) elastic waves. The ultrasonic waves propagate in the sample under evaluation before they arrive at the boundary of defects. Defects arise in the considered sample and in most cases may represent varying types of system of cracks. The propagating ultrasound waves diffract (interact) with defects and after that change their own characteristics. If placed on the boundary of the considered material the ultrasonic transducer allows one to record the scattered wave field (see Fig.1), then the change in wave characteristics can be used to analyze the image of the internal defects.

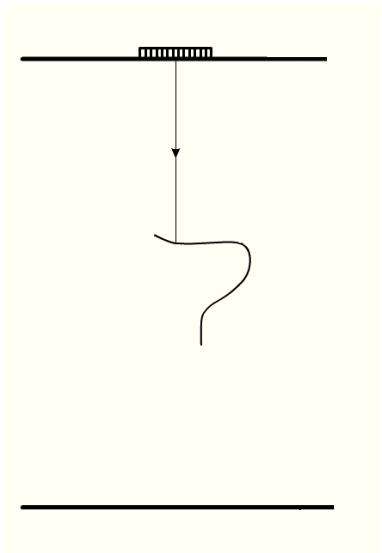

Figure 1: Ultrasound non-destructive testing

Currently, detection of the flaws position is considered to be a solved problem. From the time-of-flight information of the ultrasonic signal one can predict the location of defects with a high accuracy. The determination of the crack form is not so trivial task and nowadays theoretical researches of the described problems cannot be realized within the framework of any accurate model because the arising equations cannot be solved in real-time even on modern computers. Practically, important three-dimension problems, especially in the high-frequency range of vibration, demand too huge computer resources. The methods of acceleration of the computations described in literature can be applied only to single defects of canonical form (plane, sphere, wedge, etc.). In generic case it is necessary to analyze diffraction integrals on huge nets, because one needs to take at least 10 nodes per each wavelength. It is clear, that with the frequency rise the number of nodes in such straight numerical methods increases considerably. It leads to the instability of the calculation, as well as to intolerably large span time. It is also known that analytical

expressions lose their accuracy at medium high frequency. It is particularly noticeable in the case of a large order of multiple propagation, because in this case the divergence of the ultrasonic wave beam becomes quite substantial. Eventually, the comparison of asymptotic formulas with the direct numerical methods is possible only for rather high frequency, where, as it was mentioned above, the efficiency of the known direct numerical methods decrease due to the huge size of the computational mesh. It is obvious that the existing computational methods, described and reported in the literature, cannot perform calculation in mentioned ranges of changing physical properties, which occurs in the practice of ultrasonic nondestructive testing. In this connection it is urgent to design numerical algorithms which can be applied in real time for extremely high frequencies.

In the meantime, at the present day, many scientists look forward to the supercomputers and multiprocessor devices, which would allow to "parallelize" the problem and to solve it in a reasonable time. However, development of the fast numeric algorithms, adapted to the problem, can build up the necessary foundation for the creation of portable devices, which could solve the problem "on-fly", without having to pass measured data to the computation centre. Especially, as the fast progress in the electronics engineering during past few decades has resulted in so well developed modern portable devices which become comparable by their parameters with ten-years-old PCs

The main aim of the current research is concerned with the development of fast numerical algorithms, which take into account the physics of the ultrasonic flaw detection, and also the adaptation of some already-existing algorithms to the needs of the engineering practice.

Mathematically, recent methods of solving the dynamic crack theory problems and ultrasonic non-destructive testing reduce them to boundary integrals and integral equations taken over the surface of the considered defects.

The well known standard numerical methods are suitable for this equation. But , as mentioned above, in the three-dimensional problems, especially in high-frequency range of vibration, the computation requires huge computer resources even on present-day computers. On the other hand, the integrals in similar problems can be reduced to a form permitting application of the fast Fourier transform (FFT). Thus, in the present research we propose to use fast algorithms, which will allow us to significantly reduce the computational time for the elastic stress fields and to improve theoretical and numerical methods of strength evaluation of materials in the case of accumulation of cracks and other defects.

Another aspect, which we would like to emphasize in the current work, is a mathematical clarity of the numerical algorithms. This is due to the fact, that fast algorithms, which are well developed in the computational mathematics, are often connected with too complicated mathematical tools, and their application is not so simple for non-specialists.

0.2 Content of the work by chapters

Logically, the current dissertation is constructed in such a way, that we pass from the simple model problems to the complex one, which are close to the physical reality.

In the first chapter we propose a new alternative method, based on reduction of diffraction integrals and boundary integral equations of elastic dynamic cracks theory to the forms, which permit application of the FFT. This approach demands a special change of variables, based on a specific form of the phase function. Then, reduction to a form which permits application of the FFT based on some efficient semi-analytic realization of this change of variables. Finally, the computation of elastic wave fields can be performed in real-time

on personal computer. The developed algorithms allow us to solve this problem in the extremely high-frequency range. We apply this method to solve diffraction problem for plane rigid screen in the high frequency range. Derivation of the diffraction integral is based on Kirchhoff's physical diffraction theory. It is shown, that the developed method allows us to significantly reduce the time of computation, keeping the accuracy of direct numerical methods.

The second chapter is devoted to the application of similar technique in the contact problems. Mathematically, such problems can be treated in terms of some integral equations of the first kind. The numerical treatment of such problems is based on the application of various numerical methods, that means the change of initial integrals by finite-dimensional ones. At the same time, integrals in such problems expressed in discrete form can be considered as a convolution of two signals that allows us to use the property of the discrete Fourier transform, also known as the convolution theorem. Thus, the Fourier transform of the unknown function is expressed as a Fourier transform of the right-hand side of the integral equation and the kernel of integral operator. After this evaluation we only need to estimate the inverse transform to find the unknown quantity. The fast Fourier transform method is used to reduce significantly the time of calculation for the proposed algorithm.

At the end of the chapter we demonstrate an application of the accelerated iterative conjugate gradient method in the crack problem in the porous elastic plane, by using the model developed by Nunziato and Cowin. With the help of Fourier transform the problem is reduced to an integral equation over the boundary of the crack. Some analytical transformations are applied to calculate the kernel of the integral equation in its explicit form. We perform a numerical collocation technique to solve the derived hyper-singular integral equation. Due to convolution type of the kernel, we apply, at each iteration step, the classical iterative conjugate gradient method in combination with

the fast Fourier technique, to solve the problem in almost linear time. Some numerical examples for materials of various values of porosity are presented.

In the next chapter the new iterative approach for diffraction problems on the obstacles with arbitrary shape is developed. When the problem is reduced to the integral equations via Boundary Integral Equation (BIE) method and then discretized, this leads to the linear algebraic system with the dense matrix which can be solved by classical Gauss-elimination method in $O(N^3)$ arithmetic operations , where N is the size of the matrix. However, such matrices have special structure which permits effective algorithms of matrix-vector multiplications in such a way that it needs only linear instead of quadratic arithmetic operations. Thus, such types of techniques are used in iteration schemes where matrix-vector multiplication is the most expensive computational operation. If the iteration scheme converges rapidly, then the total cost to solve the initial problem is nearly linear depending on the size of the mesh. These compression methods are well studied, so we are concentrating on a certain improvement of the iterative schemes. We develop new iterative algorithms where on each iteration step one should solve an approximated problem with a special matrix. This is performed in such a way, that the initial matrix becomes Toeplitz after having applied this approximation. In the case of star-like obstacles it can be done analytically by constructing a linear algebraic system on the circle. In this case the matrix is circulant and the form of its exact inversion is known and can be achieved by applying fast Fourier transform which requires $O(N\,log(N))$ arithmetic operations. In the case when the obstacle has more general form, the approximate matrix is computed numerically by a certain averaging procedure. Then a conjugate gradient method is applied to solve the approximate system with the Toeplitz matrix by nearly linear amount of arithmetic operations.

In the last chapter, similar idea to construct the iteration scheme is applied

in the diffraction problem for the system of linear obstacles. The problem is reduced to a system of boundary integral equations, which are discretized by applying the Belotserkovskii-Lifanov method. In discrete form, a finite number of systems with Toeplitz matrices (the number of systems is equal to the number of barriers) are solved at each iteration step by applying the fast bi-conjugate gradients method with preconditioning. The algorithm is tested on several geometries, and its convergence in these cases is analyzed.

Chapter 1

An efficient numerical algorithm for one-dimensional diffraction integrals

1.1 Introduction

First steps in the field of the fast computations are historically connected with the operation of the matrix-vector multiplication. The well-known paper by Cooley-Tukey [1] on the algorithm of the fast Fourier transform (FFT), has greatly influenced the modern computational world, and nowadays it is widely used in different fields. Formally, this operation can be considered as the fast multiplication of the Fourier matrix, which represents the Vandermond matrix of the special form, on the vector [2,3]. Further, we will refer in detail on this representation. In the present chapter we will consider the FFT in the classical formulation as finite series. Another example, that we would like to mention here, is the fast multipole method (FMM) developed by Rokhlin in his works [4–6]. This algorithm also represents fast matrix-vector multiplication,

but in contrast to FFT, such approach is approximate. These two mentioned methods differ from their predecessor in the fact, that they allow one to reduce the number of required operations from classical N^2 for matrix-vector multiplication to almost N operations.

The ideas of application of the FFT algorithm for evaluation of diffraction integrals arising in acoustical problems were discussed in works [7,8]. Here we propose an alternative approach. To this end, let us show how mathematical model which describes the wave process of interaction of the elastics waves with cracks can be adapted to the possibility of the FFT application. In fact, integrals arising in these types of problems, are very similar in their structure to the form on which one can apply the fast Fourier transform. At least, such interpretation is possible after some substitutions of the variables. To this aim, there was developed an efficient semi-analytic method of reduction of diffraction integrals to a form permitting the application of the FFT. It is based on a special transform of coordinates adapted to current type of the phase function. It requires the combination of analytical and numerical methods.

As a result of application of the proposed method the cost of numerical computation of the current problems will be reduced practically by the order of mesh dimension, because, as already mentioned, any direct numerical calculation of integral requires N^2 operations, but the proposed technique takes only $N\,log(N)$ operations, where N is the mesh dimension. Such a method is efficient in the high-frequency range of vibration, which is typical for wave problems of ultrasonic non-destructive testing. The developed method and the connected numerical algorithm are applied to the problems of diffraction of ultrasonic waves by linear cracks.

1.2 Application of FFT to the diffraction by a plane hard screen in echo-case

1.2.1 Formulation of the problem

To demonstrate the proposed method, we consider the planar two-dimensional problem of diffraction of the ultrasonic waves by the crack in an elastic isotropic material. As a first approximation, we assume that the crack at its initial stage of growth is given by a finite interval (say, l long). Suppose that it is planar. We relate rectangular coordinate system Oxy to this interval, so that the origin of coordinates coincides with the beginning of this interval, and the horizontal axis is directed along the length. Then we locate the ultrasound-radiation source $S(x_S, y_S)$ at some distance from crack in this coordinate system. Moreover, in the present example, we will consider the case when the source and the receiver of the sound signal match that corresponds to the echo-sounding when both sensors are integrated into a single device (see Fig.1.1). It should also be stated that the echo method is one of the most popular, taking about 90% of the total measurements performed.

We will seek the scattered pressure field, considering the shape and position of the crack to be given, as well as incident wave to be known. Moreover, we assume that all the wave processes are harmonic, so the time factor $e^{-i\omega t}$ will be omitted in the subsequent calculations (where ω is the angular frequency). Technically, the issue at hand is not the object of ultrasonic testing, but it will help to understand how high-frequency diffraction integrals can be adapted to the use of fast methods.

We consider this problem (as well as the following examples) in the framework of linear acoustics, and the pressure p will be the main wave characteristic of the acoustic field. According to this model, the total perturbed wave field

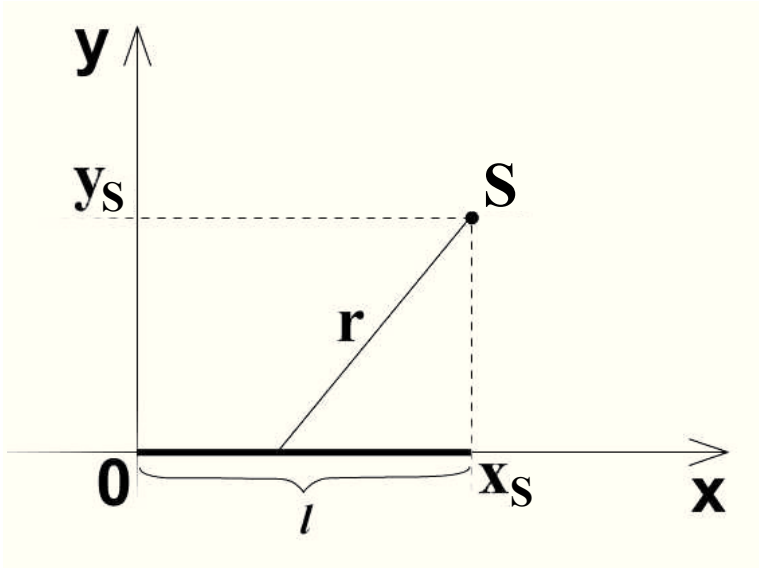

Figure 1.1: Diffraction by the plane screen in echo-case

can be represented as the sum of the direct and reflected signals respectively $p = p^{inc} + p^{sc}$ [9,10]. We assume that the cylindrical acoustic wave

$$p^{inc} = \frac{e^{ikr}}{\sqrt{r}} \tag{1.1}$$

is sent from the source S, where i is the imaginary unit, r is the distance from the source to the screen, which is expressed by the formula $r = \sqrt{(x_S - \xi)^2 + y_S^2}$, and k is the wave number connected with the wavelength λ by the ratio $k = 2\pi/\lambda$. Given the ultrasonic waves are short wavelength, the parameter k is large (recall that $\lambda = c/f$ where c is the speed of sound in the medium, and f – its temporal frequency).

Firstly, let us consider the case when the source-receiver of the signal lies outside the interval $[0, l]$, say to the right of it (i.e., $x_S > l$). It is convenient to demonstrate the logic of the solution, leaving the transparency of mathematical calculations, since in this case the distance function r increases monotonically. Next, we show how this case can be generalized to an arbitrary position of the

source S.

The physical Kirchhoff diffraction theory can be applied for the ultrasonic waves with large wave number [11]. This model is convenient because it immediately gives an expression for the reflected signal at the receiver using the integral formula of the incident wave

$$p^{sc} = 2\int_0^l p^{inc}\frac{\partial\Phi}{\partial n_\xi}d\xi \tag{1.2}$$

where Φ is the Green's function and n - normal to the surface. Thus, to find the unknown function it is sufficient to integrate the equation (1.2).

Given that [9] in the two-dimensional acoustic case the Green's function is expressed in terms of the Hankel function of the first kind, namely

$$\Phi(r) = \frac{i}{4}H_0^{(1)}(kr) \tag{1.3}$$

which in its asymptotics for large argument (in our high-frequency case $kr >> 1$) can be expressed in terms of exponential function [12]

$$H_0^{(1)}(kr) \approx \sqrt{\frac{2}{\pi kr}}e^{i(kr-\pi/4)} = \frac{2}{(1+i)\sqrt{\pi kr}}e^{ikr} \tag{1.4}$$

whence it follows that

$$\Phi(r) \approx \frac{i+1}{4\sqrt{\pi kr}}e^{ikr} \tag{1.5}$$

Normal integration can be represented as

$$\frac{\partial\Phi}{\partial n_\xi} = \frac{\partial\Phi}{\partial r}\frac{\partial r}{\partial n_\xi} \approx \frac{(i+1)y_S}{4\sqrt{\pi k}}e^{ikr}\frac{\sqrt{r}(ik-1/(2r))}{r^2} \approx \frac{(i-1)y_S}{4\sqrt{\pi}}\frac{\sqrt{k}}{r\sqrt{r}}e^{ikr} \tag{1.6}$$

Substituting this expression in equation (1.2), we obtain the integral representation for finding the unknown pressure field

$$p^{sc} \approx \frac{i-1}{2\sqrt{\pi}}y_S\sqrt{k}\int_0^l \frac{e^{2ikr}}{r^2}d\xi \tag{1.7}$$

From this equation one can obtain the exact solution with standart numerical methods. However, due to the points given in the introduction, this

approach would be time-consuming. To implement the proposed alternative approach based on the use of the FFT method, we make the following change

$$\xi = x_S - \sqrt{r^2 - y_S^2}, \quad d\xi = -r/\sqrt{r^2 - y_S^2}dr, \tag{1.8}$$

which transforms the foregoing equation to

$$\begin{array}{c} p^{sc} = \frac{i-1}{2\sqrt{\pi}} y_S \sqrt{k} \int_{\sqrt{(x_S-l)^2+y_S^2}}^{\sqrt{x_S^2+y_S^2}} \frac{e^{2ikr}}{r\sqrt{r^2-y_S^2}} dr = \\ = \frac{i-1}{2\sqrt{\pi}} y_S \sqrt{k} e^{2ika} \int_0^{\sqrt{x_S^2+y_S^2}-a} \frac{e^{2ik\eta}}{(\eta+a)\sqrt{(\eta+a)^2-y_S^2}} d\eta \end{array} \tag{1.9}$$

where $\eta = r - a$, $a = \sqrt{(x_S - l)^2 + y_S^2}$.

We assume that the wave number is given by a large initial value, i.e. $k = k_0 + \Omega$. Introducing, for convenience, constant A and denoting the subintegral function through $u(\eta)$

$$A = \frac{i-1}{2\sqrt{\pi}} y_S \sqrt{k}, \qquad u(\eta) = \frac{e^{2ik_0\eta}}{(\eta+a)\sqrt{(\eta+a)^2 - y_S^2}} \tag{1.10}$$

we obtain the final form of the integral equation

$$p^{sc}(\Omega) = A e^{2i(k_0+\Omega)a} \int_0^{\sqrt{x_S^2+y_S^2}-a} u(\eta) e^{2i\Omega\eta} d\eta \tag{1.11}$$

suitable for reduction to the discrete Fourier transform.

1.2.2 Numerical treatment

For the numerical solution of the equation (1.11) we introduce a uniform spaced grid of N nodes $\eta_n = (n + 1/2)h$, $n = 0, 1, .., N - 1$ with a constant pitch on the interval of integration $h = (\sqrt{x_S^2 + y_S^2} - a)/N$. Then, the first integral can be approximated by the approximate integral sum:

$$\int_0^{\sqrt{x_S^2+y_S^2}-a} u(\eta) e^{2i\Omega\eta} d\eta \approx h \sum_{n=0}^{N-1} u(\eta_n) e^{2i\Omega\eta_n} \tag{1.12}$$

If we take the countable set of wave numbers as

$$\Omega_m = \frac{\pi m}{\sqrt{x_S^2 + y_S^2} - a}, \quad (m = 0, 1, .., N-1) \tag{1.13}$$

then it easy to see, that the integral in the equation (1.12) represent a standard expression for the FFT [13], which according to the ideology of the FFT can be calculated for all N simultaneously, i.e. for all wave numbers. The final expression of the pressure of the reflected wave will be the following

$$p_m^{sc} \approx hAe^{2i(k_0+\Omega_m)a} e^{i\Omega_m h} \sum_{n=0}^{N-1} u_n \, e^{i2\pi mn/N} = hNAe^{2i(k_0+\Omega_m)a} e^{i\Omega_m h} \, FFT^{-1}[u_n] \tag{1.14}$$

Further, this problem is calculated numerically. Note that, unlike the existing approximate methods of matrix-vector multiplication, the approach presented here is accurate.

1.2.3 Analytical solution

In the case where the source abscissa coincides with the end of the interval ($x_S = l$), in the subintegral function $u(\eta)$ there is root singularity at the lower end of integration since $a = y_S$ and correspondingly

$$u(\eta) = \frac{e^{2ik_0\eta}}{(\eta + y_S)\sqrt{(\eta y_S)^2 + 2\eta y_S}} \tag{1.15}$$

The application of L'Hopital rule shows that $u(0) = 0$. Nevertheless, using this feature, the problem can be solved analytically. We take this feature into a single integral.

$$\int_0^L \frac{e^{2ik\eta}}{\sqrt{\eta}} \left(\frac{1}{(\eta + y_S)\sqrt{\eta + 2y_S}} - \frac{1}{y_S\sqrt{2}} \right) d\eta + \frac{1}{y_S\sqrt{2}} \int_0^L \frac{e^{2ik\eta}}{\sqrt{\eta}} d\eta \tag{1.16}$$

where $L = \sqrt{x_S^2 + y_S^2} - y_S$.

The second integral in the equation (1.16) can be represented in standard integrals. For this purpose we represent the exponential as a sum of trigonometric functions

$$\int_0^L \frac{e^{2ik\eta}}{\sqrt{\eta}}d\eta = \int_0^L \frac{cos(2k\eta)}{\sqrt{\eta}}d\eta + i\int_0^L \frac{sin(2k\eta)}{\sqrt{\eta}}d\eta \tag{1.17}$$

Replacing $z = 2k\eta$ we observe that the resulting integrals

$$\frac{1}{\sqrt{2k}}\int_0^{2kL} \frac{cos(z)}{\sqrt{z}}dz + i\frac{1}{\sqrt{2k}}\int_0^{2kL} \frac{sin(z)}{\sqrt{z}}dz = \sqrt{\frac{\pi}{k}}C_2(2kL) + i\sqrt{\frac{\pi}{k}}S_2(2kL) \tag{1.18}$$

represent the sum of the Fresnel integrals, which are given by

$$C_2(x) = \frac{1}{\sqrt{2\pi}}\int_0^x \frac{cos(t)}{\sqrt{t}}dt, \quad S_2(x) = \frac{1}{\sqrt{2\pi}}\int_0^x \frac{sin(t)}{\sqrt{t}}dt \tag{1.19}$$

For these integrals there is a good rational approximation [12]

$$\begin{aligned} C_2(2kL) &= C\left(2\sqrt{\tfrac{kL}{\pi}}\right) = \tfrac{1}{2} + q\left(2\sqrt{\tfrac{kL}{\pi}}\right)sin(2kL) - g\left(2\sqrt{\tfrac{kL}{\pi}}\right)cos(2kL) \\ S_2(2kL) &= S\left(2\sqrt{\tfrac{kL}{\pi}}\right) = \tfrac{1}{2} - q\left(2\sqrt{\tfrac{kL}{\pi}}\right)cos(2kL) - g\left(2\sqrt{\tfrac{kL}{\pi}}\right)sin(2kL) \end{aligned} \tag{1.20}$$

Therefore, using the Fresnel integrals, we rewrite the desired pressure of the reflected wave in a compact form

$$p^{sc}(k) \approx Ae^{2iky_S}\frac{(C_2(2kL) + iS_2(2kL))\sqrt{\pi}}{y_S\sqrt{2k}} \tag{1.21}$$

1.2.4 Generalization for arbitrary position of the inductor-receiver system

Similarly, the analysis is done in the case where the abscissa of the source-receiver is above the screen (see Fig.1.2). The main difference is the fact that the integrand function becomes piecewise smooth, as in this case, after the

change of variable (1.8), the integration interval is split into two sub-intervals

$$p^{sc} \approx -\frac{i-1}{2\sqrt{\pi}} y_S \sqrt{k} \int_{\sqrt{x_S^2+y_S^2}}^{\sqrt{(x_S-l)^2+y_S^2}} \frac{e^{2ikr}}{r\sqrt{r^2-y_S^2}}\, dr =$$

$$= \frac{i-1}{2\sqrt{\pi}} y_S \sqrt{k} \left(\int_{y_S}^{\sqrt{x_S^2+y_S^2}} \frac{e^{2ikr}}{r\sqrt{r^2-y_S^2}} dr + \int_{y_S}^{\sqrt{(x_S-l)^2+y_S^2}} \frac{e^{2ikr}}{r\sqrt{r^2-y_S^2}}\, dr \right) = \tag{1.22}$$

$$= \frac{i-1}{2\sqrt{\pi}} y_S \sqrt{k} \int_{y_S}^{\sqrt{x_S^2+y_S^2}} u(r) e^{2ikr} dr$$

where, the piecewise smooth function was introduced for the convenience

$$u(r) = \begin{cases} 2\frac{e^{2ikr}}{r\sqrt{r^2-y_S^2}}, & r \in [y_S, \sqrt{(x_S-l)^2+y_S^2}], \\ \frac{e^{2ikr}}{r\sqrt{r^2-y_S^2}}, & r \in (\sqrt{(x_S-l)^2+y_S^2}, \sqrt{x_S^2+y_S^2}] \end{cases} \tag{1.23}$$

For definiteness, we assume $\sqrt{(x_S-l)^2+y_S^2} < \sqrt{x_S^2+y_S^2}$ (i.e., the sound source is located to the right of the center of the screen). Then all the arguments repeat exactly the previous case and differ only in more complex derivation of Fresnel integrals. The final form of the analytical solution is as follows

$$p^{sc}(k) \approx A e^{2iky_S} \frac{(C_2(2kL) + C_2(2kL_l) + i(S_2(2kL) + S_2(2kL_l))\sqrt{\pi}}{y_S\sqrt{2k}} \tag{1.24}$$

where $L_l = \sqrt{(x_S-l)^2+y_S^2} - y_S$.

1.2.5 Numerical results

The comparative analysis of the results of fast numerical integration of the equation (1.14) (denoted as "numeric 2" in the figures) with an explicit asymptotic solution (1.21),(1.24) of the problem (in the case when the sound source is located above the screen) shows good convergence of the proposed method. Numerical experiments have also shown that the accuracy of calculation of the integral from the formula (1.14) almost coincides with the direct numerical integration of the equation (1.7)(denoted as "numeric 1" in the figures). Thus,

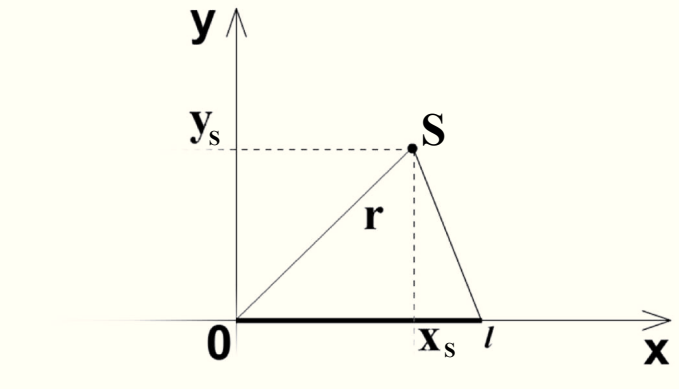

Figure 1.2: Diffraction in the case when source-receiver is above the screen

when the number of the nodes is $N = 2^{10} = 1024$ FFT method differs only in the third decimal place, which is reflected in the graph 1.3.

In the calculation of the pressure dependence of the horizontal coordinates of the source the following parameters were taken: $l = 5mm$, $y_S = 35mm$, $N = 2^{10} = 1024$, $c = 5940m/s$ (which corresponds to the propagation velocity of sound in steel). At frequencies below $f \leq 1\,MHz$ the influence of the flaw does not essentially change the magnitude of the reflected pressure. This is logical from the physical point of view, because this wave-length is almost equal to the size of the crack and there are not any diffraction effects in fact. This fact is well known to experimenters who use high-frequencies to detect small flaws. Obviously, because of the symmetry of the problem, the magnitude of the pressure module $|p|$ of the reflected field to the left of the interval will coincide with the field in the symmetric point to the right of it.

In practice, the ultrasonic amplitude variation under the variations of frequency over a wide frequency range, i.e. the so-called amplitude-frequency characteristic (AFC) is sometimes measured. The corresponding analysis for the different number of nodes $N = 2^M$ is shown in Figures 1.4–1.6. In the calculations the same parameters as the previous example were taken, how-

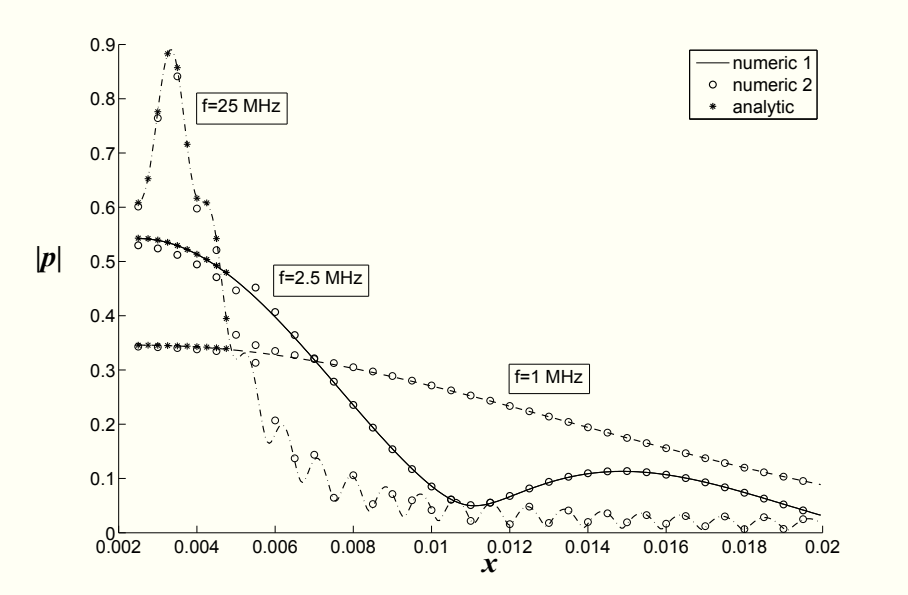

Figure 1.3: Pressure dependence of the horizontal coordinates of the source ($l = 5mm$, $y_S = 35mm$, $N = 2^{10} = 1024$, $c = 5940m/s$)

ever, the abscissa of the source was fixed at $x_S = 20mm$. Figure 1.4 shows the graphs in the frequency range $f \approx 1\,MHz - 10^4 MHz$. It can be seen that the direct numerical calculation from formula (1.7) at a certain frequency becomes unstable, which is reflected in the strong oscillations of the solution at high frequencies. This is due to the fact that the grid of the input nodes is too small for such an oscillating function. It is evident that more dense grids should be used at higher frequencies. However, the calculation on the modified formula (1.14) on the same grid falls in agreement with the solution "later", i.e. for higher frequencies. Moreover, this solution does not oscillate. This can be explained by the nature of the discrete Fourier transform, which typically converts the signal from a time-frequency range (where the function is oscillating) into the amplitude-frequency range, where the signal is represented by a more regular function. The difference of the approximate "critical" frequen-

Table 1.1: Comparison of executional time upon N

number of nodes $N = 2^M$	method	"critical" frequencies	executional time (ms)
$N = 2^8 = 256$	Straight	$2.09 \cdot 10^5$	91–188
	FFT	$2.46 \cdot 10^5$	0.5–0.8
$N = 2^9 = 512$	Straight	$4.78 \cdot 10^5$	500–624
	FFT	$5.66 \cdot 10^5$	1.2–2.12
$N = 2^{10} = 1024$	Straight	$1.08 \cdot 10^6$	827–1134
	FFT	$1.28 \cdot 10^6$	2.3–3.5
$N = 2^{11} = 2048$	Straight	$1.93 \cdot 10^6$	5939–6510
	FFT	$2.22 \cdot 10^6$	4.9–7.4
$N = 2^{12} = 4096$	Straight	$4.27 \cdot 10^6$	29182–29801
	FFT	$5.01 \cdot 10^6$	11.4–16.4
$N = 2^{13} = 8192$	Straight	$9.11 \cdot 10^6$	116285-127518
	FFT	$1.07 \cdot 10^7$	21.8–35.2

cies above at which the solution begins to diverge, for the direct numerical integration and the proposed method is shown in the comparative table 1.1. It is evident that in the case of numerical integration if we divide the screen into N nodes and perform calculations for N different frequencies, then the direct evaluation of integral (1.7) would require N^2 operations, whereas the fast Fourier transformation results in $N\,logN$ operations. For example, for $N = 2^{10} = 1024$ the difference in speed of calculation is $N^2/(N\,logN) = 102.4$. With increasing frequency the effect of the FFT grows exponentially. This is also reflected in table 1.1.

Note that the frequency step depends only on the location of the source-obstacle, and the maximum calculated frequency also depends on the number

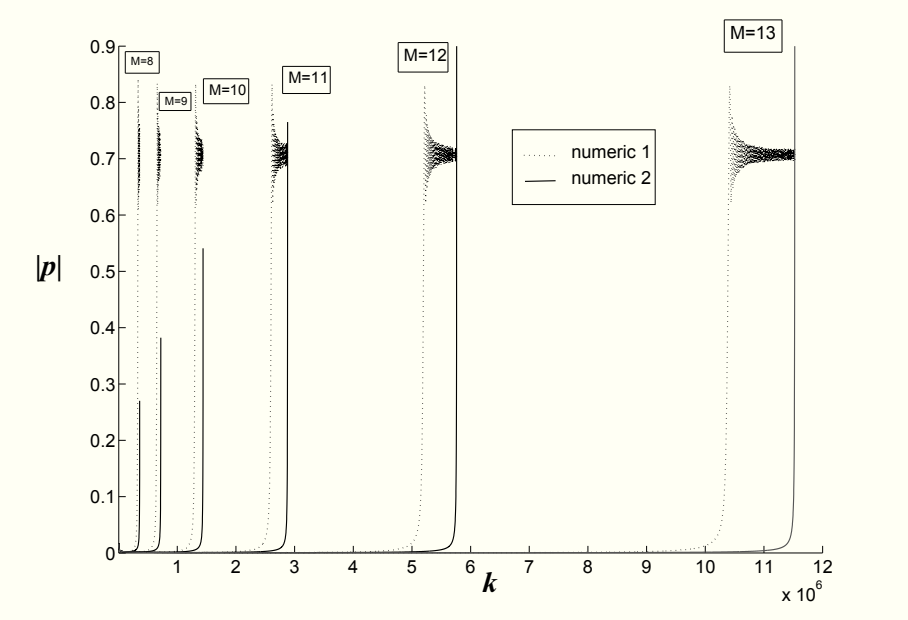

Figure 1.4: Modulus of the scattered wave pressure $|p|$ versus wave number k in a wide range

of nodes N. The range given in the previous graph is the direct consequence of this fact. It is evident that most of the solutions are not of practical interest since they refer to the hyper-sound. The range of the ultrasonic waves is defined as $f \approx 1\,MHz - 10^3 MHz$. The graph for the range is shown in figure 1.5. The figure shows that the number of nodes which equals $M = 10$, $N = 2^M = 1024$ approximates well the frequency domain $f \approx 1\,MHz - 500\,MHz$. This range is shown in more detail in the graph (1.6). To reduce the grid spacing on the frequency parameter the distance between the sound source and the screen should be increased, which is probably the only drawback of the proposed method.

It is significant that the use of the FFT provides a solution for all wave numbers only in $N\,log(N)$ operations without any approximations. In this respect, this method is equivalent to the direct numerical calculation of the

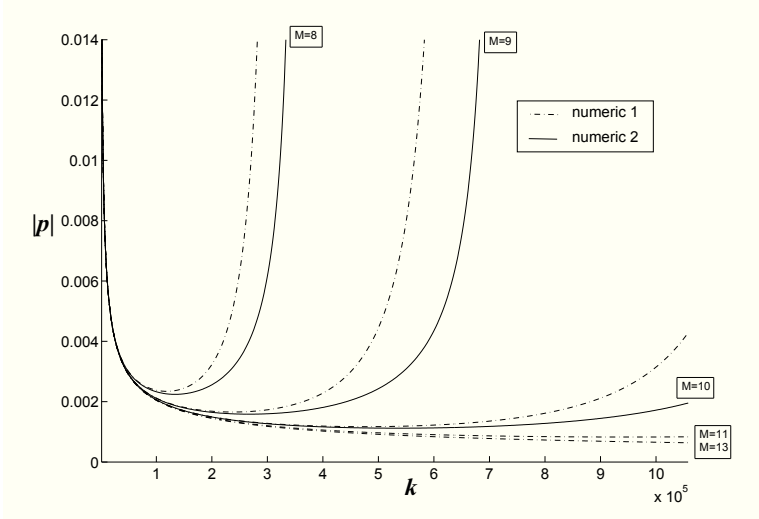

Figure 1.5: Modulus of the scattered wave pressure $|p|$ versus wave number k in ultrasound range ($f \approx 1\,MHz - 10^3 MHz$)

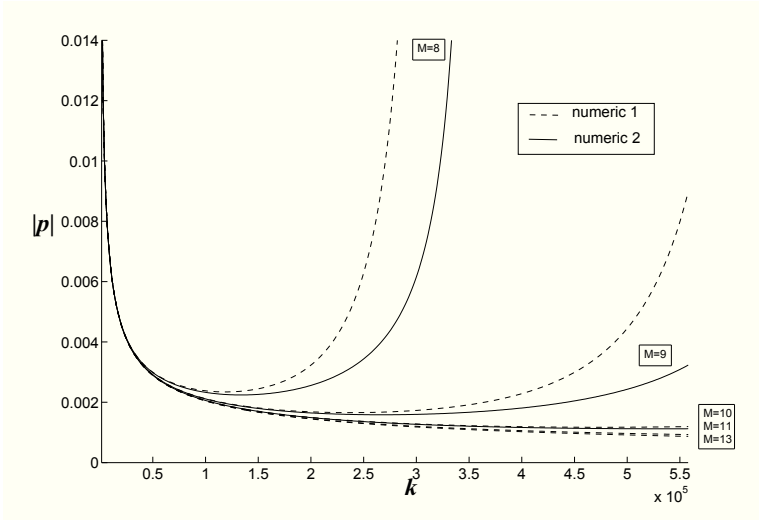

Figure 1.6: Modulus of the scattered wave pressure $|p|$ versus wave number k in the range of frequency between $1\,MHz$ and $500\,MHz$)

equation (1.7).

1.3 Extension to the case of spaced source and receiver

In practice, the sound source does not always coincide with the sound receiver. For example, in "end-to-end" test of the walls of the building, the source is located on one side of the wall, and the receiver on the back one. Therefore, in this section we consider a model of spaced source and receiver of the audio signal (see Fig.1.7)

As can be seen from the figure, the distance from the source to the screen and from the screen to the signal receiver is different, namely $r_1 = \sqrt{(\xi - x_S)^2 + y_S^2}$ and $r_2 = \sqrt{(\xi - x_R)^2 + y_R^2}$ where (x_S, y_S) and (x_R, y_R) are the coordinates of the sound source and receiver, respectively. It makes its own changes to the integral representation for the incident wave in the framework of the Kirchhoff diffraction

$$p^{sc} \approx \frac{y_R(i-1)\sqrt{k}}{2\sqrt{\pi}} \int_0^l \frac{e^{ik(r_1+r_2)}}{r_2\sqrt{r_1 r_2}}\, d\xi \tag{1.25}$$

To reduce the diffraction integral to the form of the Fourier transformation we make the following changes. As in the previous example, firstly it is necessary to replace the variable in equation (1.25) so that the integration was defined for the variable, located in the exponent. Thus, introducing a new variable

$$r(\xi) = r_1 + r_2 = \sqrt{(\xi - x_S)^2 + y_S^2} + \sqrt{(\xi - x_R)^2 + y_S^R} \tag{1.26}$$

expressing further ξ through r, and r_1 and r_2 through $\xi(r)$ we arrive at the expression

$$p^{sc} \approx \frac{y_R(i-1)\sqrt{k}}{2\sqrt{\pi}} \int_{r(0)}^{r(l)} \frac{\xi'_{1,2} e^{ikr}}{r_2\sqrt{r_1 r_2}}\, dr \tag{1.27}$$

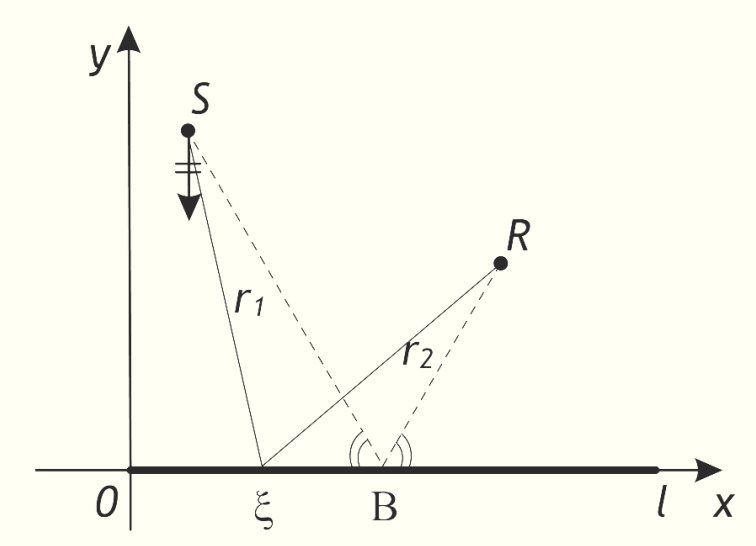

Figure 1.7: Diffraction by the plane screen. S - sound source, R - receiver, B - specular point.

The solution of the quadratic equation resulting from the conversion of (1.26) has two roots $\xi_{1,2}(r) = (-b/2 \pm \sqrt{(D/4)})/a$ where D - is the discriminant, a - is the first coefficient, b - is the second coefficient of the equation. From physical point of view it is clear that one of the roots belongs to the interval from the origin to the point of specular reflection, and the second one belongs to the other half of the interval (see Fig. 1.7). We will use the simple relations such as a condition for membership to a particular interval:

$$\xi_1(r(0)) = 0, \qquad \xi_2(r(l)) = l \tag{1.28}$$

where $\xi_1 \in [0, B), \quad \xi_2 \in (B, l]$.

Then the reflected pressure field for an acoustic wave (1.27) will be as follows

$$\frac{y_R(i-1)\sqrt{k}}{2\sqrt{\pi}} \left(- \int_{r(B)}^{r(0)} \frac{\xi_1' e^{ikr}}{r_2\sqrt{r_1 r_2}}\, dr + \int_{r(B)}^{r(l)} \frac{\xi_2' e^{ikr}}{r_2\sqrt{r_1 r_2}}\, dr \right) \tag{1.29}$$

We note that by integrating this expression at mirroring ($\xi = B$) a singularity

appears. To avoid this problem we make the following changes. We extract the summands which have this feature from each of the previous integral expression:

$$-\int_{r(B)}^{r(0)} u_1 e^{ikr} dr + \int_{r(B)}^{r(l)} u_2 e^{ikr} dr - \int_{r(B)}^{r(0)} \frac{1}{a} \frac{D'}{4\sqrt{D}} e^{ikr} dr + \int_{r(B)}^{r(l)} \frac{1}{a} \frac{D'}{4\sqrt{D}} e^{ikr} dr \tag{1.30}$$

Here, the prime denotes the derivative with respect to the variable r and functions u_1, u_2 contain the remaining members, i.e.

$$u_{1,2}(r) = \frac{-(a'(-b/2 \pm \sqrt{D/4}))/a^2 - b'/(2a)}{r_2(\xi_{1,2})\sqrt{r_1(\xi_{1,2})r_2(\xi_{1,2})}} \tag{1.31}$$

It should be pointed out that it is the discriminant D that becomes zero at the point of specular reflection. Further, replacing $\eta = r - r(B)$, we divide the integrals containing the feature into the sum of the two as follows

$$\begin{aligned}\int_0^{r(0)-r(B)} \frac{1}{\widetilde{a}} \frac{\widetilde{D}'}{4\sqrt{\widetilde{D}}} e^{ik\eta} d\eta = \int_0^{r(0)-r(B)} \frac{e^{ik\eta}}{\sqrt{\eta}} \left(\frac{1}{\widetilde{a}} \frac{\widetilde{D}'}{4\sqrt{\widehat{D}}} - \left(\frac{1}{\widetilde{a}} \frac{\widetilde{D}'}{4\sqrt{\widehat{D}}} \right) \Big|_{\eta=0} \right) d\eta + \\ + \left(\frac{1}{\widetilde{a}} \frac{\widetilde{D}'}{4\sqrt{\widehat{D}}} \right) \Big|_{\eta=0} \int_0^{r(0)-r(B)} \frac{e^{ik\eta}}{\sqrt{\eta}} d\eta\end{aligned} \tag{1.32}$$

where the wave marks the same magnitude after substituting $r = \eta + r(B)$ there. Here $\widehat{D} = \widetilde{D}/\eta$, $\widetilde{D} = 4\eta^6 + U\eta^5 + T\eta^4 + E\eta^3 + Q\eta^2 + W\eta$, and the constants U, T, E, Q, W are expressed in terms of the coordinates of the sound source and the receiver.

The resulting integrals are easily calculated as the first integral has a removable singularity at the lower limit, which is calculated by the L'Hopital rule, and the second integral can be represented as the sum Fresnel integrals, which, as mentioned above, have fairly good approximation by rational functions. Thus, the reflected pressure field can be sought as the sum of the Fresnel

integrals and integral of a known function:

$$p^{sc} \approx \frac{y_R(i-1)\sqrt{k}}{2\sqrt{\pi}} e^{ikr(B)} \Big(\int_0^{L2-L0} F(\eta) e^{ik\eta} d\eta - \\ - \left(\frac{1}{\widetilde{a}} \frac{\widetilde{D'}}{4\sqrt{\widehat{D}}} \right) \Big|_{\eta=0} \left(\int_0^{L1-L0} \frac{e^{ik\eta}}{\sqrt{\eta}} d\eta + \int_0^{L2-L0} \frac{e^{ik\eta}}{\sqrt{\eta}} d\eta \right) \Big) \tag{1.33}$$

where $L0 = r(B), \quad L2 = max\{r(0), r(l)\}, \quad L1 = min\{r(0), r(l)\}.$

The first integral of the formula (1.33) can be represented as an integral sum:

$$\int_0^{L2-L0} F(\eta) e^{ik\eta} d\eta = l \int_0^{(L2-L0)/l} F(\chi l) e^{i\Omega\chi} d\chi = lh \sum_{m=0}^{N-1} F(\chi_m l) e^{i\Omega\chi_m} \tag{1.34}$$

which after selecting the dimensionless units

$$\chi_m = mh = m\frac{L2-L0}{Nl}, \quad \Omega_n = \frac{2\pi l\, n}{L2-L0} \tag{1.35}$$

represent a standard expression for the fast Fourier transformation. According to the FFT this sum can be calculated for all N at once, i.e. for all wave numbers simultaneously. Thus, with the increase of the number of points of division the maximum wave number for which one can calculate the pressure field increases as well, as $k_n = \Omega_n/l = 2\pi l\, n/(L2-L0), \quad n = 0, 1, .., N-1.$

Next, as in the previous section, we represent each integral of the second summand of the equation (1.33) as the sum of the Fresnel integrals. Then, the final form of the reflected pressure field will be as follows

$$p^{sc} \approx e^{ikr(B)} y_R \left[\frac{\sqrt{\Omega l}}{\sqrt{2\pi}} h \cdot FFT(F(\chi_m l)) - \left(\frac{1}{\widetilde{a}} \frac{\widetilde{D'}}{4\sqrt{\widetilde{D}}} \right) \Big|_{\eta=0} \Big(C_2(\Omega(L2-L0)/l) + \right. \\ \left. + C_2(\Omega(L1-L0)/l) + i\Big(S_2(\Omega(L2-L0)/l) + S_2(\Omega(L1-L0)/l) \Big) \Big) \right] \tag{1.37}$$

The graphs 1.8, 1.9 show that this method gives results similar to direct numerical simulations as well as the asymptotic behavior of the expression (1.37)

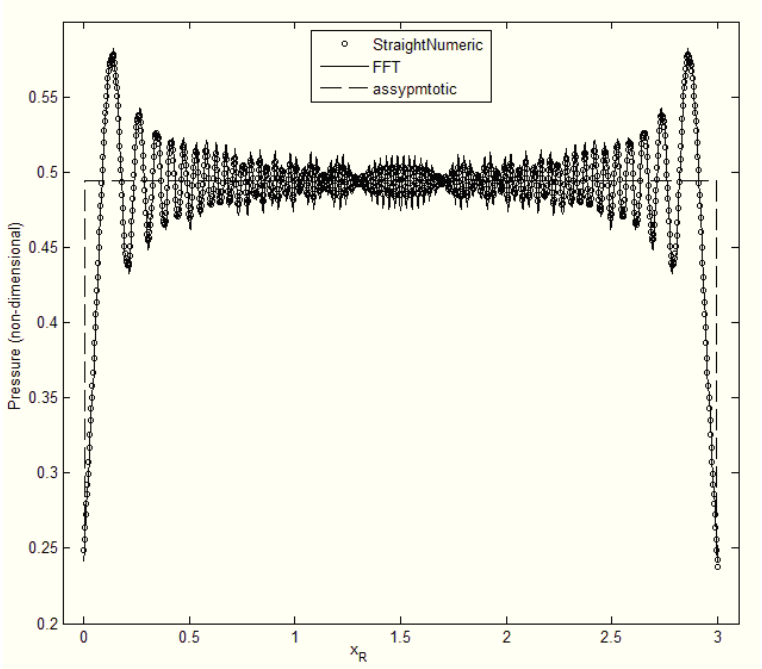

Figure 1.8: Pressure of scattered wave field versus x-coordinate of the sound receiver

given that the wave number tends to infinity. It should be noted that the Fresnel integrals mainly contribute to the asymptotic solution. When constructing these graphs the following values were taken: $l = 3, \quad x_S = 0.3, \quad y_S = 3.2, \quad x_R = 0.6, \quad y_R = 0.9.$

After $\Omega \approx 4000$ direct numerical calculation becomes erratic, as shown in Figure 1.10. This is due to the fact that one wavelength has less than ten nodes. However, the proposed method saves the results which are close to the asymptotic behavior almost all along the axis (see Fig. 1.11). For clarity, all the graphics are shown for $N = 2^{10}$, since the convergence of the numerical calculation and the proposed method based on the FFT is virtually absolute with the increase of this parameter. The numerical implementation of this problem when the number of nodes $N = 16384$ (which corresponds to 2^{14}) in the programming environment Visual C++, took 44.99 seconds, while the

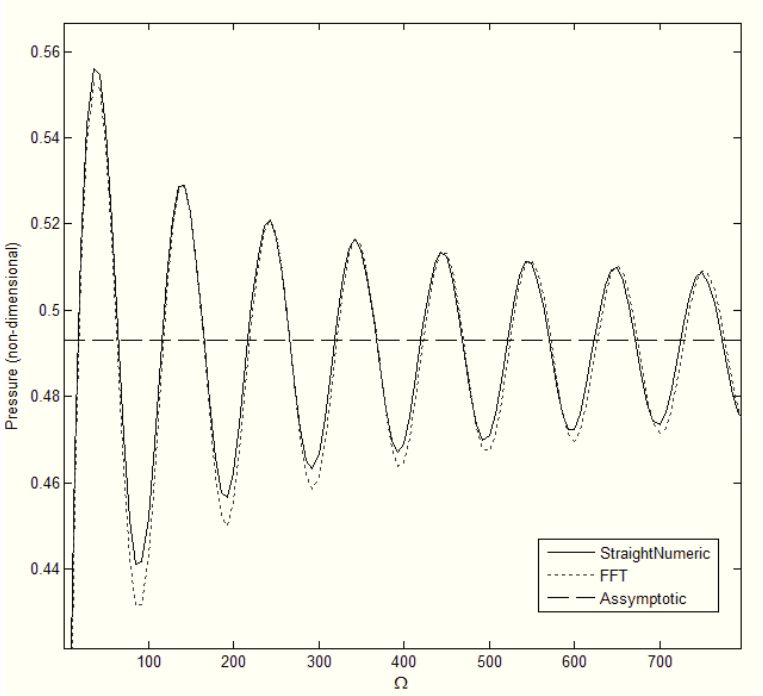

Figure 1.9: Pressure of scattered wave field versus wave number in a short range

proposed method using FFT demanded just 0.124 seconds! i.e. about 500 times faster.

It is clear that the proposed approach has three major advantages: 1) short calculating time; 2) calculation of the wave field for the frequency range, and 3) good convergence with the asymptotic theory where conventional numerical methods are erratic. Thus, the developed method showed good accuracy of calculations in the problem of diffraction on the solid plane screen, allowing to reduce the computation time of the considered integrals by many times.

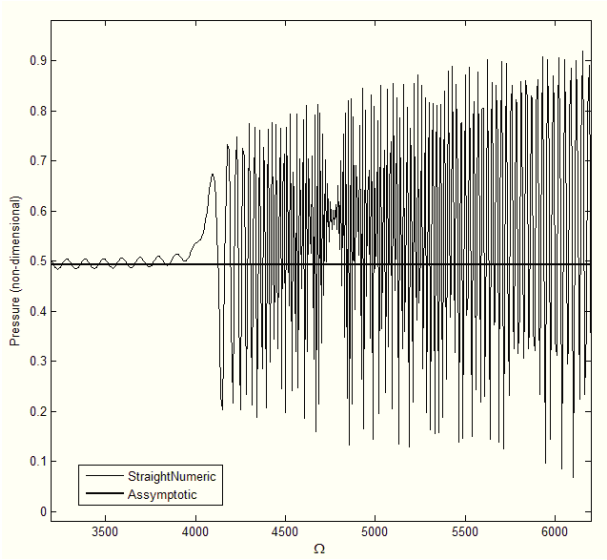

Figure 1.10: Pressure of scattered wave field versus wave number. Comparison between asymptotic solution and direct numerical treatment ($N = 1024$)

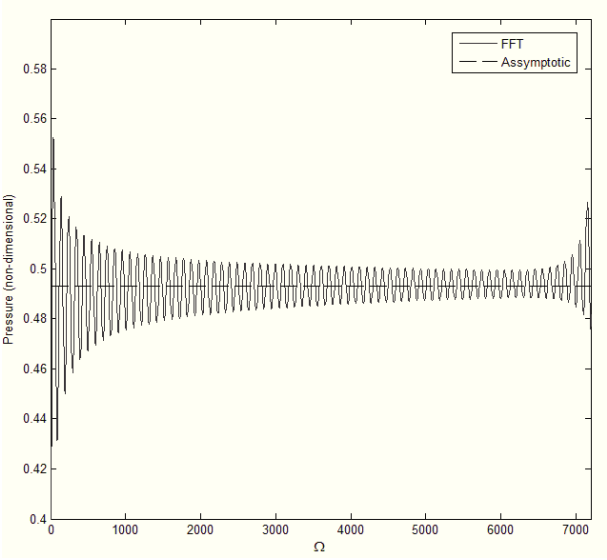

Figure 1.11: Pressure of scattered wave field versus wave number. Comparison between asymptotic solution and FFT-based method ($N = 1024$)

Chapter 2

Application of the FFT to solve integral equations in mechanics of continua

2.1 Introduction

As we have already pointed out, the external loads give rise to defects in the exploited materials. The study of the changes in the crack shape under load allows predicting the crack growth and the condition of the material strength. Mathematically, contact problems are the closest to the crack problems. Both problems can be reduced to integral equations of the first or the second kind. Numerical treatment of such problems is based on application of various algorithms which reduce the initial integral equations to a finite-dimensional form. If there is a need to solve the problem on a large grid for different right-hand sizes, the numerical calculations of the received linear algebraic system is computer-intensive. On the other hand, the kernel of the integral in such problems represents, in the discrete form, a certain matrix of a specific structure.

Thus, one can apply well-developed fast algorithms of computational linear algebra for structured matrices. Note that, the use of the FFT is directly related to the solution procedure, based on the application of the analytical Fourier transformation.

2.2 Application of the fast sine and cosine transforms in contact problems on elastic layer

For example, let us consider the contact problem of the distributed load action on an infinite layer. In this section, we will present the form of the integral equation. Its derivation for the problem of a crack in a porous elastic material will be considered in detail in the relevant chapter.

So, let us assume that the distributed load p_0 applied on the interval $[0, a]$ $(y = h)$ acts on the infinite, linear-elastic, isotropic and homogeneous layer $(|x| < \infty,\ 0 \leq y \leq h)$, with the height of h, clamped to the base $y = 0$.

As is well known [14], the displacement field for such a problem can be expressed by the formula

$$u(x) = \int_0^a p_0(\xi) K(x - \xi) d\xi \tag{2.1}$$

where the kernel of the integral operator

$$K(x) = \int_0^\infty \frac{ch(2s) - 1}{s(sh(2s) + 2s)} cos(sx) ds \tag{2.2}$$

2.2.1 Case of the point load

Let us consider a simple example, when a single-point force acts on the layer instead of a distributed load, such as applied at the origin, i.e. $p_0(\xi) = p_0\delta(x)$ (see Fig.2.1). Then, using the property of Dirac delta function $\delta(x)$, the equa-

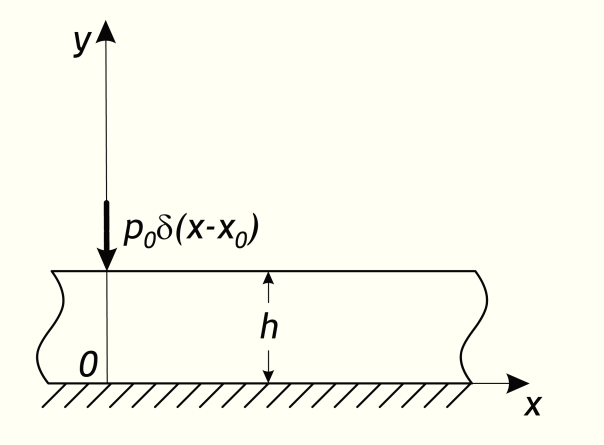

Figure 2.1: Contact problem on elastic layer in the case of single-point force

tions (2.1),(2.2) are reduced to a rather simple form:

$$u(x) = p_0 \int_0^\infty \frac{ch(2s) - 1}{s(sh(2s) + 2s)} cos(sx) ds \tag{2.3}$$

Further, not to lose the accuracy because of the deletion of points at infinity when substituting the integral by the finite-dimensional sum, we distinguish the additive component in an explicit form in the integrand corresponding to the asymptotic behavior at infinity:

$$u(x) = p_0 \int_0^\infty \left(\frac{ch(2s) - 1}{s(sh(2s) + 2s)} - \frac{1}{\sqrt{s^2 + 1}} \right) cos(sx) ds + p_0 \int_0^\infty \frac{cos(sx)}{\sqrt{s^2 + 1}} ds \tag{2.4}$$

Using the L'Hopital rule, we find that the integrand at the lower limit is 1/3. The second component is the standard integral and is exactly the modified Bessel function (MacDonald function) $K_0(x)$ [12].

Numerical experiment shows that the distinguished root feature already at $s > 10$ differs from the original function only in the third decimal place. In our calculations we have limited first integral upper limit to $A = 350$ where the difference is reduced to $O(10^{-8})$. Then, by introducing nodes grid $s_n = nh =$

nA/N, $n = 0, 1, .., N-1$, the first integral is replaced by the integral sum

$$\int_0^A f(s)cos(sx)ds \approx h \sum_{n=0}^{N-1} f(s_n)cos\left(xn\frac{A}{N}\right) \tag{2.5}$$

, which, when selected $x_k = 2\pi m/A$, $m = 0, 1.., N-1$ reduces to the fast cosine transform. Here

$$f(s) = \frac{ch(2s) - 1}{s(sh(2s) + 2s)} - \frac{1}{\sqrt{s^2 + 1}} \tag{2.6}$$

Then the final form of the expression for the strain field is given by the following formula

$$u(x_m)/p_0 \approx h\, FCT[f(s_n)] + K_0(x_m) \tag{2.7}$$

where FCT - is the fast cosine transform algorithm. The rational approximation is used for the numerical calculation of the modified Bessel function [12].

Below there is a comparative graph (Fig. 2.2) of the proposed method (shows by the points) and the direct numerical calculation of the equation (2.4). The results are given for the following design parameters: $N = 2^{13} = 8192$, $p_0 = 1$, $A = 350$.

The direct numerical computation in the programming environment Visual C++ took 4.72 seconds. The proposed approach took only 0.045 seconds, that is about 100 times faster. It is worth noting that in the first case, it is necessary to calculate the integral for each coordinate separately, whereas the use of fast transform allows finding it immediately for the entire interval. Moreover, the bigger the number of nodes N we take for the numerical score, the greater the length of this interval is, because, $x_N = N\pi/A$.

2.2.2 Case of the uniform load

Likewise the problem of a uniformly distributed load p, acting on the interval $[0, a]$ can be considered. Indeed, it is easy to notice that in this case the

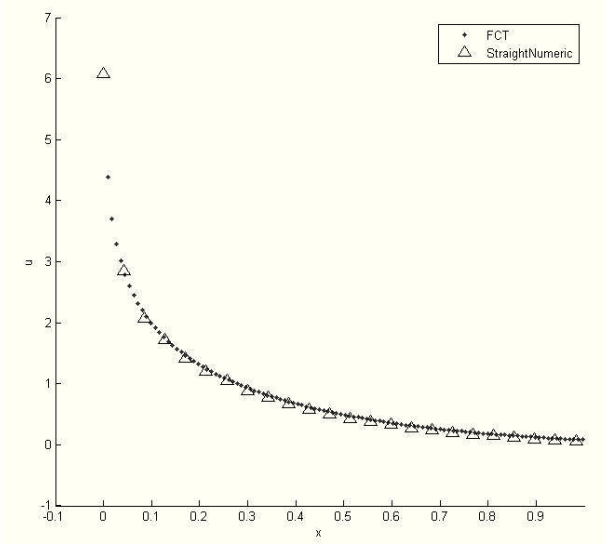

Figure 2.2: Displacement vector u versus x-coordinate in the case of point load

equation (2.1) takes the form:

$$u(x) = p \int_0^a \int_0^\infty \frac{ch(2s) - 1}{s(sh(2s) + 2s)} cos(s(x - \xi)) ds \, d\xi \tag{2.8}$$

Exchanging the order of integration in (2.8) and integrating over the interval of loading, we obtain the expression (2.9)

$$u(x) = p \int_0^\infty \frac{ch(2s) - 1}{s^2(sh(2s) + 2s)} \left(sin(sx) + sin(s(a - x))\right) ds \tag{2.9}$$

which in our view is convenient to consider as the sum of two integrals , i.e. for each sinus separately. Note that the integral in the equation (2.9) allows one to use the fast sine transform almost immediately. For this it is only necessary to select appropriately the partition mesh for both variables. However, as in the previous example, we distinguish the additive component in an explicit form in the integrand corresponding to the asymptotic behavior at infinity for the greater accuracy of the numerical integration:

$$\begin{gathered} \int_0^\infty \frac{2sh^2(s)}{s^2(sh(2s)+2s)} sin(sx) ds = \int_0^\infty \left(\frac{2sh^2(s)}{s^2(sh(2s)+2s)} - \frac{1}{2s} \right) sin(sx) ds + \\ + \frac{1}{2} \int_0^\infty \frac{sin(sx)}{s} ds \approx \int_0^A f(s) sin(sx) ds + \frac{Si(Ax)}{2} \end{gathered} \tag{2.10}$$

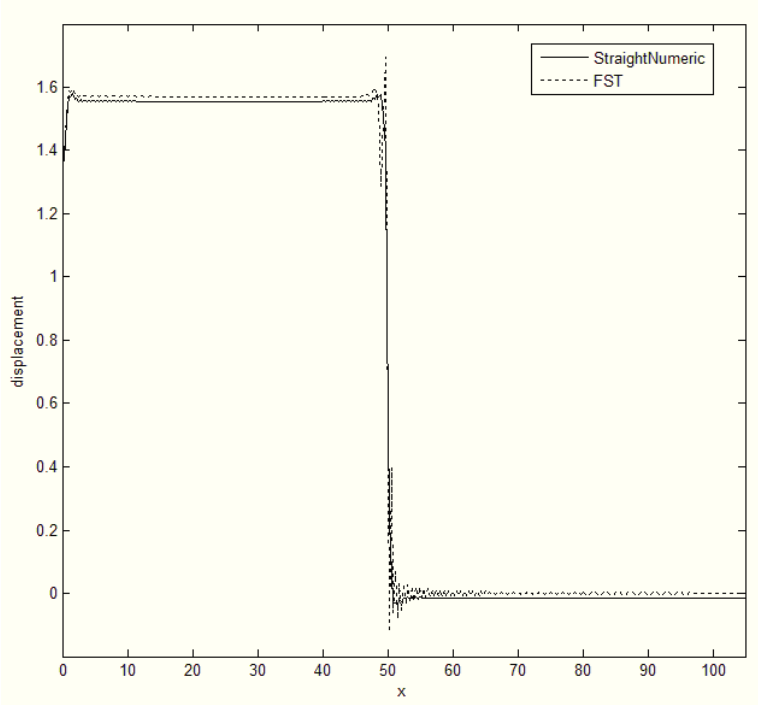

Figure 2.3: Displacement vector u versus x-coordinate in the case of uniform load

It can be seen that the second component is the standard integral, namely the integral sine $Si(Ax)$ where A - is the upper limit of integration. Further, replacing the first integral by the integral sum, we arrive at a form that when chosen $x_k = k\pi/A$ is reduced to a fast sine transform [15]:

$$\int_0^A f(s)sin(sx)ds \approx h\sum_{j=0}^{N-1} f(s_j)sin(s_j x) \tag{2.11}$$

where $h = A/N$, $s_j = jh$, $j = 0, 1, .., N-1$. Then the final expression for the displacement field will have the form

$$u(x_k)/p \approx h\sum_{j=0}^{N-1} f(s_j)sin(s_j x_k) + h\sum_{j=0}^{N-1} f(s_j)sin(s_j(x_k - a)) + \\ + \frac{Si(Ax_k) - Si(A(x_k - a))}{2} \tag{2.12}$$

The graph 2.3 comparing this technique with direct numerical integration of equation (2.10) is given above. The calculations were performed for the

following parameters: $A = 10$, $a = 50$, $N = 2^{13} = 8192$, $p = 1$. The rational approximation was used for the numerical calculation of the integral sine [12]. Here a direct numerical calculation in the programming environment Visual C++ took 32.46 seconds, and the present method - 0.008 seconds.

2.2.3 Case of the non-uniform load

From the previous section it is evident that the FFT is a fast and efficient method for integration. However, the equations kernels do not always allow bringing them to the form suitable for direct use of the FFT. Nevertheless, over a wide problem class the integrals presented in discrete form can be considered as the convolution of two signals, that allows to use the discrete Fourier transformation property, also known as the convolution theorem. Thus, the Fourier transform of the unknown function is expressed in terms of the Fourier transform of the right-hand side of the integral equation and the kernel of the integral operator. After their calculation it is only necessary to perform the inverse transform to find the unknown value. Obviously, to increase the calculation speed of the proposed algorithm the method of fast Fourier transform is used.

To demonstrate the proposed approach, we assume that in the previous problem the load is distributed unevenly and is given as a function of force distribution $p(x)$ $(0 \le x \le a,\ y = h)$ (see Fig. 2.4). Obviously, in this case, the discretization of the integral equation (2.1)–(2.2) leads to the following sum

$$u_n \approx h_1 \sum_{0}^{N-1} p_j K_{nj}, \quad n = 0, 1, .., N-1 \tag{2.13}$$

where $h_1 = a/N$, $u_n = u(x_n)$, $p_j = p(\xi_j)$, and the coefficients of the matrix

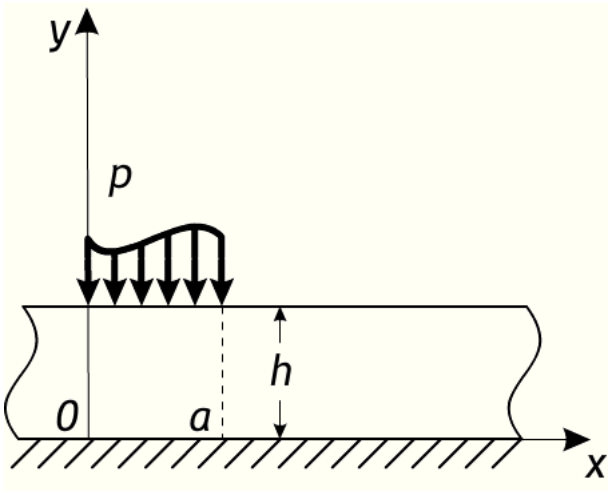

Figure 2.4: Contact problem on elastic layer in the case of non-uniform load

K_{nj} are given by the following expression

$$K_{nj} = K(x_n - \xi_j) \approx h_2 \sum_{n=0}^{M-1} \frac{ch(2s_m) - 1}{s_m(sh(2s_m) + 2s_m)} cos(s_m(x_n - \xi_j)), \quad h_2 = A/M \tag{2.14}$$

Here, the constant A is the upper limit of integration arising when replacing the integral finite sum, and the nodes are calculated using the formulas $x_n = nh_1$, $\xi_j = jh_1$, $s_m = mh_2$.

In the case where the unknown function is the displacement field, the direct calculation of the double sum (2.13) for only one fixed position x_i takes $N \times M$ operations. On the other hand, the right-hand side of the equation (2.13) can be regarded as a convolution of two discrete signals. Thus, by applying the discrete Fourier transform to this equation and using the convolution theorem [13], we obtain

$$\widehat{u} = DFT\left[h_1 \sum_{j=0}^{N-1} p(\xi_j) K(x_n - \xi_j)\right] = h_1 \widehat{p}\widehat{K} \tag{2.15}$$

Here the values $\widehat{u}$, $\widehat{p}$, $\widehat{K}$ denote the Fourier transform of functions u, p, K respectively, and DFT - is the Discrete Fourier Transform. Therefore, the solu-

tion of the direct problem is obtained by applying the inverse Fourier transform to the equation (2.15), i.e.

$$u = DFT^{-1}\left[h_1 \widehat{p}\widehat{K}\right] \tag{2.16}$$

For the efficient computation of Fourier transforms made in the proposed method, the FFT algorithms are used. However, the solution of this problem can be even more effective if we note that the discretized kernel of integral operator (2.14) by means of a special choice of the partition mesh can be presented in the form of fast cosine transformation, which in turn can be expressed by the inverse discrete Fourier transform. Such an approach would present the kernel as the inverse discrete Fourier transform of the integrand, as a result there is no need to apply the direct conversion in the formula (2.16), since instead integrand kernel can be directly used. Mathematically, it is as follows. Since

$$K(x_j) \approx h_2 \sum_{m=0}^{M-1} f_m \, cos(s_m \, x_j), \quad f_m = \frac{ch(2s_m) - 1}{s_m(sh(2s_m) + 2s_m)} \tag{2.17}$$

when selecting a partition mesh of $x_j = j\pi/(h_2 M)$ this expression takes the form of fast cosine transformation [15].

To bring the resulting sum to an inverse Fourier transform we expand the discretized integrand so that it is even with respect to $m = M$:

$$f_{2M-m} = f_m, \quad m = 0, 1, .., M-1 \tag{2.18}$$

Then the inverse FFT of the extended functions will be:

$$F_j = \frac{1}{2M} \sum_{m=0}^{2M-1} f_m \, e^{-i\frac{\pi j m}{M}} \quad m = 0, 1, .., M-1 \tag{2.19}$$

The second half of this sum from $m = M$ to $2M - 1$ can be simplified if we use replacement $m' = 2M - m$:

$$\sum_{m=M}^{2M-1} f_m \, e^{-i\frac{\pi j m}{M}} = \sum_{m'=0}^{M-1} f_{2M-m'} e^{-i\frac{\pi j(2M-m')}{M}} = \sum_{m'=0}^{M-1} f_{m'} e^{i\frac{\pi j m'}{M}} \tag{2.20}$$

Thus

$$F_j = \frac{1}{2M}\sum_{m=0}^{M-1} f_m \left[e^{-i\frac{\pi jm}{M}} + e^{i\frac{\pi jm}{M}}\right] = \frac{1}{M}\sum_{m=0}^{M-1} f_m \, cos(\pi jm/M) \tag{2.21}$$

Finally, we obtain that the kernel of the integral operator is expressed through the inverse discrete Fourier transform of f as follows:

$$K_j = Mh_2F_j \tag{2.22}$$

Substituting this expression in equation (2.15), we obtain

$$\widehat{u} = DFT\left[h_1\sum_{j=0}^{N-1} p(\xi_j)K(x_n - \xi_j)\right] = h_1h_2M\widehat{p}f \tag{2.23}$$

Consequently, the required displacement field is obtained from the following equation:

$$u = DFT^{-1}\left[h_1h_2M\widehat{p}f\right] \tag{2.24}$$

The described approach is quite versatile and can be applied to various integral equations with difference kernels. When the right-hand side of the original equation (2.1) has a rather simple form, it is more expedient to bring the numerical integration to the fast transforms by a special change of variable.

2.3 Fast numerical solution of the crack problem in the porous elastic material

In the examples above, we restricted ourselves to the evaluation of integrals, however, FFT algorithms can be successfully applied to the solution of integral equations (i.e. in cases where the integrand is unknown). Let us demonstrate application of this idea in the crack problem for a medium with voids. Materials of this nature play important role in many fields, such as soil mechanics, civil engineering, ultrasonic non-destructive testing and others. The used theory

for the behavior of the porous elastic media has been proposed by Nunziato and Cowin in 1980s [16,17]. In accordance to this model, there is introduced an unknown function which takes into account a certain volume fraction field. This new function of volumetric density significantly influences the stress-strain state, being introduced as a product of material density field and the volume fraction field. The general theory, developed in detail, has been tested on numerous concrete problems for special domains under particular boundary conditions (see, for example, [18–21]) and shows good agreement with both experimental data and physical conclusions. The application of this theory for the crack problem in porous materials has been presented in [22] and our further treatment is based upon this work.

Mathematically, when the problem for linear crack is reduced to the linear algebraic system by a collocation technique, the obtained matrix has a Toeplitz-like structure. The algorithms to solve such matrix equations are well-developed and there are many different approaches presented in literature. For $N \times N$ systems direct "fast" methods require $N \log^2(N)$ arithmetic operations. To improve such approaches, there have been developed faster methods based on a preconditioned conjugate gradient method with circulant pre-conditioners.

2.3.1 Formulation of the problem and review of previous results

Let us consider a linear crack of length $2a$ in the considered porous material with a distributed load p_0 acting on its boundary. We couple with this crack a fixed system of rectangular Cartesian coordinates $Oxyz$ in such a way that the center of the system is located at the center of the crack (see Fig.2.5). As proposed in [16,17], we call ν_ρ^0 the constant volume fraction. In this frame the

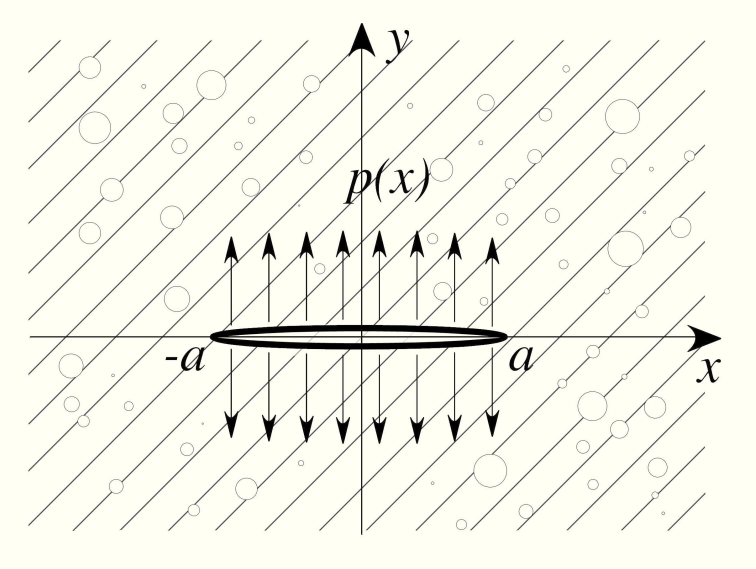

Figure 2.5: Linear crack in the porous elastic material

constant mass density ϱ is represented as a product of two fields: the density of the matrix material γ and the volume fraction field ν_ρ $(0 < \nu_\rho \leq 1)$, i.e. $\varrho = \gamma\nu_\rho$. This representation introduces an additional degree of kinematic freedom and, in absence of the volume fraction field, this theory reduces to the classical theory of elasticity.

Assume that ϕ $(\phi = \nu_\rho - \nu_\rho^0)$ represents the change in volume fraction from the reference one, $\bar{u}$ denotes the displacement vector, μ and λ are usual elastic constants, and α, β, ζ represent some constants related to porosity of the medium. Then, according to the Nunziato and Cowin model [16,17], it is possible to describe the behavior of the homogeneous and isotropic elastic material using the following system of partial differential equations

$$\begin{cases} \mu\ \Delta\ \bar{u} + (\lambda + \mu)\ grad\ div\ \bar{u} + \beta\ grad\ \phi = 0 \\ \\ \alpha\ \Delta\ \phi - \zeta\ \phi - \beta\ div\ \bar{u} = 0 \quad , \end{cases} \tag{2.26}$$

It is clear that $\beta = 0$ corresponds to the case when the elastic and the "porosity"

fields are independent from each other. Thus, in the case $\beta = 0$ the stress-strain state is insensitive with respect to function ϕ. The components of the stress tensor are represented by the following formulas

$$\begin{cases} \sigma_{ij} = \lambda\ \delta_{ij}\ \varepsilon_{kk} + 2\ \mu\ \varepsilon_{ij} + \beta\ \phi\ \delta_{ij} \\ \varepsilon_{ij} = \frac{1}{2}(u_{i,j} + u_{j,i})\ . \end{cases} \tag{2.27}$$

where δ_{ij} is Kronecker's delta.

In the plane problem, where $u = \{u_x(x,y),\ u_y(x,y),\ 0\}$, one can rewrite system (2.26)-(2.27) in the two-dimensional form

$$\begin{cases} \frac{\partial^2 u_x}{\partial x^2} + c^2\ \frac{\partial^2 u_x}{\partial y^2} + (1-c^2)\ \frac{\partial^2 u_y}{\partial x \partial y} + H\ \frac{\partial \phi}{\partial x} = 0 \\ \frac{\partial^2 u_y}{\partial y^2} + c^2\ \frac{\partial^2 u_y}{\partial x^2} + (1-c^2)\ \frac{\partial^2 u_x}{\partial x \partial y} + H\ \frac{\partial \phi}{\partial y} = 0 \\ l_1^2 \left(\frac{\partial^2 \phi}{\partial x^2} + \frac{\partial^2 \phi}{\partial y^2} \right) - \frac{l_1^2}{l_2^2}\ \phi - \left(\frac{\partial u_x}{\partial x} + \frac{\partial u_y}{\partial y} \right) = 0, \end{cases} \tag{2.28}$$

with

$$\begin{cases} \frac{\sigma_{xx}}{\lambda+2\mu} = \frac{\partial u_x}{\partial x} + (1-2c^2)\ \frac{\partial u_y}{\partial y} + H\phi\ , \\ \frac{\sigma_{yy}}{\lambda+2\mu} = (1-2c^2)\ \frac{\partial u_x}{\partial x} + \frac{\partial u_y}{\partial y} + H\phi\ , \\ \frac{\tau_{xy}}{\mu} = \frac{\partial u_x}{\partial y} + \frac{\partial u_y}{\partial x}\quad . \end{cases} \tag{2.29}$$

Here, for the sake of convenience, some new positive physical parameters are added. Two of them are dimensionless:

$$c^2 = \frac{\mu}{\lambda + 2\mu}\ , \quad H = \frac{\beta}{\lambda + 2\mu}\ , \tag{2.30}$$

and

$$l_1^2 = \frac{\alpha}{\beta}\ , \quad l_2^2 = \frac{\alpha}{\zeta} \tag{2.31}$$

are measured in meters.

The boundary conditions over the line $y = 0$ are given as follows:

$$\begin{aligned} &\sigma_{yy} = p_0(x) \equiv \sigma_0,\ |x| \le a; \quad u_y = g(x) = \begin{cases} u_0(x),\ |x| \le a, \\ 0,\ |x| > a. \end{cases} \\ &\tau_{xy} = 0\ (y = 0), \quad \frac{\partial \phi}{\partial y} = 0 \end{aligned} \tag{2.32}$$

Here, for simplicity, the tangential load is assumed to be absent. The last boundary condition refers to an elastic material with voids and it follows from the balance principle (see [20]).

In order to transform the problem into an integral equation problem, it is convenient to apply the Fourier transform along the x-axis [22]. We recall here that, for arbitrary function $f(x)$ and respective Fourier image $F(s)$, the Fourier transform can be written as

$$F(s) = \int_{-\infty}^{\infty} f(x)\; e^{isx}\; dx\;, \qquad f(x) = \frac{1}{2\pi}\int_{-\infty}^{\infty} F(s)\; e^{-isx} ds\;. \tag{2.33}$$

By applying the Fourier transform (2.33) to system (2.28), one reduces the system of partial differential equations to a system of ordinary differential equations with constant coefficients regarding images of functions u_x, u_y, ϕ. Obviously, these functions depend only on variable y:

$$\begin{cases} c^2 U_x'' - s^2\, U_x + (1-c^2)(-is)\, U_y' - is\, H\, \Phi = 0 \\ (1-c^2)(-is)\, U_x' + U_y'' - c^2\, s^2\, U_y + H\, \Phi' = 0 \\ is\, U_x - U_y' + l_1^2\, \Phi'' - \left(\frac{l_1^2}{l_2^2} + l_1^2\, s^2\right)\, \Phi = 0\;. \end{cases} \tag{2.34}$$

In [18,19] it is shown that solution of homogeneous system (2.34) can be found by classical exponential substitution. This leads to a couple of double characteristic values (the same as in the classical linear elasticity) and a simple value, arising due to porosity of the material. Finally, the general solution is constructed in the form

$$\begin{pmatrix} U_x \\ U_y \\ \Phi \end{pmatrix} = D_1 \begin{pmatrix} \frac{isH}{1-CN} \\ \frac{H\sqrt{s^2+1-CN}}{1-CN} \\ 1 \end{pmatrix} e^{-y\sqrt{s^2+1-CN}} \;+\; D_2 \begin{pmatrix} i\; sign(s) \\ 1 \\ 0 \end{pmatrix} e^{-|s|y} + \tag{2.35}$$

$$+D_3 \begin{pmatrix} \frac{1-CN+c^2}{(-is)(CN-1+c^2)} + iy\ sign(s) \\ y \\ \frac{2CNc^2}{H(1-CN-c^2)} \end{pmatrix} e^{-|s|y} \quad , \tag{2.36}$$

where the dimensionless physical parameter $CN = (l_2^2/l_1^2)\, H,\ 0 \leq CN < 1$ is usually called the "Coupling Number". The constants D_1, D_2, D_3, which depend on s, can be found by substituting the above equation into the boundary conditions, since we have three boundary conditions for three unknowns.

Finally, the application of the inverse Fourier transform to the images of the unknown functions leads to the following representation [18,19]

$$\begin{aligned} &u_{x,y}(x,y) = \tfrac{1}{2\pi} \int_{-\infty}^{\infty} Y_{x,y}(s,y) \left[\int_{-a}^{a} u_0(\xi) e^{is\xi} d\xi \right] e^{-isx} ds = \\ &= \tfrac{1}{2\pi} \int_{-a}^{a} u_0(\xi) d\xi \int_{-\infty}^{\infty} Y_{x,y}(s,y) e^{is(\xi - x)} ds \end{aligned} \tag{2.37}$$

Function ϕ can be written by analogy. It is proposed in [22] to use the second equation of system (2.29), to obtain an integral equation for the stress-deformation relation. This approach gives the following integral representation

$$\begin{aligned} \tfrac{\sigma_{yy}(x,y)}{\lambda+2\mu} = \tfrac{1}{2\pi} \int_{-a}^{a} u_0(\xi) d\xi \int_{-\infty}^{\infty} \{ &(1-2c^2)(-is) Y_x(s,y) + \\ &+ \tfrac{\partial Y_y(s,y)}{\partial y} + H Y_\Phi(s,y) \Big\} \cdot e^{is(\xi - x)} ds \end{aligned} \tag{2.38}$$

where coefficients Y_x, Y_y, Y_Φ are given by the formulas

$$\begin{cases} iY_x(s,y) = \frac{2CNc^2s^3}{(CN-1)^2\sqrt{s^2+1-CN}} e^{-y\sqrt{s^2+1-CN}} + \\ \\ + \left(\frac{(1-CN)c^2 - 2CNc^2s^2}{(CN-1)^2} sign(s) + \frac{1-CN-c^2}{CN-1} ys \right) e^{-y|s|} \\ \\ Y_y = -\frac{2CNc^2s^2}{(CN-1)^2} e^{-y\sqrt{s^2+1-CN}} + \\ \\ + \left(\frac{(CN-1)^2 + 2CNc^2s^2}{(CN-1)^2} + \frac{CN-1+c^2}{CN-1} y|s| \right) e^{-y|s|} \\ \\ HY_\Phi(s,y) = \frac{2CNc^2|s|}{(CN-1)} \left(\frac{s}{\sqrt{s^2+1-CN}} e^{-y\sqrt{s^2+1-CN}} - e^{-y|s|} \right) \end{cases} \tag{2.39}$$

After some routine mathematical transformations, by putting $y = 0$, it is possible to connect the unknown displacement and the stress on the boundary of the crack:

$$\frac{\sigma_{yy}(x)}{\lambda + 2\mu} = \frac{c^2}{\pi} \int_{-a}^{a} L(\xi - x) u_0(\xi) d\xi \tag{2.40}$$

where the kernel function $L(x)$ is given by the expression

$$\begin{array}{l} L(x) = \int_{-\infty}^{\infty} \left\{ \frac{2CNc^2s^4}{(1-CN)^2\sqrt{s^2+1-CN}} - \right. \\ \left. - \frac{|s|\left[2CNc^2s^2 + (1-CN)(1-c^2)\right]}{(1-CN)^2} \right\} e^{isx} ds \end{array} \tag{2.41}$$

The authors of [22] show that the kernel can be reduced to a more explicit form. This based on some classical tabulated integrals [12,23]. Thus, if one takes into account that the integrand is even, then integral in (2.40) can be rewritten on the semi-interval $(0, \infty)$ as follows:

$$\begin{array}{l} L(x) = \frac{4CNc^2}{(1-CN)^2} \int_0^\infty \frac{s^4}{\sqrt{s^2+1-CN}} \cos sx \, ds - \\ - \frac{4CNc^2}{(1-CN)^2} \int_0^\infty s^3 \cos sx \, ds - \frac{2(1-c^2)}{(1-CN)} \int_0^\infty s \cos sx \, ds \end{array} \tag{2.42}$$

It is easy to check that the last integral is the same as in the classical linear problem. Moreover, with $CN \to 0$ (no voids), there remains only the last term, like in the crack problem for the ordinary material without voids.

It is shown in [22] that the kernel is hyper-singular. Thus, for a stable numerical calculation for every x on the interval $[-a, a]$ (outside the origin) the kernel can be divided to regular and irregular parts

$$L(x) = 4CNc^2 \left[K_0(|x|b) \left(1 + \tfrac{3}{(xb)^2}\right) + K_1(|x|b) \left(\tfrac{2}{|x|b} + \tfrac{6}{(|x|b)^3}\right) - \right. \\ \left. - \tfrac{6}{(xb)^4} - \tfrac{1}{2(xb)^2} \right] + \tfrac{2(1-c^2b^2)}{(xb)^2} = L_0(x) + \left(\tfrac{2}{b^2} - 2c^2\right) \tfrac{1}{x^2} \tag{2.43}$$

where we have introduced parameter $b = \sqrt{1-CN}$, and $L_0(x) = O(\ln|x|)$, $x \to 0$ is a function with a more regular behavior when compared with the characteristic hyper-singular part. Finally, integral equation (2.40) takes the form appropriate for an efficient numerical treatment:

$$\int_{-a}^{a} L_0(x-\xi) u_0(\xi) d\xi + \left(\frac{2}{b^2} - 2c^2\right) \int_{-a}^{a} \frac{u_0(\xi)}{(x-\xi)^2} u_0(\xi) d\xi = \frac{\pi}{\mu}\sigma_0, \quad |x| \le a. \tag{2.44}$$

2.3.2 Discrete implementation and fast algorithms

To perform the numerical calculation needed to solve Eq. (2.44), one may use the collocation technique proposed in [24]. In this case the interval of the crack boundary $(-a, a)$ is divided into n small subintervals of length $h = 2a/N$. The set of nodes $\xi_m = -a + mh$, $m = 0, ..., N$ are chosen in discretization over internal variable, and in dicretization of the external variable one should take the nodes $x_n = -a + (n - 1/2)h$, $n = 1, ..., N$ placed at the central points of each sub-interval $[\xi_{i-1}, \xi_i]$. Thus, the initial integral equation can be approximated by the following linear algebraic system

$$\sum_{n=1}^{N} A_{nm} u_m = \sigma_n, \qquad (\sigma_n = \sigma_0\, \pi/\mu,\, \forall n), \tag{2.45}$$

where the non-diagonal elements of the matrix A_{nm}, $(n \neq m)$ are equal to

$$A_{nm} = \left(\frac{2}{b^2} - 2c^2\right)\left(\frac{1}{x_n - \xi_m} - \frac{1}{x_n - \xi_{m-1}}\right) + hL_0(x_n - \xi_m) \tag{2.46}$$

with $u_m = u_0(\xi_m)$. The diagonal elements of the matrix $(n = m)$ are calculated as

$$A_{nn} = \left(\frac{2}{b^2} - 2c^2\right)\left(\frac{1}{x_n - \xi_n} - \frac{1}{x_n - \xi_{n-1}}\right) \tag{2.47}$$

System (2.45)–(2.47) can be solved by classical numerical methods (for example, by Gauss elimination), but this requires $O(N^3)$ number of arithmetic operations [15]. When the number of nodes N is large, such a technique takes too much computational time. Thus, a faster iterative approach should be applied to reduce the computational cost of the solution. The advantage of iterative techniques is connected with the fact that one may stop the algorithm, when a desired precision is attained. In fact, in practical computing with applications we are usually interested in some accurate solution but not exact one, because computer implementation itself does bring some deficiency in the solving process. Moreover, real electronic devices installed in the industry never give exact input or output data, because of presence of "noise".

Generally, iterative methods are faster when compared to direct methods. In the present work we test the conjugate gradients method (CG)[2] as one of the most efficient and popular techniques in the nowadays computational mathematics. This method provides a minimization of the function

$$t(x) = \frac{1}{2}uAu - \sigma u \tag{2.48}$$

Such a minimization problem is solved when the gradient of function t is equal to zero:

$$grad(t) = Au - \sigma = 0 \tag{2.49}$$

which is equivalent to the initial problem (2.45). The principal advantage of this method is that its recurrence relations are very compact and can be

represented only by few lines:

$$\begin{aligned} \alpha_j &= (r_{j-1}, r_{j-1})/(Az_j, z_j), \\ u_j &= u_{j-1} + \alpha_j z_j, \\ r_j &= r_{j-1} - \alpha_j A z_j, \\ \beta_j &= (r_j, r_j)/(r_{j-1}, r_{j-1}), \\ z_{j+1} &= r_j + \beta_j z_j. \end{aligned} \tag{2.50}$$

At the first step one should set the initial residual vector $r_0 = \sigma - Ax_0$ and the initial basis vector to be $z_1 = r_0$. The initial solution x_0 can be set trivial or taken from some general assumptions (for example, from the asymptotic behavior). It is clear from (2.50) that the most computer-expensive operation is a matrix-vector multiplication in the first and third lines of the iteration algorithm. If one operates with a general dense matrix, this operation is performed in N^2 numerical operations. Thus, the overall numerical cost of such a method is $O(N_{it}N^2)$, where N_{it} is the number of iterations needed to achieve the desired precision.

However, let us notice that the matrix in system (2.45) has a special form, because its elements depend only on difference of subscripts, i.e. $A_{nm} = A_{n-m}$, and then all the information about the matrix is collected in its first row and first column. This also means that the overall computer memory storage required for this kind of matrix includes only an array of length $2N - 1$, or even N in the case of symmetric matrix. This is much lower than the classical N^2 required for matrices with a dense structure. Just this fact was an origin for development of the algorithms which solve such a system in a reasonable computational time [25]. In fact, in the present day the solution of matrix systems with Toeplitz and Toeplitz-type matrices is an intensively developing area of computational mathematics.

Actually, there are various approaches to solve LAS with Toeplitz matrices. The most convenient way is a construction of a certain numerical scheme that

calculates the unknown vector u. The algorithms of such a kind are based on the developed results of computational mathematics and often include too complex numerical schemes. One of disadvantages of such approaches is that they are very unstable for ill-conditioned systems and as, a result, give inaccurate solutions. To improve the stability of such a technique, there have been proposed few approached of complexity $O(N \log^3 N)$ [26,27]. It is easy to check that if $N = 10^3$, then such an algorithm requires almost $O(N^2)$ operations. However, real applications usually require to solve LAS (2.45) for different right-hand sides. This means that we should apply any "fast" algorithm several times (as much as the number of right-hand sides we have).

Another idea is based on the fact that the inverse of a Toeplitz matrix can also be represented in compact manner (as a sum of products of Toeplitz matrices, i.e. $A^{-1} = W_1V_1 + W_2V_2$, where A, W_1, V_1, W_2, V_2 are Toeplitz matrices [28]). Below we will show some fast ideas for the product of general Toeplitz matrices by using an algorithm based on a FFT method which requires only $O(2N \log(2N))$ operations. It becomes clear from this fact that the inversion of any Toeplitz matrix can by multiplied by a right-hand side vector just in $O(8N \log(2N))$ operations. This again justifies the efforts of many authors to develop fast inversion algorithms for such matrices. In fact, an obvious advantage of this approach is that, when a system has to be solved with several right-hand sides, the algorithm is applied only once, followed by only matrix-vector multiplications. A shortcoming of such methods is that they are also unstable in the case of ill-conditioned systems.

Both approaches described above can be implemented using two classical algorithms: direct or iterative. The earliest works in this domain were concentrated on the development of the direct methods. As a rule, their complexity is quadratic (instead of a cubic) number of operations, which is a considerable advantage. Generally, this methods impose some restrictions to matrix A. As

an example, the invertibility of the $(N-1)\times(N-1)$ principal sub matrix of A was required for first "fast" Toeplitz solvers such as well-known Levinson and Trench algorithms [29,30]. Further, faster algorithms of quasi-linear complexity $O(N\log^2 N)$ have been developed by de Hoog, Ammar and others [31,32] and now known as "superfast" solvers. The key idea of these methods is to solve the problem recursively. As a rule, such algorithms dealt with well-conditioned, symmetric positive-define Toeplitz matrices and were unstable in the case of poor conditioning. To overcome the obstacle various look-ahead algorithms have been recently developed for the Teoplitz systems with singular or ill-conditioned principal sub-matrix.

However, in the case of Toeplitz matrices, the iterative approach is clearer and easier to implement. In fact, the most popular way of solving Toeplitz systems in engineering mechanics is represented by the simple and rather efficient conjugate gradient method with preconditioning (PCG), where the power of the fast Fourier transform is intensively used. It has been shown that the solution of such a LAS by the conjugate gradient method requires a quasilinear number of operations if preconditioning is applied to the matrix of the system [33, 34]. This approach has been widely used in applications because of its convenient implementation. It is this approach that we used in our study. Below, we describe it in more detail, following [2].

Recall that the preconditioning technique is based on the simple idea that a system

$$A_{n-m}u_m = \sigma_n \tag{2.51}$$

with an ill-conditioned matrix A is replaced by a preconditioned system

$$AC^{-1}u = \sigma \tag{2.52}$$

where the preconditioning matrix C is chosen so that the matrix of the product AC^{-1} has a low condition number. Theoretically, any matrix can be improved

with this technique as soon as a suitable preconditioner has been found.

PCG can be compactly rewritten as the following recurrence relations [2]

$$\begin{aligned} \alpha_j &= (r_{j-1}, C^{-1}r_{j-1})/(Az_j, z_j), \\ u_j &= u_{j-1} + \alpha_j z_j, \\ r_j &= r_{j-1} - \alpha_j A z_j, \\ \beta_j &= (r_j, C^{-1}r_j)/(r_{j-1}, C^{-1}r_{j-1}), \\ z_{j+1} &= C^{-1}r_j + \beta_j z_j. \end{aligned} \tag{2.53}$$

In the contrast to the classical CG, here at the first step the initial basis vector is set to be a solution of the system $Cz_1 = r_0$ or, equivalently, $z_1 = C^{-1}r_0$ if the inverse matrix is known. Likewise, this inverse matrix appears two times at each iteration of PCG algorithm. Therefore, the inversion of the matrix C^{-1} and the multiplication of the matrices C^{-1} and A by the corresponding residual and basis vectors are the most expensive operations and, as we said earlier, in the general case the first operation requires a cubic number of operations, while the second one, a quadratic number of operations. Hence, this approach is faster then CG method only in the case when the inverse to matrix C can be found at least in N^2 (or even less) operations and both the multiplication of matrix C^{-1} by vector and construction of preconditioning matrix C can be performed in sufficiently less operations than N^2.

In the case of Toeplitz matrices, both operations are reduced to quasilinear complexity by applying the properties of circulant matrices, which are a discrete representation of the convolution operation. A circulant matrix is a periodic Toeplitz matrix with $c_{-k} = c_{N-k}$ for $1 \leq k \leq N-1$. Here, the vector $\bar{c}$ is the first row of the matrix C.

In the modern literature on computational mathematics there are many various techniques to construct a preconditioning matrix [35]. Advanced approaches use a generating function of the matrix and are known as "function-based". For symmetric matrices a classical preconditioner, which is built from

the elements of the given matrix, generally works well. This idea has initially been proposed by G. Strang in 1986 [33] and in his algorithm is constructed from a half of elements of the first row and first column of original Toeplitz matrices:

$$c_j = \begin{cases} A_j, & 0 \le j < \frac{N+1}{2} \\ A_{j-N}, & \frac{N+1}{2} \le j < N \end{cases} \tag{2.54}$$

recalling that $A_{n-m} = A_{nm}$. This circulant matrix minimizes norms $||C - A||_1$ and $||C - A||_\infty$.

Let us also recall the so-called optimal circulant preconditioned matrix proposed by T.Chan [34]. This matrix is the nearest, in the Frobenius-norm, circulant matrix to the given Toeplitz matrix. Namely, this solves the optimization problem: $\min ||C - A||_F$. The first row of this matrix is built from the elements of the initial Toeplitz matrix by the following formula

$$c_j = \frac{(N-j)A_j + jA_{j-N}}{N}, \quad 0 \le j < N \tag{2.55}$$

In the case of poor conditioning, one can use the technique described in [36].

The advantage of using circulant preconditioned matrices is justified by the fact that circulant matrices can be easily inverted and both initial and inverse matrices can be multiplied with any vector in $O(N \log(N))$ arithmetic operations by the fast Fourier transform. It is well known that circulant matrices have explicit singular value decomposition (SVD) with the help of Fourier matrices: $C = F^{-1}\Lambda F$, where the Fourier matrix F is a special type of Vandermonde matrix with the elements $F_{kl} = e^{2\pi ikl/N}$. The matrix-vector multiplication of such matrices can be performed in $O(N \log(N))$ operations by applying Fast Fourier transform algorithms [3]. It is easy to see that by using this decomposition, the inverse to the circulant matrix also has an explicit representation, specifically, $C^{-1} = F\Lambda^{-1}F^{-1}$, where matrix Λ is a diagonal

matrix with singular values of C on its diagonal, and is obtained by multiplying a Fourier matrix by the first row of C. Hence, the inversion of this matrix requires only $O(N)$ operations. It has been shown that, with a good choice of a circulant preconditioner, PCG is faster than available direct superfast Toeplitz solvers and the number of iterations is independent of the dimension of the problem.

Let us show how one can multiply a Toeplitz matrix A by a vector using the aforecited decomposition of circulant matrices. First of all, let us analyze the difference between the circulant and the Toeplitz matrices. The accepted notations for Toeplitz matrix imply that its elements are constant along every diagonal parallel to the principal one, i.e.

$$A = \begin{pmatrix} a_0 & a_1 & \dots & a_{N-2} & a_{N-1} \\ a_{-1} & a_0 & a_1 & & a_{N-2} \\ \vdots & a_{-1} & a_0 & \ddots & \vdots \\ a_{-(N-2)} & & \ddots & \ddots & a_1 \\ a_{-(N-1)} & a_{-(N-2)} & \dots & a_{-1} & a_0 \end{pmatrix}. \tag{2.56}$$

From the other hand, the circulant matrix is just a periodic Toeplitz matrix, where $c_{-k} = c_{N-k}$ for $1 \leq k \leq N-1$, i.e.

$$C = \begin{pmatrix} c_0 & c_1 & \dots & c_{N-2} & c_{N-1} \\ c_{N-1} & c_0 & c_1 & & c_{N-2} \\ \vdots & c_{N-1} & c_0 & \ddots & \vdots \\ c_2 & & \ddots & \ddots & c_1 \\ c_1 & c_2 & \dots & c_{N-1} & c_0 \end{pmatrix}. \tag{2.57}$$

It is clear that the original Toeplitz matrix can be extended to the matrix of larger size, of circulant structure:

$$A^c = \begin{pmatrix} A & \boxtimes \\ \boxtimes & A \end{pmatrix} \tag{2.58}$$

where matrix $\boxtimes$ is constructed in a special way, to provide the final matrix A^c to be circulant ($a^c_{-k} = a^c_{2N-k}$, $1 \leq k \leq 2N-1$). Again, positive subscripts of vector a correspond to the first row of A^c and negative ones – to the first column. The vector which is to be multiplied by matrix A is also filled (usually by zeros) in order to reach the length $2N$. The final product of the extended matrix by this vector produces a certain vector of length $2N$, from which one keeps only first N elements and remove the remaining part. It is easy to control that this procedure precisely represents the matrix-vector product:

$$\begin{pmatrix} A & \boxtimes \\ \boxtimes & A \end{pmatrix} \begin{pmatrix} u \\ 0 \end{pmatrix} = \begin{pmatrix} Au \\ \boxtimes u \end{pmatrix} \tag{2.59}$$

This can be executed as the multiplication of a circulant matrix by a vector using FFT algorithm. As already discussed, the advantage of this approach is that the number of required operations is only $O(2N \log(2N))$, instead of $O(N^2)$. Thus, if the CG algorithm results in a desired precision with N_{it}, then the overall required cost of the algorithm is only $O(6N\, N_{it} \log(2N))$.

In the works of T.Chan it has been shown that the required number of iterations N_{it} of PCG with optimal circulant preconditioner for Toeplitz systems is considerably small and does not depend on the number of nodes N. In fact, in our numerical experiments N_{it} does not exceed 25 steps, while the number of nodes is varied from 256 to 1024. This fact allows us to conclude that the numerical scheme is "quasi-linear" in the sense that it is much smaller than classical $O(N^2)$ but not yet linear $O(N)$.

2.3.3 Some numerical results

We have performed a number of computational experiments in accordance with Eq.(2.45) for various values of parameter CN and for different types of materials. Some of them are reflected in figures 2.6–2.9. The applied vertical

stress σ_0 is accepted to be of unit value.

In figure 2.6 we present an example of dependence of the displacement vector for concrete with Young's modulus $E = 30\,(GPa)$ and Poisson's ratio $\nu = 0.2$ versus parameter CN (GPa represents one gigapascal). It can be noted that, with growing "coupling number" CN, the opening of the crack becomes smaller. Thus, one can conclude that the crack in the materials with voids is less sensitive to the load (recall, that value $CN = 0$ corresponds to the classical linear elasticity). However, the qualitative behavior is similar to those obtained for analogous classical problem.

In figure 2.7 we show another example where the displacement profile is calculated for different types of materials with $CN = 0.5$. In our computer simulations we have used different types of real materials with the following values of physical parameters: concrete - $\nu = 0.2$, $E = 30\,(GPa)$; glass - $\nu = 0.25$, $E = 60\,(GPa)$; aluminum - $\nu = 0.34$, $E = 70\,(GPa)$; steel - $\nu = 0.3$, $E = 200\,(GPa)$. One can conclude from these numerical experiments that increasing of Young's modulus E results in decreasing of opening u.

Figure 2.8 shows the correlation between vector u and the "coupling number" CN for different types of materials, at the central point over the crack's faces: $x = 0$, where vector u has its maximum. From this figure one can also see the properties outlined in the two previous paragraphs.

Other numerical experiments are demonstrated in figure 2.9. The dependence of u versus length of the crack shows that for larger cracks the opening grows less rapidly.

Another series of numerical experiments have been performed to examine the efficiency of the proposed numerical algorithm to solve LAS (2.45). These results are represented in tables 2.1, 2.2. First of all, let us estimate the number of numerical operations needed. It is well known that the straightforward Gauss elimination technique requires $O(N^3)$ numerical operations to

solve LAS $N \times N$. Iterative CG method uses only a matrix-vector multiplication on each iteration, thus the overall cost of the classical CG approach is $O(N_{it}N^2)$, where N_{it} is the number of iterations needed to arrive to a desired precision and $O(N^2)$ is the cost of the matrix-vector multiplication on each step. In order to speed-up this algorithm, we use a fast matrix-vector multiplication, as described in the previous section. Since such a treatment implies a double size of the initial matrix, with the use of FFT method 3 times, one attains $O(N_{it}6N\log(2N))$ cost. In the case of the preconditioned algorithm it is added supplementary a LAS solver at every iteration step. For the circulant preconditioner it can be done also by applying FFT algorithm, i.e. we have additional $O(3N\log(N))$ operations at each step. Since the difference between $\log(N)$ and $\log(2N)$ is considerably small, we can approximately estimate the cost of PCG as $O(N_{it}9N\log(2N))$.

The implementation of fast algorithms is more interesting on large meshes. For example, it is seen from the table, that in the case $N = 2^{10}$ our approach requires around a second only, instead of 4 minutes. When the number of numerical calculations are almost equal, the classical straight-forward Gauss elimination technique is more preferable. It is interesting to note the difference between classical CG and CG with fast Toeplitz matrix-vector multiplication for $N = 2^6$, where the classical approach is even faster, but twice more expansive when compared with the fast CG algorithm. For other cases ($M > 6$, $N = 2^M$) one can see a considerable speed-up of the fast methods. However it should be noted that the number of iterations grows rapidly in the CG standard algorithm, while in PCG this remains near 20. Moreover, this quantity does not depend upon a type of material or the value of its porosity. Also, in our numerical experiments both T. Chan and Strang preconditioners give the same number of iterations for PCG. However, in more complex problems some more advanced techniques can be used (see, for example [36]).

Table 2.1: Dependence of execution time upon N

number of nodes $N = 2^M$	method	number of num.calc.	execution time (ms)
$N = 2^5 = 32$	Gauss	32768	0.89
	CG	41984	3.02
$log(2N) = 4.15$	fast CG	32739	3.35
	fast PCG	20362	2.21
$N = 2^6 = 64$	Gauss	262144	6
	CG	245760	6
$log(2N) = 4.8$	fast CG	111790	7
	fast PCG	50305	4
$N = 2^7 = 128$	Gauss	2097152	35
	CG	1376256	32
$log(2N) = 5.5$	fast CG	357730	23
	fast PCG	114984	6
$N = 2^8 = 256$	Gauss	16777216	320
	CG	7929856	249
$log(2N) = 6.2$	fast CG	1159430	70
	fast PCG	287461	18
$N = 2^9 = 512$	Gauss	134217728	2347
	CG	42991616	1297
$log(2N) = 6.9$	fast CG	3492130	245
	fast PCG	670744	36
$N = 2^{10} = 1024$	Gauss	1073741824	24097
	CG	231735296	7524
$log(2N) = 7.6$	fast CG	10352890	535
	fast PCG	1545906	77

Table 2.2: Number of iterations versus N

$N = 2^M$	CG	PCG
$2^5 = 32$	41	17
$2^6 = 64$	60	18
$2^7 = 128$	84	18
$2^8 = 256$	121	20
$2^9 = 512$	164	21
$2^{10} = 1024$	221	22

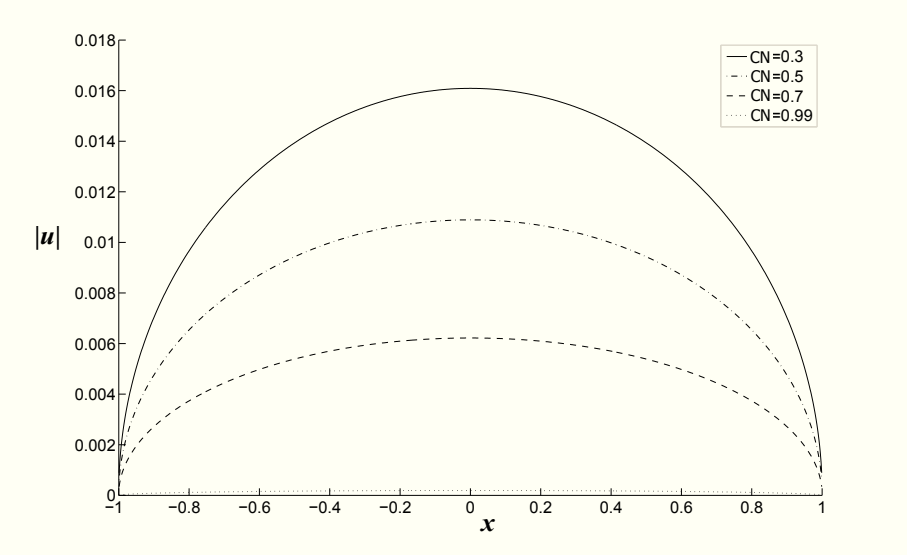

Figure 2.6: Opening u of the crack, $-1 < x < 1$, versus "coupling number" CN for concrete ($\nu = 0.2, \quad E = 30\,(GPa)$, $N = 2^{10}$)

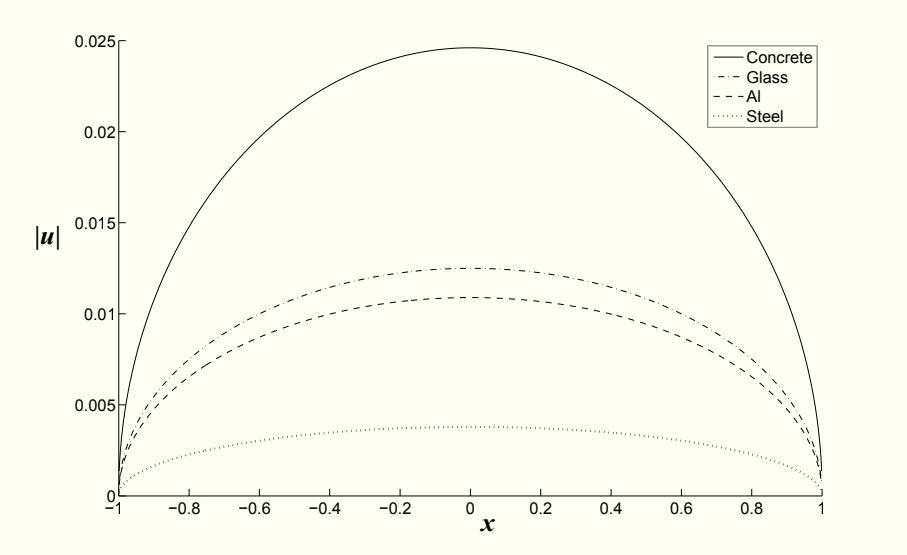

Figure 2.7: Displacement vector u over the crack boundary $-1 < x < 1$ for different types of materials ($CN = 0.5$, $N = 2^{10}$)

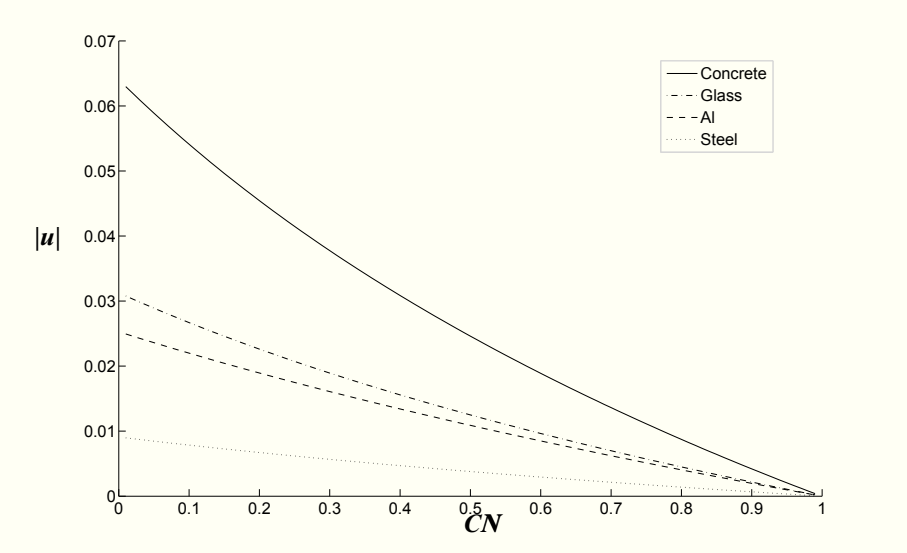

Figure 2.8: The maximum of the opening ($\max u = u(0)$) versus CN for different types of materials ($N = 2^{10}$)

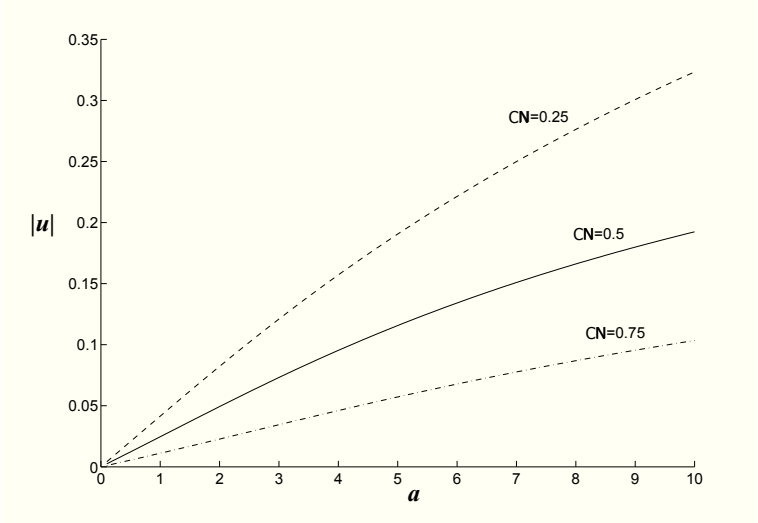

Figure 2.9: The maximum of the opening ($\max u = u(0)$) versus half-length of the crack a for concrete with different values of porosity CN ($N = 2^{10}$)

Some figures for the opening of the crack for different types of material are presented. Qualitatively, the vertical displacement field is similar to the classical linear elasticity, but the quantitative behavior is different. One can conclude from the figures that with porosity increasing the shape of cracks's opening becomes more uniform. This property is quite natural from the physical point of view.

Chapter 3

A fast iteration method for integral equations of the first and second kind

3.1 Introduction

In the last chapter we have shown how integral equations arising in the problems of continuum mechanics, can be reduced to the linear algebraic equations of convolution type. For fast solution of the integrals we used the properties of circulant and toeplitz matrices, which permits to accelerate computations by using FFT. However, in the diffraction problems such types of matrices arise only in the case, when the reflecting object is of special geometry and nodes of computational grid are arranged on equal distance between each other. Specifically, circulant matrix corresponds to the diffraction on the circle obstacle, and diffraction problem for the linear obstacle of finite length can be reduced to the system with Toeplitz matrix. In the first chapter we demonstrated fast method of evaluation of the diffraction integrals, which is based upon physical

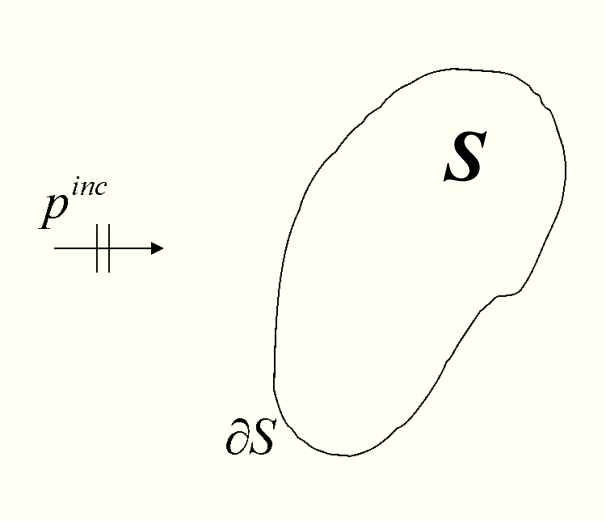

Figure 3.1: Diffraction by an arbitrary shaped object

Kirchhoff theory. For more accurate solution of the diffraction problems by arbitrarily shaped body (see Fig.3.1) we use the Boundary Integral Equation (BIE) method. In frames of this approach the unknown function is under the integral and for numerical solution there is a need to solve respective LAS (in contrast to Kirchhoff theory, which reduces the estimation of the reflected field to the evaluation of a certain integral).

In fact, in wave problems of mathematical physics the BIE method represents one of the most powerful instruments to find and analyze solutions of arising boundary value problems. The basic advantage of this method is that such equations are more tractable from mathematical point of view than the original differential equations. In the case of 2D scattering by hard or soft obstacles the problem can be reduced respectively to a first- or second-kind integral equations of Fredholm type [37]. In order to construct numerical solution to the diffraction problem, it is used a certain appropriate quadrature formula, which reduces the problem to some linear algebraic systems (LAS) whose matrix has a fully dense structure. Therefore, the direct numerical treat-

ment with a grid containing N nodes implies that the matrix has N^2 nonzero elements, and classical approaches require $O(N^3)$ arithmetic operations (for example, by the Gauss elimination technique). As we said in introduction, with the frequency increasing, if one keeps at least 10 nodes per wavelength, such a treatment becomes computationally too expensive. Just for this reason there have been proposed recently some "fast" numerical methods.

The most popular approach is based on some iteration scheme (such as conjugate gradients (CG) method or generalized minimal residual (GMRES) method). As mentioned in previous chapter, these methods usually require calculation of a matrix-vector product on each step of iterations, which appears to be the most expensive operation in such approaches, since in the general case of matrices with dense structure it can be done in $O(N^2)$ operations with matrix storage of $O(N^2)$. Hence, in order to reduce computational cost the most intensive efforts were directed to arrange some fast matrix-vector multiplication algorithms. As a rule, they are based on some special numerical techniques connected with a representation of big data arrays by relatively small number of parameters in a "easy-to-use" form. Such approaches are related to some approximation methods which are in active use in statistics, speech recognition, image processing etc. As a rule, these methods are quasi-linear, since the CPU cost of matrix-vector multiplication is $O(N \log(N))$ operations with $O(N)$ storage dimension.

Some basic ideas of this sort have been proposed by Rokhlin and Greengard [4,5] in 1985 that is known now as a fast multipole method (FMM). Similar method was also developed by Hackbusch and Novak [38,39], this is known as a panel clustering method. Further, both method were generalized in H^2- and H-matrix approaches [40–42]. Some other methods are based upon a certain approximation of the initial matrix by a matrix of block structure, with the matrix rank equal to 1. This method, proposed by Tyrtyshnikov in 1993 [43,44], is

known as mosaic-skeleton method. The other, interpolation method, reduces the problem to a dense matrix of a smaller regular grid. The constructed matrix in this case is Toeplitz or block-Toeplitz one, for which there exist some fast matrix-vector multiplication algorithms based on the Fast Fourier Transform. This idea was considered by Nechepurenko in 1985 [45]. Further development in this direction was performed by A. Brandt [46], who applied these ideas to irregular grids. Other powerful methods are based upon wavelet analysis, when the initial matrix transforms to a pseudo-sparse form (or T-sparse, by A. Harten definition [47,48] which means that the matrix is sparse if one neglects its small elements). This idea is currently under active development [49,50]. Some alternative fast treatments of BIE arising in diffraction theory are proposed in [51–54].

All above methods are based upon a special decomposition of the initial matrix. Depending on structure of the operator, as well as on disposition of the "source" and the "observation point" , the elements of the initial matrix are divided to two groups related to the so-called "long-range" and "short-range" interaction. Typically, the elements located near the principal diagonal correspond to "short-range" interaction, just these elements are associated with the singularities. All operations with such blocks are performed in a standard way. The matrix blocks, out of the diagonal, connected with the "long-range" action zone, may be approximated by some matrices of a specific structure. The algorithms discussed above operate just with these blocks.

The first attempts in this research direction were founded on some special analytical decomposition of the kernel in the considered integral equation. The evident lack of such an approach is that there is a need to construct a specific computational code for every specific kernel. Besides, some types of kernels do not permit the required decomposition. Recently, there are created the algorithms which operate only with the elements of the matrix and do not use

any information about the kernel [43,55]. In the present work we use one of such methods, namely, "adaptive cross approximation" (ACA) algorithm [43]. In this algorithm the elements out of the principal diagonal are approximated by matrices of small rank. In practice, we used the C++ library HLibPro, to realize a fast matrix-vector multiplication by the ACA method [56].

This modern fast matrix methods implies numerous applications of new efficient algorithms in many branches of applied mathematics and mechanics. Mentioned fast algorithm gives a good basis to apply an iterative solver to construct a fast numerical scheme. Therefore, the main aim of the present chapter is to propose an alternative iterative scheme. The method we present at each iteration step requires to solve a convolution integral equation, or in discrete form, a linear algebraic system with circulant or Toeplitz matrix. This can be attained by a fast method. In frames of such approach, the computation time required to solve systems of linear algebraic equations generated by BIE is linear instead of quadratic or cubic in classical methods that is a big advantage when solving problems of huge mesh dimension.

3.2 Integral equation of the first kind arising in 2D diffraction by soft obstacles

In applications to diffraction problems many authors prefer to treat a second-kind Boundary Integral Equation (BIE) which, as predicted by the classical Fredholm theory, provides a continuous inverse operator for every wave number different from an enumerable set [37]. This property leads to stability of the numerical treatment. In frames of the direct BIE method integral equations of the second kind arise in the case of acoustically hard boundary (Neumann boundary-value problem). Analogous direct treatment for acoustically soft

obstacles results in a first-kind BIE where the Fredholm theory is not valid. It is known that indirect BIE formulation allows one to come again to an integral equation of the second kind [37]. Nevertheless, it is very interesting to study fast numerical methods applied to direct integral equation of the first kind in the case of acoustically soft boundary.

It is well known [9,37] that the direct BIE method reduces the diffraction problem for acoustically soft obstacle (Dirichlet-type boundary condition) to the Fredholm integral equation of the first kind

$$\int_l \Phi(|y_0 - y|) \frac{\partial p(y)}{\partial n}\, dl_y = p^{inc}(y_0), \qquad y_0 \in l, \tag{3.1}$$

where l is the boundary contour of the obstacle, dl_y is the elementary arc-length of the boundary line coupled with point $y \in l$, $p^{inc} = \exp[ik(y_1^0 \cos\alpha + y_2^0 \sin\alpha)]$ is the incident plane wave, α defines the direction of incidence, and k is the wave number. As we mentioned in the first chapter, in the 2D-case Green's function is represented by the Hankel function

$$\Phi(r) = \frac{i}{4} H_0^{(1)}(r), \qquad r = |y_0 - y|\,. \tag{3.2}$$

Let us consider, to be more specific, a star-like obstacle described in the polar coordinate system by a single-valued polar-radius function ρ:

$$\begin{aligned} y_1 &= \rho(\theta)\cos\theta, \qquad y_2 = \rho(\theta)\sin\theta, \qquad 0 \le \theta \le 2\pi, \\ y_1^0 &= \rho(\psi)\cos\psi, \qquad y_2^0 = \rho(\psi)\sin\psi, \qquad 0 \le \psi \le 2\pi, \end{aligned} \tag{3.3}$$

Then Eq. (3.1) can be rewritten over the interval $[0, 2\pi]$:

$$\begin{aligned} &\tfrac{i}{4}\int_0^{2\pi} H_0^{(1)}\left\{ k\left|\sin\tfrac{\theta-\psi}{2}\right| \sqrt{\left[\tfrac{\rho(\theta)-\rho(\psi)}{\sin\frac{\theta-\psi}{2}}\right]^2 + 4\rho(\theta)\rho(\psi)} \right\} g(\theta)d\theta = p^{inc}(\psi), \\ &g(\theta) = \tfrac{\partial p(\theta)}{\partial n} \sqrt{\rho'^2(\theta) + \rho^2(\theta)}\,, \qquad (0 \le \psi,\, \theta \le 2\pi). \end{aligned} \tag{3.4}$$

Integral equation of the first kind in its general form (3.1), as well as in the star-like polar representation (3.4), for complex geometries and high frequencies is difficult-to-solve, since any direct approach demonstrates instability for

some examples. However, the numerical treatment can be performed by the simplest quadrature rule, on the uniform grid:

$$\theta_m = mh, \quad \psi_j = jh, \quad h = \frac{2\pi}{N}\,, \qquad (m, j = 0, 1, .., N-1), \tag{3.5}$$

that leads to the following algebraic system

$$Cg = f, \ \sim \sum_{m=0}^{N-1} c_{jm} g_m = f_j, \quad j = 0, 1, .., N-1; \ g_m = g(\theta_m), \ f_j = p^{inc}(\psi_j),$$
$$c_{jm} = \frac{ih}{4} H_0^{(1)}\left\{ k \left|\sin\tfrac{\theta_m - \psi_j}{2}\right| \sqrt{\left[\frac{\rho(\theta_m)-\rho(\psi_j)}{\sin\frac{\theta_m-\psi_j}{2}}\right]^2 + 4\rho(\theta_m)\rho(\psi_j)} \right\}, \quad m \neq j. \tag{3.6}$$

The diagonal elements should be calculated more accurately, by arranging integration of a logarithmic function which is the asymptotic representation of the Hankel function for small argument: $(i/4)H_0^{(1)}(z) \to -(1/2\pi)[\ln(z/2) + \gamma]$, $z \to 0$ (where $\gamma = 0.57721566$ is Euler's constant) [12]:

$$c_{jj} = -\tfrac{1}{2\pi} \int_{\psi_j - h/2}^{\psi_j + h/2} \left\{ \ln\left[k \left|\sin\tfrac{\theta-\psi_j}{2}\right| \sqrt{\rho'^2(\psi_j) + \rho^2(\psi_j)} \right] + \gamma \right\} d\theta \approx$$
$$\approx -\tfrac{h}{2\pi} \left[\ln \tfrac{kh\sqrt{\rho'^2(\psi_j)+\rho^2(\psi_j)}}{4} + \gamma - 1 \right]. \tag{3.7}$$

The classical Gauss elimination gives a natural tool to deal with LAS (3.6). The alternative strategy to arrange fast computations is to proceed with a matrix of a specific structure. The essence of the algorithm proposed is to arrange a circulant matrix in the left-hand side of system (3.6)-(3.7). This can be done by the following averaging in the argument of the Hankel function:

$$H_0^{(1)}\left\{ k \left|\sin\tfrac{\theta-\psi}{2}\right| \sqrt{\left[\frac{\rho(\theta)-\rho(\psi)}{\sin\frac{\theta-\psi}{2}}\right]^2 + 4\rho(\theta)\rho(\psi)} \right\} \approx H_0^{(1)}\big(Ak \left|\sin\tfrac{\theta-\psi}{2}\right| \big)\,,$$
$$A = \big(\tfrac{1}{2\pi}\big)^2 \int_0^{2\pi}\int_0^{2\pi} \sqrt{\left[\frac{\rho(\theta)-\rho(\psi)}{\sin\frac{\theta-\psi}{2}}\right]^2 + 4\rho(\theta)\rho(\psi)}\ d\theta d\psi\,. \tag{3.8}$$

This allows us to rewrite the system in the following equivalent form:

$$C^0 g = f + (C^0 - C)\, g, \qquad c^0_{jj} = -\tfrac{h}{2\pi}\left(\ln\tfrac{Akh}{8} + \gamma - 1\right),$$
$$c^0_{jm} = \tfrac{ih}{4}\, H_0^{(1)}\Big(Ak \left|\sin\tfrac{\theta_m-\psi_j}{2}\right| \Big), \qquad m \neq j\,. \tag{3.9}$$

As pointed out in previous chapter, solution of LAS and matrix-vector multiplication with such a matrix both are $O(N \log N)$ expensive, where solution is attained by a simple convolution scheme. It is obvious that circulant matrix operator, or a convolution integral operator in the continuous form, is related to a problem of diffraction by a certain round obstacle [57]. This is the physical meaning of the algorithm. Now, if the norm of the matrix operator in the right-hand side is sufficiently small: $\zeta = ||C^0 - C|| \ll 1$ (that is certainly valid for any contour close to a circle), and operator C^0 in the left-hand side of Eq. (3.9) is invertible: $||(C^0)^{-1}|| < B$, then operator equation (3.9) is equivalent to: $g = F + (C^0)^{-1}(C^0 - C)\, g$, $F = (C^0)^{-1} f$. Hence, by classical Banach theory, this provides the norm $||(C^0)^{-1}(C^0 - C)|| < 1$, therefore the solution to this equation may be obtained either as the Neumann operator series or by successive iterations [58]:

$$C^0 g_{n+1} = f + \left(C^0 - C\right) g_n, \qquad n = 0, 1, ..., \tag{3.10}$$

where the solution on the initial step (i.e. for $n = 0$) may be taken trivial.

Each iteration step requires a certain kind of fast circulant solver that is performed by convolution theorem. As we mentioned before, the computational cost of such solver is $O(N \log N)$, by using an appropriate FFT algorithm. The most expensive operation in this scheme is the matrix-vector multiplication in the right hand side of (3.10). This can also be done in $O(N \log N)$ operations by using some efficient methods, such as wavelet-transform, Fast Multipole Method (FMM), skeletonization and others. As noted in the Introduction, in our algorithm we used for this purpose a C++ code of the ACA algorithm as a part of the standard library HLibPro [56].

In practice, in the low-frequency case the method demonstrates powerful convergence. An example of this sort is presented in Fig. 3.2.

For higher frequencies, good convergence takes place only for geometries of

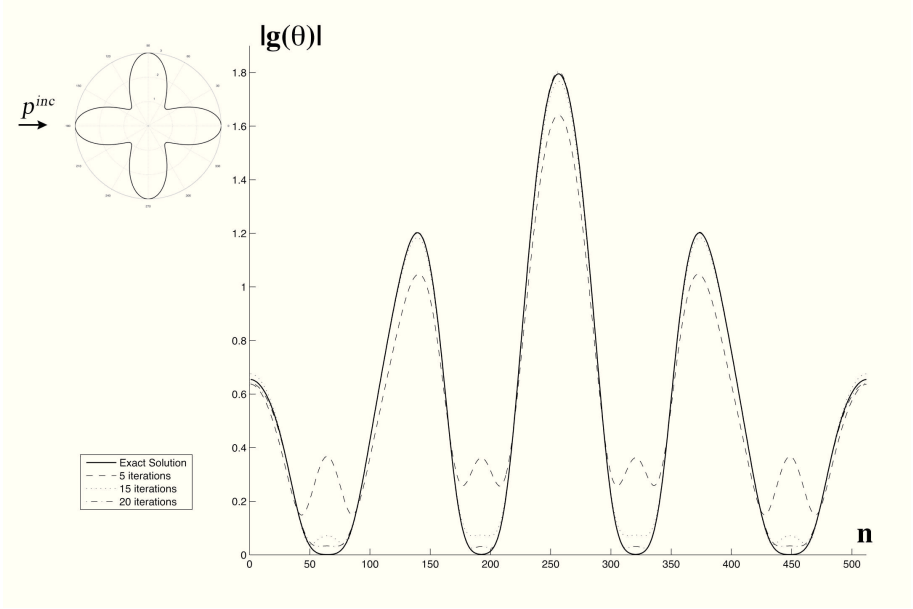

Figure 3.2: Diffraction by a soft four-leaves rose: $\rho(\theta) = 2 + \cos(4\theta)$, $k = 0.1$, $N = 2^9 = 512$

not very complex shape, like in example shown in Fig. 3.3.

3.2.1 Extension to other parametric representations of the boundary contour

The approach developed in the previous section for star-like contours can successfully be applied for some alternative representations of the boundary contour. For example, in the case of a simple elliptic obstacle the equation of the boundary contour in the polar coordinate system is not very simple:

$$\rho(\theta) = \frac{ab}{\sqrt{a^2 \sin^2\theta + b^2 \cos^2\theta}}\,, \quad y_1(\theta) = \rho(\theta)\cos\theta, \quad y_2(\theta) = \rho(\theta)\sin\theta. \tag{3.11}$$

Much more natural parametric form, to describe this contour, is given as

$$y = \{a\cos\theta, b\sin\theta\}, \qquad y_0 = \{a\cos\psi, b\sin\psi\}, \qquad (0 \le \psi,\, \theta \le 2\pi), \tag{3.12}$$

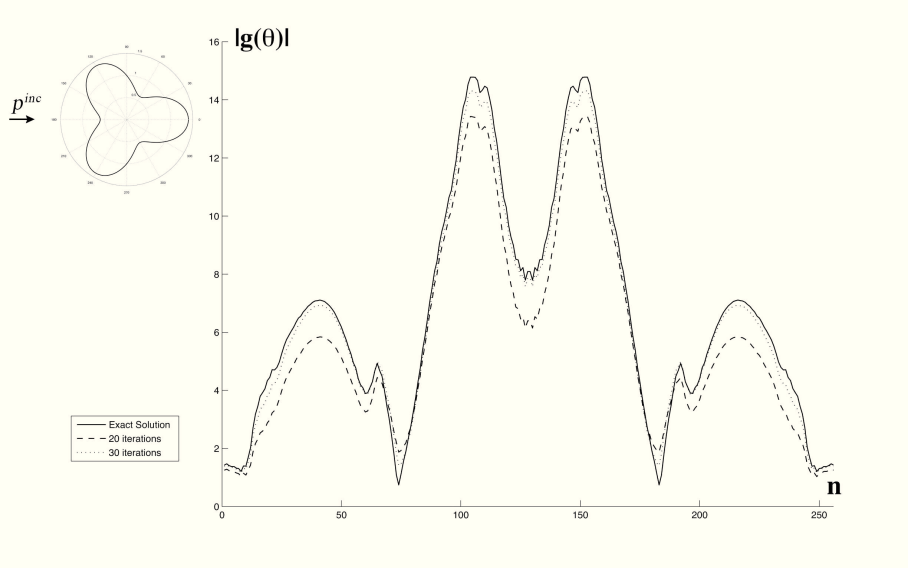

Figure 3.3: Diffraction by a soft three-leaves rose: $\rho(\theta) = 1 + 0.4\cos(3\theta)$, $k = \pi$, $N = 2^8 = 256$

where parameters ψ, θ are no longer polar angles. Such a parametrization results in the following integral equation

$$\begin{aligned} &\tfrac{i}{4}\int_0^{2\pi} H_0^{(1)}\left[2k\left|\sin\tfrac{\theta-\psi}{2}\right|\sqrt{(a^2-b^2)\sin^2\tfrac{\theta+\psi}{2}+b^2}\,\right] g(\theta)d\theta = p^{inc}(\psi), \\ &g(\theta) = \tfrac{\partial p(\theta)}{\partial n}\sqrt{a^2\sin^2\theta + b^2\cos^2\theta}, \qquad (0\le\psi,\,\theta\le 2\pi), \end{aligned} \tag{3.13}$$

which is again equivalent to the one similar to Eq. (3.9):

$$\begin{aligned} &D^0 g = f + (D^0 - D)\,g, \qquad d^0_{jj} = -\tfrac{h}{2\pi}\left(\ln\tfrac{Akh}{4} + \gamma - 1\right), \\ &d^0_{jm} = \tfrac{ih}{4}H_0^{(1)}\Big(2Ak\left|\sin\tfrac{\theta_m-\psi_j}{2}\right|\Big), \qquad m\ne j\,, \\ &A = \left\{\left(\tfrac{1}{2\pi}\right)^2 \int_0^{2\pi}\int_0^{2\pi}\left[(a^2-b^2)\sin^2\tfrac{\theta+\psi}{2}+b^2\right]d\theta d\psi\right\}^{1/2} = \left(\tfrac{a^2+b^2}{2}\right)^{1/2}, \end{aligned} \tag{3.14}$$

with

$$\begin{aligned} &d_{jm} = \tfrac{ih}{4}H_0^{(1)}\left[2k\left|\sin\tfrac{\theta_m-\psi_j}{2}\right|\sqrt{(a^2-b^2)\sin^2\tfrac{\theta_m+\psi_j}{2}+b^2}\,\right], \quad m\ne j\,. \\ &d_{jj} = -\tfrac{h}{2\pi}\left[\ln\tfrac{kh\sqrt{(a^2-b^2)\sin^2\psi_j+b^2}}{4} + \gamma - 1\right]. \end{aligned} \tag{3.15}$$

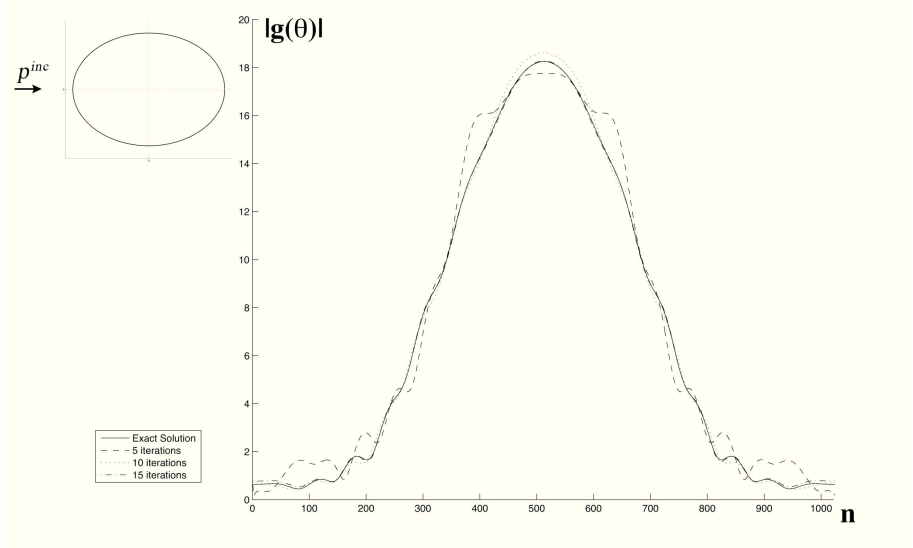

Figure 3.4: Diffraction by a soft ellipse, $k = 10$, $b/a = 0.9$, $N = 2^{10} = 1024$

The iterative process is absolutely analogous to (3.10). An example for a soft elliptic obstacle is demonstrated in Fig. 3.4.

3.2.2 The estimate of the number of required iteration steps

It is conventionally accepted for many classical iteration algorithms (see, for example [28]) that they must provide a consistent criterion to stop the iterations. Let us give some appropriate estimates of this sort for the algorithm proposed in the present work.

As follows from Eq. (3.10), the difference between the solution on the cur-

rent step and exact solution g_* is (recall that $f = Cg_*$):

$$\begin{aligned} & g_{n+1} - g_* = (C^0)^{-1} f + (C^0)^{-1} (C^0 - C)\, g_n - g_* = \\ & = (C^0)^{-1} (C^0 - C)\, g_n + [(C^0)^{-1} C - (C^0)^{-1} C^0]\, g_* = (C^0)^{-1} (C^0 - C)\, (g_n - g_*) \\ & \cdots = [(C^0)^{-1} (C^0 - C)]^{n+1} (g_0 - g_*), \end{aligned} \tag{3.16}$$

where g_0 is the chosen initial iteration. Therefore,

$$||g_{n+1} - g_*|| \leq ||(C^0)^{-1}||^{n+1}\ ||C^0 - C||^{n+1}\ ||g_0 - g_*||. \tag{3.17}$$

where the following norm for arbitrary vector $c = \{c_j\}$ and arbitrary matrix $C = \{c_{kj}\}$ are used in the standard functional space l_∞ [58]:

$$||c|| = \max_{1 \leq j \leq N} |c_j|, \qquad ||C|| = \max_{1 \leq k \leq N} \sum_{j=1}^{N} |c_{kj}|. \tag{3.18}$$

The first term in the right-hand side of Eq. (3.17) can easily be estimated from the concept of *condition number* [28] which is

$$cond(C^0) = ||C^0||\ ||(C^0)^{-1}||. \tag{3.19}$$

Since the norm of the circulant matrix $\delta = ||C^0||$ can easily be calculated directly by its definition on a pre-processing step and since the calculation of the condition number for any matrix is a simple technical procedure [28], one can simply estimate the norm of inverse to the circulant matrix, as $||(C^0)^{-1}|| = \delta/\beta,\ \beta = cond(C^0)$. It should also be noted that the norm $\zeta = ||C^0 - C||$ is again calculated directly by its definition. Then Eq. (3.17) gives a good basis for the sought estimate of the required number of iteration steps, if one applies after n iteration steps the following approximation $g_* \approx g_n,\ \Rightarrow g_0 - g_* \approx g_0 - g_n$. With all these comments made, Eq. (3.17) can be arranged less that the required arbitrarily small quantity: $||g_{n+1} - g_*||/||g_*|| \leq \varepsilon \ll 1$ provided

$$\left(\frac{\delta\zeta}{\beta}\right)^{n+1} \frac{||g_0 - g_n||}{||g_n||} \leq \varepsilon. \tag{3.20}$$

This gives a finite-number-of-steps stopper at least for boundary contours sufficiently close to a circle, since as noted above, in this case $\zeta \ll 1$. It is interesting to note that with the trivial initial step $g_0 = 0$ the last inequality becomes even simpler: $(\beta\zeta/\delta)^{n+1} \leq \varepsilon$.

3.3 Integral equation of the second kind arising in 2D diffraction by hard obstacles

In the previous chapter we have proposed an alternative iterative approach to diffraction by the soft obstacles, which requires at each iteration step to solve only a LAS with circulant matrix. Since, in the case of the star-like contours, the kernel of integral equation contains a certain exactly convolution term, the approximation procedure can be based on reducing the remaining part to a constant by averaging over the polar angle. Such an approach is very attractive, but, unfortunately, it is not clear how to construct such a matrix for more general kernel functions. The main goal of the present chapter is to extend this approach to the diffraction problems for hard obstacles. At the same time, we apply here a different, improved, strategy to construct circulant matrix. Namely, the proposed method is based upon the algebraic instead of analytical construction of the circulant matrix. Another goal is to evaluate convergence of the proposed method versus frequency and obstacle's geometry.

Let us consider 2D diffraction of a plane incident wave p^{inc} by a hard obstacle with smooth closed boundary curve ℓ. The governing equation is the Helmholtz partial differential equation with the Neumann-type boundary condition [37]:

$$\Delta p + k^2 p = 0, \quad p = p^{inc} + p^{sc}, \qquad \left.\frac{\partial p}{\partial n}\right|_l = 0 \quad \sim \quad \left.\frac{\partial p^{sc}}{\partial n}\right|_l = -\left.\frac{\partial p^{inc}}{\partial n}\right|_l. \tag{3.21}$$

By applying Green's integral formula, this can directly be reduced to the

following integral equation of the second kind:

$$\frac{p(y_0)}{2} - \int_l p(y)G(y,y_0)dl_y = p^{inc}(y_0), \quad y_0 \in l; \quad y = (y_1, y_2), \quad y_0 = (y_1^0, y_2^0).$$

$$G(y,y_0) = \frac{\partial \Phi(r)}{\partial n_y} = -\frac{ik}{4} H_1^{(1)}(kr) \frac{(\bar{r} \cdot \bar{n}_y)}{r}. \tag{3.22}$$

Here dl_y is the elementary arc-length of the boundary line coupled with point $y \in l$, $\bar{n}_y$ is the outer unit normal vector to contour at this point, $\Phi(r)$ is Green's function expressed in terms of Hankel transcendental function.

Now, by dividing contour ℓ to N small subintervals of length Δl_j and choosing nodes y_j, $j = 0, 1, \ldots, N-1$, say at the central points of each small subinterval, one can reduce BIE in a standard way to the following LAS with respect to quantities $p_j = p(y_j)$ [59]:

$$\sum_{j=0}^{N-1} p_j c_{mj} = p^{inc}(y_m), \quad m = 0, 1, \ldots, N-1, \tag{3.23}$$

where with the simplest approach $c_{mm} = 1/2$; $c_{mj} = -G(y_j, y_m)\Delta l_j$, $(j \neq m)$.

3.3.1 Iteration algorithm

In the previous chapter we showed analytical approximation of the kernel. Here we arrange the algebraic averaging over the elements belonging to any diagonal parallel to the principal one. Actually, there is no need to collect all elements of the circulant matrix, since they can be collected in a vector of dimension N, sufficient to represent the matrix. To this end, we build an approximated vector d_i with N elements, where $i = 0, \ldots, N-1$, that satisfies the relation

$d = \sum_{j=1}^{N} e_j/N$. That is clearly shown in the following scheme:

$$C = \begin{pmatrix} \bullet & \bullet & \bullet & e_1 & \bullet & \bullet & \bullet & \bullet \\ \bullet & \bullet & \bullet & \bullet & e_2 & \bullet & \bullet & \bullet \\ \bullet & \bullet & \bullet & \bullet & \bullet & \ddots & \bullet & \bullet \\ \bullet & \bullet & \bullet & \bullet & \bullet & \bullet & e_{m-1} & \bullet \\ \bullet & \bullet & \bullet & \bullet & \bullet & \bullet & \bullet & e_m \\ e_{m+1} & \bullet & \bullet & \bullet & \bullet & \bullet & \bullet & \bullet \\ \bullet & \ddots & \bullet & \bullet & \bullet & \bullet & \bullet & \bullet \\ \bullet & \bullet & e_N & \bullet & \bullet & \bullet & \bullet & \bullet \end{pmatrix} \Longrightarrow$$

$$C^c = \begin{pmatrix} \bullet & \bullet & \bullet & d & \bullet & \bullet & \bullet & \bullet \\ \bullet & \bullet & \bullet & \bullet & d & \bullet & \bullet & \bullet \\ \bullet & \bullet & \bullet & \bullet & \bullet & \ddots & \bullet & \bullet \\ \bullet & \bullet & \bullet & \bullet & \bullet & \bullet & d & \bullet \\ \bullet & \bullet & \bullet & \bullet & \bullet & \bullet & \bullet & d \\ d & \bullet & \bullet & \bullet & \bullet & \bullet & \bullet & \bullet \\ \bullet & d & \bullet & \bullet & \bullet & \bullet & \bullet & \bullet \\ \bullet & \bullet & d & \bullet & \bullet & \bullet & \bullet & \bullet \end{pmatrix} \tag{3.24}$$

This algebraic approximation is convenient from the computational point of view, since it allows one to organize a unique machine code for many different physical problems with different geometry of obstacles. So, by using this approximation, one can rewrite LAS (3.23) in the equivalent form

$$C^c p = f + (C^c - C)\, p \tag{3.25}$$

and then arrange iteration scheme

$$C^c p_{q+1} = f + (C^c - C) p_q, \qquad q = 0, 1, \ldots, \tag{3.26}$$

where the initial-step solution may be taken trivial: $p_0 = 0$.

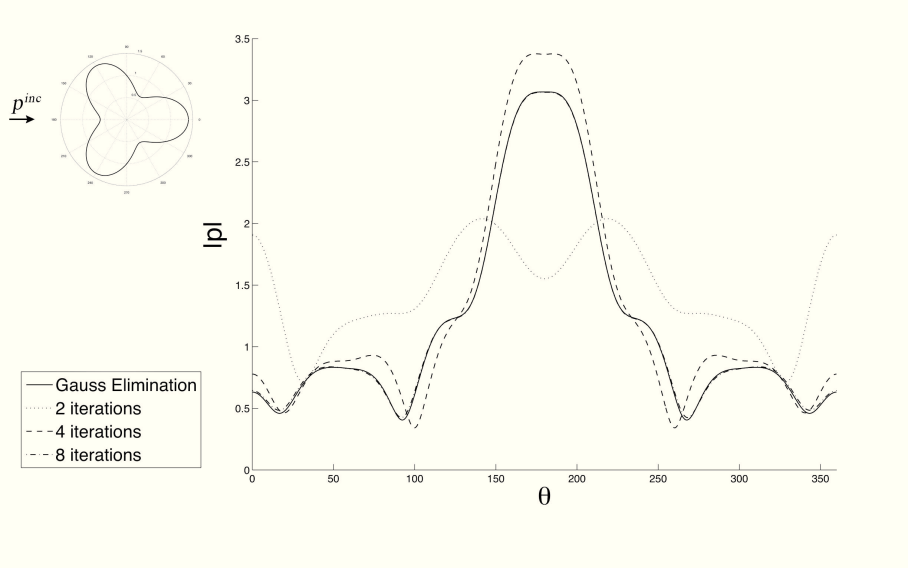

Figure 3.5: Diffraction by a hard three-leaves rose: $\rho(\theta) = 2 + 1.5\cos(3\theta)$, $k = 2$

As follows from the classical results of functional analysis, given in the previous chapter, if $||C^c - C||$ is sufficiently small then the iteration process is certainly convergent.

The convergence of the proposed algorithm has been tested on many examples. One of them is demonstrated in Fig. 3.5, for a three-leaves rose which in the polar coordinate system is described in the legend to Fig. 3.5. The number of nodes with the discretization is $N = 2^{10}$ here and all other examples below. In this case the classical CG method diverges. The proposed method converges, and one can see that the 8th iteration is practically indistinguishable from the exact diagram constructed by the Gauss elimination.

The numerous calculations carried out show that convergence of the iterative scheme takes place up to significantly higher frequencies when compared with the standard CG method. The number of iterations in the proposed algorithm does not depend on the size of numerical grid, being more sensitive to the wave number and to the shape of the obstacle. In particular, for geometry

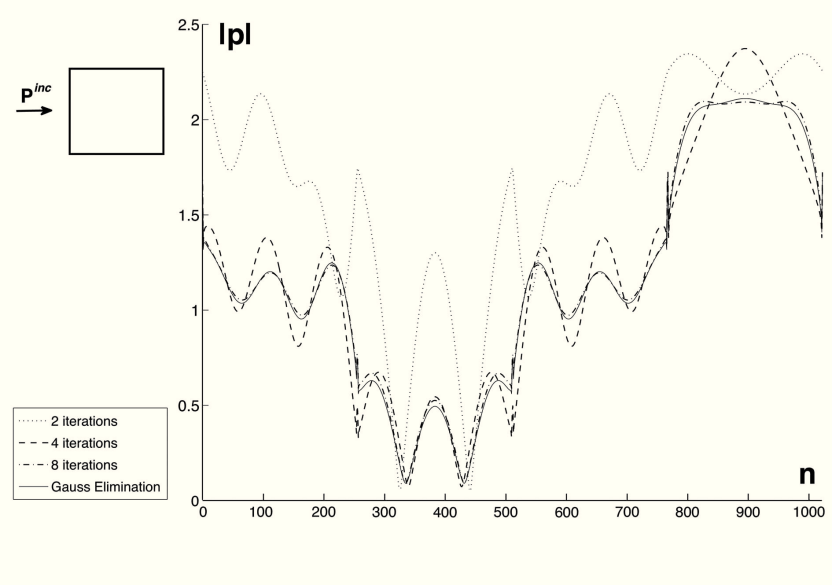

Figure 3.6: Diffraction by a hard quadratic obstacle with a unit side, k=8. The first node is near the left lowest boundary point

shown in Fig. 3.5 our algorithm converges for $0 < k \leq 5.6$.

For a four-leaves rose $\rho(\theta) = 2 + 1.5\cos(4\theta)$, $(0 \leq \theta < 2\pi)$, the proposed method converges for $0 < k \leq 0.8$, and we did not succeed in finding any, even very small, value of k when the direct CG algorithm converges for this geometry.

With further increasing of the number of leaves, the upper frequency boundary of convergence is naturally decreases. Thus, in the case of 8-leaves rose, $\rho(\theta) = 2 + 1.5\cos(8\theta)$, $(0 \leq \theta < 2\pi)$, the algorithm converges only for $0 < k \leq 0.35$.

In the example of diffraction by a simple quadratic obstacle the proposed iteration algorithm converges for $0 < k \leq 8.7$. Fig. 3.6 demonstrates convergence for $k = 8$, and the direct CG iterations again diverge in this example.

It is very interesting to study the convergence in the class of elliptic obstacles with various aspect ratio. Let us set the bigger semi-axis of the ellipses to

be unit: $a = 1$. Then with variation of the second semi-axis one can observe the following: $b = 0.3$ – convergence for $0 < k \leq 5$; $b = 0.1$ – convergence for $0 < k \leq 3$; and the critique value is $b = 0.0022$ when the convergence breaks even for extremely low frequencies.

3.4 Application of the fast BIE iteration method for an arbitrary body in a flow of incompressible inviscid fluid

In the present chapter let us demonstrate the variation of the method we propose on the 2d problem about an arbitrary body placed in a flow of incompressible inviscid fluid. Since the solution of Toeplitz system by the PCG (preconditioned conjugate gradients) method with a circulant pre-conditioner is $O(N \log N)$ expensive, we try here to approximate the exact matrix by a certain Toeplitz one instead of circulant, and then apply a fast algorithm for this matrix, on each iteration step. We illustrate the convergence of this iteration scheme by a number of numerical examples, both for hard and soft boundary conditions. It appears that the method is highly efficient for hard boundaries (indeed, the most natural case), being much less efficient for soft bodies (which are of less interest in practice).

To be more specific, the flow is assumed stationary in time and uniform at infinity. Then the classical Boundary Element Method (BEM), or Boundary Integral Equation (BIE) method can be formulated here either in terms of velocity potential $\varphi(y)$, $y = (y_1, y_2)$, $\bar{v} = \operatorname{grad} \varphi$, or in terms of stream function $\psi(y)$. Again, to be more specific, we treat the problem by using function φ. Then, the classical theory [60] determines potential φ' to the perturbed value of the velocity vector $\bar{v}$, at arbitrary point $y_0 = (y_1^0, y_2^0)$ in the flow, through the

integral taken over the boundary contour l to the body under consideration:

$$\varphi'(y_0) = \int\limits_l \left[\varphi(y) \frac{\partial \Phi(y, y_0)}{\partial n_y} - \frac{\partial \varphi(y)}{\partial n_y} \Phi(y, y_0) \right] dl_y \tag{3.27}$$

If the boundary of the body is absolutely hard: $\partial\varphi/\partial n_y|_l = 0$ then (3.27) is simplified to

$$\varphi'(y_0) = \int\limits_l \varphi(y) \frac{\partial \Phi(y, y_0)}{\partial n_y} dl_y \tag{3.28}$$

Here $\varphi = \varphi' + \varphi_\infty$, Green's function is $\Phi(y, y_0) = -\ln r/(2\pi)$, $r = |y - y_0| = [(y_1 - y_1^0)^2 + (y_2 - y_2^0)^2]^{1/2}$, $\bar{n}_y$ is the outer unit normal vector to contour l, $\varphi_\infty(y) = v_0(y_1 \cos\alpha + y_2 \sin\alpha)$, where α is the angle between axis y_1 and flow's velocity vector at infinity $\bar{v}_0$.

It should be noted that representation (3.28) is valid only in the case when the velocity circulation is zero. We thus leave aside all questions related to the Kutta-Zhukovsky hypothesis if the body has a sharp edge on its boundary.

Now, by setting point x approaching to the boundary line from the fluid: $y_0 \to x \in l$, and taking into account the standard properties of the double layer potential [9,60], Eq. (3.28) is directly reduced to the following second-kind BIE of Fredholm type:

$$\frac{\varphi(x)}{2} - \int\limits_l \varphi(y) \frac{\partial \Phi(y, x)}{\partial n_y} dl_y = f(x), \qquad x \in l, \tag{3.29a}$$

$$f(x) = \varphi_\infty(x) = v_0(x_1 \cos\alpha + x_2 \sin\alpha). \tag{3.29b}$$

Eq. (3.29) is valid for smooth contours only, but it can easily be rewritten in an appropriate form if there is a sharp edge on contour l [60].

The natural way to arrange a direct numerical treatment of the basic BIE (3.29) is to apply the so-called *collocation technique* [9]. One may arrange a dense set of nodes $x_j \in l$, $j = 1, \ldots, N$, distributed over contour l along its full length: the same nodes for "internal" variable $y \in l$ and "external"

variable $x \in l$. One then can associate the nodes for variable y with subscripts j, x_j; and for variable x with subscripts i, x_i. If we approximate the integral in (3.29a) by a quadrature formula, the simplest one is indeed to put the integrand approximately constant over each elementary arc, then this leads to the following LAS (linear algebraic system):

$$C\varphi = f\,, \sim \quad \sum_{j=1}^{N} c_{ij}\varphi(x_j) = f_i, \quad i = 1, \ldots, N; \quad f_i = v_0(x_1^i \cos\alpha + x_1^i \sin\alpha), \tag{3.30a}$$

$$c_{ii} = \frac{1}{2}; \qquad j \neq i: \; c_{ij} = -\frac{\partial G(x_j, x_i)}{\partial n_y}\, l_j = \frac{(x_1^j - x_1^i)n_1^j + (x_2^j - x_2^i)n_2^j}{(x_1^j - x_1^i)^2 + (x_2^j - x_2^i)^2}\, \frac{l_j}{2\pi}, \tag{3.30b}$$

where l_j denotes the length of elementary arc. Besides, only in this section we accept the notation more standard for discrete mathematics, when the elements of any vector vary over $1, \ldots, N$, instead of $0, 1, \ldots, N-1$.

It should be noted that the integral in (3.29a), after discretization, gives a certain contribution to the diagonal terms c_{ii}. It is well known that this is defined by the value of the curvatue of the boundary line l at node x_i. However, this contribution contains again a small factor l_j, being asymptotically small at $N \to \infty$, when compared with the term $c_{ii} = 1/2$ given by that present outside the integral.

3.4.1 An application of the proposed iterative scheme

Typically, LAS (3.30) can be treated directly, by the Gauss elimination process. In the meantime, there is a case when the matrix $\{c_{ij}\}$ has a specific structure. We mean the case when the body placed in the flow is a circle, then with the set of the nodes, arranged with a uniform step h_θ over the polar angle, the

matrix elements become ($x_1(\theta) = a\cos\theta$, $x_2(\theta) = a\sin\theta$):

$$\begin{cases} x_1^j = a\cos\theta_j, \\ x_2^j = a\sin\theta_j, \end{cases} \quad \begin{cases} n_1^j = \cos\theta_j, \\ n_2^j = \sin\theta_j, \end{cases} \quad \begin{array}{l} \theta_j = (j-\frac{1}{2})h_\theta, \quad h_\theta = 2\pi/N, \\ l_j = a\,h_\theta, \quad j = 1,\ldots,N, \end{array}$$

$$(x_1^j - x_1^i)n_1^j + (x_2^j - x_2^i)n_2^j = a[1-\cos(\theta_i - \theta_j)] = a\{1-\cos[(i-j)h_\theta]\},$$

$$(x_1^j - x_1^i)^2 + (x_2^j - x_2^i)^2 = 2a^2\{1-\cos[(i-j)h_\theta]\}. \tag{3.31}$$

Therefore, the elements of the matrix depend on the difference of subscripts $(i-j)$, i.e. the matrix is of convolution type or, by other words, this is a periodic Toeplitz matrix. Note that in this particular case of hard boundary the matrix is even degenerated since the numerator and the denominator cancel to each other. However, periodic Toeplitz structure of the matrix remains valid in all problems for round geometries, including with full (not only degenerated) structure.

The principal idea of the method we propose here is to arrange, in the case of arbitrary geometry of the body, an iterative process when at each iteration step there is a need to solve a certain LAS with a Toeplitz matrix. This idea looks very attractive since solution to Toeplitz LAS can be constructed more efficiently than in the case of matrices of general structure. The required Toeplitz matrix, for arbitrary shape of boundary contour l, can be constructed if we change in matrix c_{ij} (3.30) all elements on every diagonal parallel to the principal one by the average value of all elements situated over this chosen diagonal. Such an approach yields a new matrix $\{c_{ij}^t\}$ with the elements:

$$c_{ij}^t = d_{i-j}, \quad d_{k+n-1,k} = \frac{\sum_{j=1}^{N-n+1} c_{j+n-1,j}}{N-n+1}, \quad n = 1,\ldots,N; \quad k = 1,\ldots,N-n+1;$$

$$d_{k,k+n-1} = \frac{\sum_{j=1}^{N-n+1} c_{j,j+n-1}}{N-n+1}, \quad n = 2,\ldots,N; \quad k = 1,\ldots,N-n+1. \tag{3.32}$$

This formal definition is clearly demonstrated here:

$$C = \begin{pmatrix} \bullet & \bullet & \bullet & e_1 & \bullet & \bullet & \bullet & \bullet \\ \bullet & \bullet & \bullet & \bullet & e_2 & \bullet & \bullet & \bullet \\ \bullet & \bullet & \bullet & \bullet & \bullet & \ddots & \bullet & \bullet \\ \bullet & \bullet & \bullet & \bullet & \bullet & \bullet & e_{m-1} & \bullet \\ \bullet & \bullet & \bullet & \bullet & \bullet & \bullet & \bullet & e_m \\ \bullet & \bullet & \bullet & \bullet & \bullet & \bullet & \bullet & \bullet \\ \bullet & \bullet & \bullet & \bullet & \bullet & \bullet & \bullet & \bullet \\ \bullet & \bullet & \bullet & \bullet & \bullet & \bullet & \bullet & \bullet \end{pmatrix} \quad d = \frac{\sum_{j=1}^{m} e_j}{m} \quad \Longrightarrow$$

$$C^t = \begin{pmatrix} \bullet & \bullet & \bullet & d & \bullet & \bullet & \bullet & \bullet \\ \bullet & \bullet & \bullet & \bullet & d & \bullet & \bullet & \bullet \\ \bullet & \bullet & \bullet & \bullet & \bullet & \ddots & \bullet & \bullet \\ \bullet & \bullet & \bullet & \bullet & \bullet & \bullet & d & \bullet \\ \bullet & \bullet & \bullet & \bullet & \bullet & \bullet & \bullet & d \\ \bullet & \bullet & \bullet & \bullet & \bullet & \bullet & \bullet & \bullet \\ \bullet & \bullet & \bullet & \bullet & \bullet & \bullet & \bullet & \bullet \\ \bullet & \bullet & \bullet & \bullet & \bullet & \bullet & \bullet & \bullet \end{pmatrix} \tag{3.33}$$

With so constructed Toeplitz matrix C^t let us represent LAS (3.30) in the equivalent form:

$$C^t\varphi = f + (C^t - C)\varphi \tag{3.34}$$

This allows us to organize the iteration process

$$C^t\varphi_{q+1} = f + (C^t - C)\varphi_q, \qquad q = 0, 1, \ldots, \tag{3.35}$$

where $\varphi_0 = 0$ is accepted as the initial iteration step, which is obviously to solve the LAS with the Toeplitz matrix in the left-hand side and the true right-hand side.

Numerical experiments performed show that the rate of convergence is independent of the number nodes, but is quite sensitive to the geometry of the boundary line l. This is quite natural from the physical point of view. In fact, the number of nodes must increase also in standard approaches of direct treatment if the geometry of the object becomes more complicated.

Generally speaking, for bodies of arbitrary complex geometry it is not so easy to give a strict proof of the convergence for the proposed iteration algorithm. However, this can be done for some particular classes of boundary contours. For example, let us restrict the consideration by the class of elliptic domains:

$$x_1^j = a\cos\theta_j, \quad x_2^j = b\sin\theta_j, \quad (a>b); \quad l_j = h_\theta\sqrt{a^2\sin^2\theta_j + b^2\cos^2\theta_j}\ ,$$

$$n_1^j = \frac{b\cos\theta_j}{\sqrt{a^2\sin^2\theta_j + b^2\cos^2\theta_j}}\ , \quad n_2^j = \frac{a\sin\theta_j}{\sqrt{a^2\sin^2\theta_j + b^2\cos^2\theta_j}}\ ,$$

$$\theta_j = \left(j-\tfrac{1}{2}\right)h_\theta, \qquad h_\theta = 2\pi/N, \qquad j = 1,\ldots,N. \tag{3.36}$$

Then the elements of matrix C in (3.30) become

$$c_{ii} = \tfrac{1}{2}; \qquad j\neq i: \ c_{ij} = \frac{(x_1^j - x_1^i)n_1^j + (x_2^j - x_2^i)n_2^j}{(x_1^j - x_1^i)^2 + (x_2^j - x_2^i)^2}\ \frac{l_j}{2\pi} =$$

$$= \frac{a(\cos\theta_j - \cos\theta_i)b\cos\theta_j + b(\sin\theta_j - \sin\theta_i)a\sin\theta_j}{a^2(\cos\theta_j - \cos\theta_i)^2 + b^2(\sin\theta_j - \sin\theta_i)^2}\ \frac{h_\theta}{2\pi} = \tag{3.37}$$

$$= \frac{ab\,h_\theta}{4\pi\left[(a^2-b^2)\sin^2\frac{\theta_i+\theta_j}{2} + b^2\right]} = \frac{ab\,h_\theta}{4\pi\left[(a^2-b^2)\sin^2\frac{(i+j-1)h_\theta}{2} + b^2\right]}\ ,$$

therefore, Eq. (3.32) implies

$$C^t = \tfrac{1}{2}(I+D), \quad d_{k+n-1,k} = \frac{ab\,h_\theta}{2\pi(N-n+1)}\sum_{j=1}^{N-n+1}\frac{1}{(a^2-b^2)\sin^2\frac{(2j+n-2)h_\theta}{2} + b^2}\ , \tag{3.38}$$

$$d_{k,k+n-1} = d_{k+n-1,k} \ \ (n=2,\ldots,N; \ \ k=1,\ldots,N-n+1); \quad d_{ii} = 0,$$

where D is evidently a Toeplitz matrix. Such a representation allows us to rewrite Eq. (3.34) as a second-kind matrix operator equation:

$$(I+D)\varphi = 2f + 2(C^t - C)\varphi, \implies \varphi = F + 2(I+D)^{-1}(C^t - C)\varphi, \quad F = 2(I+D)^{-1}f. \tag{3.39}$$

Let us estimate the elements of matrix D in (3.38) in the class of ellipses of small eccentricity, i.e. with $a=(1+\varepsilon)b,\ \varepsilon<<1$, when the ellipse is very close to a circle. Let us keep in all expressions only linear terms over parameter ε. Then one deduces from (3.38):

$$\begin{gathered} d_{k,k+n-1}=d_{k+n-1,k}=\tfrac{h_\theta}{2\pi(N-n+1)}\sum_{j=1}^{N-n+1}\tfrac{2ab}{(a^2+b^2)-(a^2-b^2)\cos[(2j+n-2)h_\theta]}\approx \\ \approx \tfrac{h_\theta}{2\pi(N-n+1)}\sum_{j=1}^{N-n+1}\tfrac{1+\varepsilon}{1+\varepsilon\{1-\cos[(2j+n-2)h_\theta]\}}\approx \\ \approx \tfrac{h_\theta}{2\pi(N-n+1)}\sum_{j=1}^{N-n+1}\{1+\varepsilon\cos[(2j+n-2)h_\theta]\}= \\ =\tfrac{h_\theta}{2\pi}\Big\langle 1+\tfrac{\varepsilon}{N-n+1}\Big\{\tfrac{\sin[(N-n+2)h_\theta]}{\sin h_\theta}\cos[(N-n+1)h_\theta]-\cos[(n-2)h_\theta]\Big\}\Big\rangle= \\ =\tfrac{1}{N}\Big\langle 1+\tfrac{\varepsilon}{N-n+1}\Big\{\tfrac{1}{2}-\tfrac{\sin[2\pi(2n-3)/N]}{2\sin(2\pi/N)}-\cos[2\pi(n-2)/N]\Big\}\Big\rangle, \end{gathered} \tag{3.40}$$

where we have used a tabular value of a finite sum for trigonometric functions [61].

For all estimates we introduce the standard normalized space l_∞ of dimension N, where the norm for arbitrary vector $c=\{c_j\}$ and arbitrary matrix $C=\{c_{kj}\}$ are, respectively [58,62]

$$||c||=\max_{1\le j\le N}|c_j|,\qquad ||C||=\max_{1\le k\le N}\sum_{j=1}^{N}|c_{kj}|. \tag{3.41}$$

Then

$$\begin{gathered} \sum_{j=1}^{N}|d_{kj}|=\sum_{n=2}^{N+1-k}|d_{k,k+n-1}|+\sum_{n=2}^{k}|d_{k,k-n+1}|=\sum_{n=2}^{N+1-k}|d_{k,k+n-1}|+\sum_{n=2}^{k}|d_{k+n-1,k}|= \\ =\tfrac{1}{N}\left(\sum_{n=2}^{N+1-k}+\sum_{n=2}^{k}\right)\Big|1+\tfrac{\varepsilon}{N-n+1}\Big\{\tfrac{1}{2}-\tfrac{\sin[2\pi(2n-3)/N]}{2\sin(2\pi/N)}-\cos[2\pi(n-2)/N]\Big\}\Big| \end{gathered} \tag{3.42}$$

Let us notice that for $N>>1$

$$\begin{gathered} \Big|\tfrac{\varepsilon}{N-n+1}\Big\{\tfrac{1}{2}-\tfrac{\sin[2\pi(2n-3)/N]}{2\sin(2\pi/N)}-\cos[2\pi(n-2)/N]\Big\}\Big|\le\tfrac{\varepsilon}{N-n+1}\times \\ \times\Big\{\tfrac{3}{2}+\tfrac{|\sin[2\pi(2N-2n+3)/N]|}{2\sin(2\pi/N)}\Big\}\le\tfrac{\varepsilon}{N-n+1}\Big\{\tfrac{3}{2}+\tfrac{2\pi(2N-2n+3)/N}{4\pi/N}\Big\}\approx\varepsilon\ll 1, \end{gathered} \tag{3.43}$$

hence expression under the modulus in (3.42) is positive. Therefore,

$$\sum_{j=1}^{N}|d_{kj}| =$$

$$\begin{aligned}
&= \tfrac{1}{N}\left(\sum_{n=2}^{N+1-k}+\sum_{n=2}^{k}\right)\left\langle 1+\tfrac{\varepsilon}{N-n+1}\left\{\tfrac{1}{2}-\tfrac{\sin[2\pi(2n-3)/N]}{2\sin(2\pi/N)}-\cos[2\pi(n-2)/N]\right\}\right\rangle = \\
&= \tfrac{N-1}{N}+\tfrac{\varepsilon}{N}\left(\sum_{n=2}^{N+1-k}+\sum_{n=2}^{k}\right)\tfrac{1}{N-n+1}\left\{\tfrac{1}{2}-\tfrac{\sin[2\pi(2n-3)/N]}{2\sin(2\pi/N)}-\cos[2\pi(n-2)/N]\right\}\leq \\
&\leq 1-\tfrac{1}{N}+\tfrac{\varepsilon}{N}\sum_{n=2}^{N}\tfrac{1}{N-n+1}\left(\tfrac{3}{2}+\tfrac{1}{4\pi/N}\right)<1, \quad (\varepsilon << 1), \implies ||D||<1.
\end{aligned} \tag{3.44}$$

Now, if in operator equation of the second kind (3.39) the norm of operator $||D|| < 1$, then, by Banach theorem [58], equation (3.39) is uniquely solvable and $||(1+D)^{-1}|| \leq 1/(1-||D||)$ is finite.

Let us estimate the norm of operator $C^t - C$ in Eq. (3.39). Obviously, both these matrices have the constant elements $1/2$ on the principal diagonal which is canceled when calculating their difference. Then, for the elements outside the principal diagonal one obtains from (3.38)

$$\tfrac{4\pi}{ab\,h_\theta}\,(d_{k+n-1,k}-c_{k+n-1,k}) =$$

$$\begin{aligned}
&= \tfrac{1}{N-n+1}\sum_{j=1}^{N-n+1}\frac{1}{(a^2-b^2)\sin^2\frac{(2j+n-2)h_\theta}{2}+b^2}-\frac{1}{(a^2-b^2)\sin^2\frac{(2k+n-2)h_\theta}{2}+b^2} = \\
&= \tfrac{1}{N-n+1}\sum_{j=1}^{N-n+1}\left[\frac{1}{(a^2-b^2)\sin^2\frac{(2j+n-2)h_\theta}{2}+b^2}-\frac{1}{(a^2-b^2)\sin^2\frac{(2k+n-2)h_\theta}{2}+b^2}\right]= \\
&= \tfrac{a^2-b^2}{N-n+1}\sum_{j=1}^{N-n+1}\frac{\sin^2\frac{(2k+n-2)h_\theta}{2}-\sin^2\frac{(2j+n-2)h_\theta}{2}}{\left[(a^2-b^2)\sin^2\frac{(2j+n-2)h_\theta}{2}+b^2\right]\left[(a^2-b^2)\sin^2\frac{(2k+n-2)h_\theta}{2}+b^2\right]}\,.
\end{aligned} \tag{3.45}$$

This implies

$$\begin{aligned}
&|d_{k+n-1,k}-c_{k+n-1,k}| \leq \tfrac{ab\,h_\theta}{4\pi}\tfrac{a^2-b^2}{N-n+1}\sum_{j=1}^{N-n+1}\tfrac{2}{b^4} \;\approx\; \tfrac{2\varepsilon}{N}\,, \implies \\
&||C^t-C|| = \max_{1\leq k\leq N}\sum_{j=1}^{N}|d_{kj}-c_{kj}| \leq 2\varepsilon << 1,
\end{aligned} \tag{3.46}$$

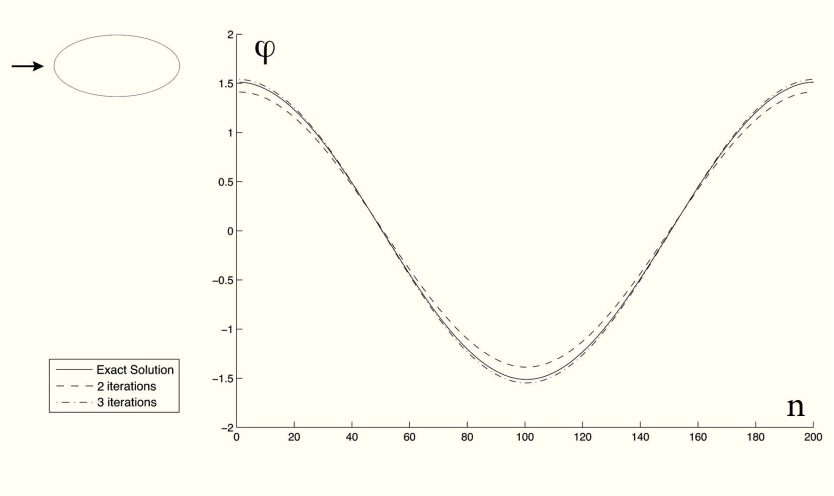

Figure 3.7: Flow over a hard ellipsis, $b/a = 0.5$, $N = 200$, $(1 \leq n \leq N)$. The first node is near rightmost boundary point

that yields the following final estimate in Eq. (3.39):

$$\varphi = F + 2(I+D)^{-1}(C^t - C)\varphi, \;\; ||2(I+D)^{-1}(C^t - C)|| \leq 2||(I+D)^{-1}||||C^t - C|| \leq \frac{2\varepsilon}{1-||D||} \tag{3.47}$$

the value which can be attained arbitrarily small for small ε. Again, according to the classical Banach theory, if the last norm is less than unit value then operator equation of the second kind (3.47) is uniquely solvable and its solution can be constructed by the standard successive iteration process, or equivalently, by Neumann's operator series [58].

When evaluating practical convergence of the proposed iteration algorithm, one may notice that this converges provided all above estimates are valid. For example, the real range of convergence in the class of elliptic objects is much wider that those with small eccentricity. Further examples show that the convergence is perfect also for various geometries different from elliptic ones.

Figures 3.7 and 3.8 demonstrate convergence of the iteration process for the ellipse with aspect ratio $\varepsilon = b/a = 1/2$ and for quadratic domain. For

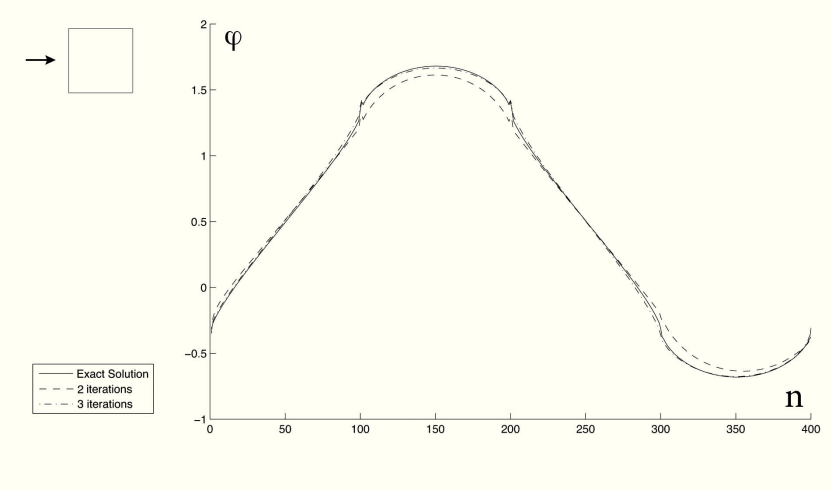

Figure 3.8: Flow over a hard quadrate, $N = 400$, $(1 \leq n \leq N)$. The first node is near left lowest boundary point

such simple geometries 10 iteration steps provide relative error less than 10^{-5} in the solution, when compared to the Gauss elimination technique. Note that in these and all forthcoming examples the enumeration of nodes is arranged counterclockwise when passing along the boundary contour.

Fig. 3.9 demonstrates a 8-leaves contour, for a correct treatment one needs to take at least 800 nodes, 100 nodes per every leaf.

Since during the intensive investigation we could not find any geometry where the method proposed diverges, let us restrict the calculations by the class of ellipses with varying aspect ratio. By decreasing $\varepsilon = b/a$ up to value $\varepsilon = 0.02$ we come to the geometry demonstrated with its BIE solution in Fig. 3.10. With further decrease of parameter ε the calculations show that for extremely small values of ε the iteration process diverges. The critical value separating convergence from divergence is somewhere near $\varepsilon^* = 0.014$.

When looking at so stable convergence of the proposed algorithm, one may suppose that all considered examples are taken only for objects close, in some

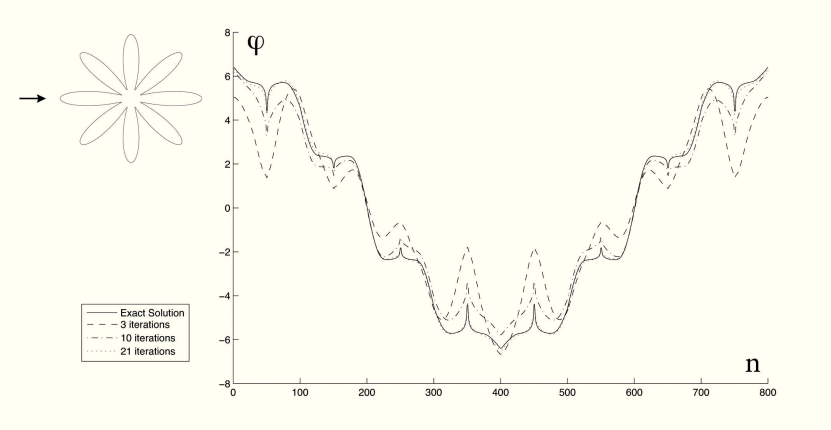

Figure 3.9: Flow over a hard 8-leaves flower, $N = 800$, $(1 \leq n \leq N)$. The first node is near rightmost boundary point

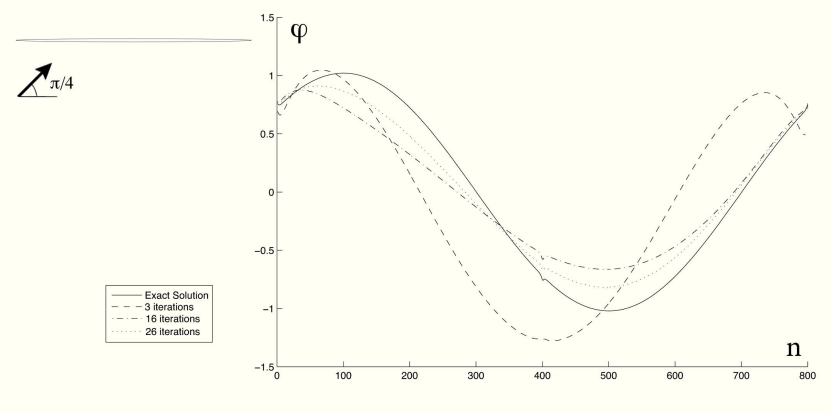

Figure 3.10: Flow over a hard ellipsis, $b/a = 0.02$, $N = 800$, $(1 \leq n \leq N)$. The first node is near rightmost boundary point

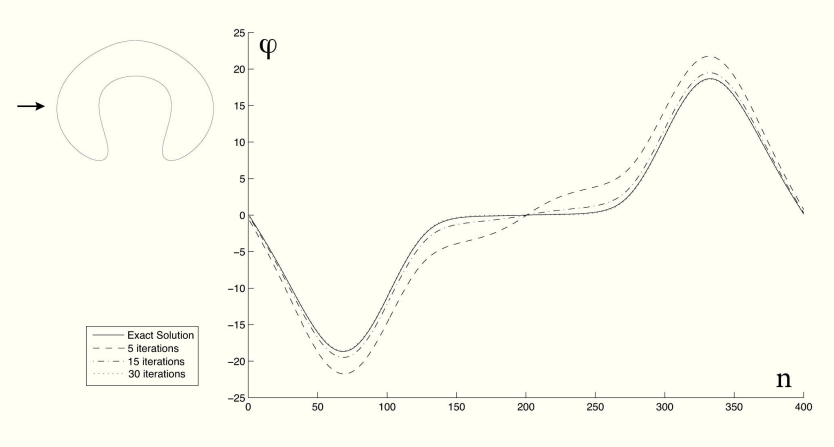

Figure 3.11: Flow over a hard roll, $N = 400$, $(1 \leq n \leq N)$. The first node is near upper boundary point

sense, to a round shape which exactly generates a real Toeplitz matrix. In order to study this question, let us consider two other geometries which seem absolutely different, both topologically and quantitatively, from any circular domain, see Figures 3.11 and 3.12.

As a final remark in this section we note that the structure of the exact matrix C is such that its principal diagonal in (3.30a) $c_{ii} = 1/2$ is Toeplitz-like. Since the principal diagonal is usually dominant for well-posed matrices, one may assume that this property makes the iteration process convergent and stable. The next section demonstrates the convergence in the case when the principal diagonal is of more general structure.

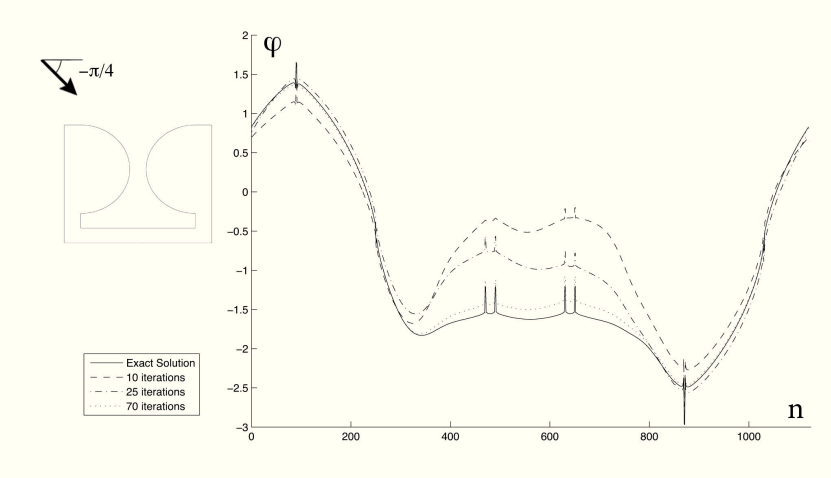

Figure 3.12: Flow over a hard body of a complicated shape, $N = 1120$, $(1 \le n \le N)$. The first node is close to the center of the lower boundary segment

3.4.2 Flow over a soft body

If the boundary condition is $\varphi|_e = 0$, then Eq. (3.27) immediately yields the following integral equation

$$\begin{aligned} &\int_l g(y) \ln|y - x| dl_y = f(x), \quad x \in l, \\ &g(y) = \tfrac{\partial \varphi}{\partial n}\big|_l = v_n|_l, \quad f(x) = -2\pi\varphi_\infty(x) = -2\pi v_0(x_1 \cos\alpha + x_2 \sin\alpha). \end{aligned} \tag{3.48}$$

which is the basic BIE in the case of soft boundary.

The same discretization like in the case of hard body, applied to Eq. (3.48), leads to the following LAS

$$\begin{aligned} &\textstyle\sum_{j=1}^N c_{ij} g_j = f_i, \quad c_{ij} = \ln|x_j - x_i| \Delta l_j, \quad j \ne i, \\ &f_i = f(x_i), \quad x_i \in l, \quad i = 1, \ldots, N. \end{aligned} \tag{3.49}$$

In order to write out correctly the diagonal elements of the matrix here, $j = i$,

one needs to calculate explicitly the contribution over small arc:

$$c_{ii} = \int\limits_{x_i-\frac{\Delta l_i}{2}}^{x_i+\frac{\Delta l_i}{2}} \ln|y-x_i|dy = 2\int\limits_{0}^{\Delta l_i/2} \ln y\, dy = \Delta l_i \left(\ln\frac{\Delta l_i}{2} - 1\right) \tag{3.50}$$

The same iteration scheme proposed in the previous section can be applied to system (3.49)-(3.50) too. Let us note that if the length of the elementary arc varies with i: $\Delta l_i \neq const$, then diagonal elements (3.50) are different for different i, and so matrix c_{ij} is not of Toeplitz type.

The detailed numerical analysis shows that the proposed iteration algorithm converges in many cases also in the case of soft boundary, like for the hard contour. First of all, it is very interesting to find the critical value $\varepsilon^* = b/a$ for ellipses, if exists, analogous to that in the case of absolutely hard body. This is found to be around $\varepsilon^* = 0.15$. The comparison with $\varepsilon^* = 0.014$ from the previous section leads to the supposition that the developed iteration technique is less applicable in the soft case. Numerous examples considered confirm that this is so indeed. The quadratic domain gives the example when the method converges, respective solution is reflected in Fig. 3.13. However, for geometries used in Figures 3.11 and 3.12 the iterations diverge.

One may assume that the supposition indicated above is valid, namely that the Toeplitz-type principal diagonal predetermines convergence, therefore such a diagonal structure takes place for hard body with good convergence but it is not Toeplitz for soft boundaries. However, on example related to Fig.3.12 the constant elementary arc length $\Delta l_j = const, \forall j$ can easily be arranged, but even in this case the iteration process diverges.

Let us try to improve the convergence of the iteration algorithm by passing to the indirect BIE method which reduces the Dirichlet boundary value problem to a second-kind integral equation. This means that one may seek the

solution as a double-layer potential:

$$\varphi'(y_0) = \int\limits_l u(y) \frac{\partial \Phi(y, y_0)}{\partial n_y} dl_y, \tag{3.51}$$

where $y_0 = (y_1^0, y_2^0)$ is an arbitrary point in the flow, and $u(y)$ is a certain unknown function on the boundary contour. If the boundary of the body is absolutely soft: $\varphi|_l = 0$, $\varphi = \varphi' + \varphi_\infty$, then (3.51) implies

$$\frac{u(x)}{2} + \int\limits_l u(y) \frac{\partial \Phi(y, x)}{\partial n_y} dl_y = -\varphi_\infty(x), \quad x \in l\,, \tag{3.52}$$

where the boundary property of the double-layer integral has again been applied. Let us note that, like with the direct BIE treatment for rigid boundary, equation (3.52) is indeed the Fredholm integral equation of the second kind.

However, a detailed numerical analysis performed for Eq. (3.52) in its discrete form, analogous to what is presented by expressions (3.30), shows that convergence of the iteration scheme is even worse than with the treatment by the first-kind integral equation, see Eqs. (3.48), (3.49). In particular, for elliptic obstacles iterations converge if $0.738 < b/a < 1$ only. It is completely unexpected, since the only difference between the integral operators in the left-hand sides of Eqs. (3.29) and (3.52) is opposite signs in front of integral. This property indicates implicitly that such a poor behavior of the proposed algorithm in the case of soft boundary is connected with the physical nature of the flow for soft obstacles rather than with the type of integral equation.

3.5 Conclusions

In the present chapter we propose a new numerical iteration method to solve BIEs arising in various boundary value problems of mathematical physics. The essence of the algorithm is demonstrated for integral equations of the first and second kind as a direct BIE method to diffraction by acoustically

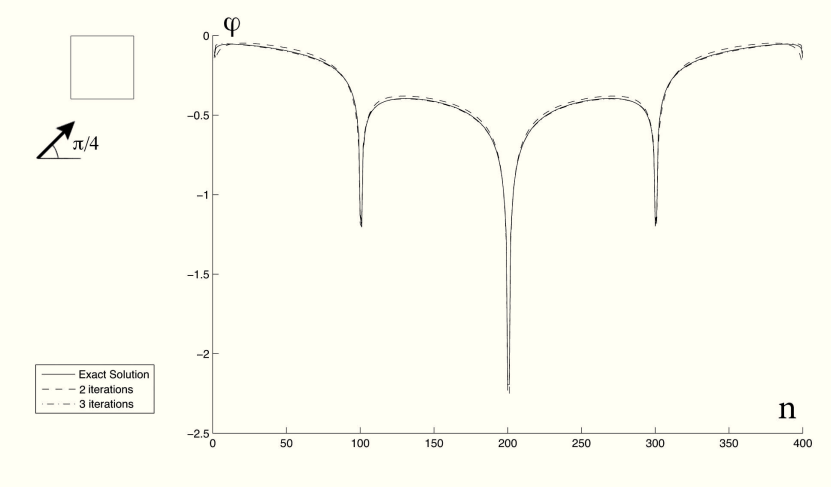

Figure 3.13: Flow over a soft quadrate, $N = 400$, $(1 \leq n \leq N)$. The first node is near left lowest boundary point

soft and hard obstacles, and also for a flow of inviscid incompressible fluid around a body, in the two-dimensional formulation. At each iteration step there is a need to solve a certain LAS with a circulant or Teplitz matrix, which is constructed both analytically and algebraically, by a certain averaging along diagonals parallel to the principal one. As Toeplitz solvers we use some special techniques known from literature, and give an estimate of respective computational expenses which shows an evident significant acceleration of the algorithm, when compared to standard Gauss elimination.

The fast methods known in literature, to solve BIE arising in mathematical physics, are typically based upon some iteration techniques like CG method and others. This has rather weak relationship with the physical nature of the considered problem. Particularly, such an approach is indifferent with respect to geometry of the obstacle and to the frequency of the oscillations. In practice, the efficiency of these fast methods is determined by the condition number of respective matrix equation, after discretization. Usually, they become less

efficient with the frequency increasing.

The method proposed is more coupled with the physical essence of the diffraction problem. This is developed for integral equations of the first kind as a direct BIE method to diffraction by acoustically soft obstacles. It is based on an iterative scheme whose each iteration step requires to solve a certain BIE with a convolution kernel, that is equivalent to a circulant matrix in the discrete form. The meaning of this idea is that the method proposed operates at each step with a BIE which is close to a certain physical obstacle with respective convolution kernel. Naturally, this is chosen in the first paragraph as a kernel corresponding to round obstacle, but this is not the only choice. In fact, for volumetric obstacles the circle represents a natural geometry with convolution kernel, which in numerical implementation on uniform grid represent circulant matrix. However, for thin obstacles one may recall linear screens which also provide convolution-type, hypersingular kernels, holding again as first-kind integral equations [24], and after discretization give Toepliz matrix.

Essentially, the new feature of the proposed method is a new iteration scheme. Like in the more standard approaches, each iteration requires a fast matrix-vector multiplication. This can be done by analogy to what is applied for this purpose in other known methods (a brief survey is given in the Introduction). In our computations we used an ACA standard algorithm, in frames of the Hierarchical matrix technique.

The computational cost of the proposed algorithm is quasi-linear, like in some other fast methods mentioned in the Introduction when solving boundary value problems of mathematical physics of this kind. Therefore, there arises a natural question: what is the advantage of this method compared, say to the straightforward CG in terms of accuracy and efficiency? By our opinion, there are several motivations. First of all, this leads to exact solution for any round obstacle. Then, for complex shapes this demonstrates a clear physical sense,

showing how close is the real geometry respectively a round shape. Finally, in the cases of convergence, the method demonstrates very efficient practical convergence.

The method demonstrates a perfect practical convergence for low frequencies with complex geometry of the obstacles with hard boundary. Only a few iterations are sufficient to attain good precision. With the frequency increasing the convergence becomes less optimistic. However, this is still efficiently applicable for the obstacles which do not permit multiple reflections on the interior parts of the boundary curve – the phenomenon playing important role in diffraction just at higher frequencies.

Another principal question with the proposed method is related to the problem of its convergence. Unfortunately, the convergence cannot be proved strictly for arbitrary geometry of the object. However, we demonstrate a proof in the class of ellipses with sufficiently small eccentricity. The scheme of the proof shows that the key point for the convergence is that operator $I + D$ in Eq. (3.39) must be invertible. As follows from the Fredholm theory [58], this property is valid for a wider class of boundary contours, not necessarily with the condition $||D|| < 1$. Therefore, the practical significance of the method is that this is applicable not only for the class of elliptic objects of small eccentricity with the given proof.

As stated above, if geometry of the obstacle is sufficiently close to a round shape then this converges for arbitrary frequency. Certainly, practical convergence is absolutely different from theoretical one. We studied this question thoroughly with a lot of numerical experiments, trying to distinguish examples where it converges and where it does not. By collecting together the results of such experiments, we could establish that convergence breaks if either complex geometry or high frequency takes place.

The method demonstrates wonderful stability for hard boundaries of var-

ious complex geometry. There has been performed a special investigation, to find the cases when the algorithm diverges. We could only detect that this diverges for extremely elongated ellipses, and we did not succeed in finding any other examples.

Unfortunately, in the case of the Dirichlet boundary condition the efficiency of the algorithm is poorer. This is so when applied to the first-kind Fredholm integral equation of the direct BIE method, and unexpectedly even worse convergent when applied to the second-kind equation of the indirect method. Therefore, we come to the conclusion that probably the convergence is more dependent on physical nature of the problem, rather than upon the kind of the integral equation.

In the case of perfect convergence, i.e. with the Neumann-type boundary condition, the number iterations is insensitive with respect to the numerical grid dimension. This significantly depends on geometry of the body only. The more complex the geometry the more iterations are required. This means in practice that the complexity of the algorithm is free of number of iterations, being determined only by the computational expenses to solve Toeplitz-type LAS.

When comparing the method proposed with other existing fast methods in diffraction, we only note that, as indicated by those authors, their approaches become, as a rule, less efficient for high frequencies. Our method converges for any frequency if the geometry is sufficiently close to a certain circle. Since, with the frequency increasing, the geometry must be too close to the round shape, one can conclude that both the standard and the proposed method loose their efficiency if the frequency is high enough.

Chapter 4

Fast Iteration Method in the Problem of Waves Interacting with Set of Thin Screens

In the current section we propose a similar iterative technique for the wave equation describing the scattering of a harmonic wave from an arbitrary configuration in the form of an array of thin straight barriers.

Scattering of waves by a set of breakwaters representing barriers or screens is an important problem in the fluid dynamics of waves. In the first approximation, they can be assumed to be thin rigid bodies. Classical research techniques for this scattering problem are available for a single screen, in which case an exact solution in the form of an infinite series in Mathieu functions can be constructed (see [63]). It is well known that this series expansion becomes ineffective in the case of short wavelengths. In this context, asymptotic methods have been widely used, which are designed for both short and long wavelengths [11, 64]. An alternative approach to such problems is based on the numerical solution of boundary integral equations (BIE) [9, 65]. For sets of plane scat-

terers, effective methods have been developed in the case of periodic arrays of barriers, where the underlying integral equation for wave scattering can be derived using the periodicity of the problem. Both asymptotic [66] and variational methods and techniques based on series expansions in certain systems of functions have been found fruitful as applied to such integral equations (see [67, 68]).

However, classical methods cannot be applied if a set of barriers (obstacles) has no special geometric configuration. A method applicable to such problems is based on scattering T matrices (see [69]). Another possible technique for solving such problems is the BIE method. For any numerical method, as the number of barriers grows, the computational dimension of the problem increases considerably. For example, in the case of the BIE method, an increasingly larger number of nodes has to be chosen, and the numerical solution of the arising systems of linear algebraic equations turns out to be an extremely complicated task for modern computers. This restriction is much more critical for short wavelengths, since, as we already mentioned, a finer grid with at least 10 nodes per wavelength has to be used in that case. As a result, it is practically not possible to investigate important physical features associated with mode locking and other wave effects in such problems (see [68, 69]).

In this chapter, we develop an approach applicable to an arbitrary configuration in the form of an array consisting of an arbitrary number of thin straight barriers. The idea underlying the proposed algorithm is that, in the case of a single obstacle, the corresponding BIE has a convolution kernel. As a result, discretizing the matrix of the corresponding LAS, we obtain a Toeplitz matrix and such a system can be solved using special fast methods for Toeplitz matrices described in previous chapters. In the case of several barriers, we propose an iteration process. At each iteration step, an integral equation is solved for each screen separately. The solutions for the other screens are taken from the

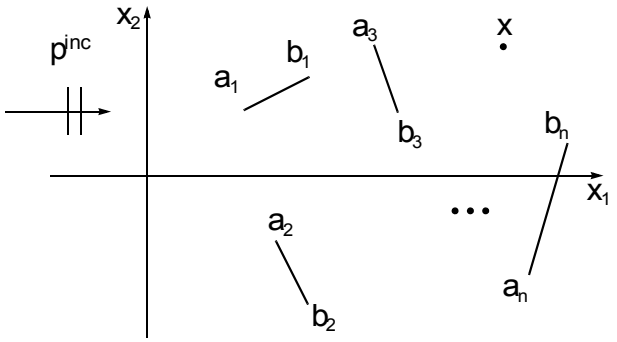

Figure 4.1: Geometry of the problem of a plane wave interacting with a set of thin screens.

previous iteration. Hence, they appear on the right-hand side of the operator equation. Thus, each iteration step in the discrete formulation involves a LAS of Toeplitz structure, which can be solved using well-known fast computational methods.

4.1 Statement of the problem and reduction to a system of boundary integral equations

Consider the gravity driven oscillations of a free surface of an ideal incompressible fluid in a channel of constant depth h (see [70]). Assume that these are small harmonic linear oscillations of constant circular frequency ω. Assume also that the channel is much longer than the wavelength. As in the previous chapters, the pressure in the incident wave is denoted by p^{inc}.

Let N rigid disjoint barriers high enough to prevent a wave from completely covering it be placed perpendicularly to the bottom. The width of the barriers is much less than their length, and their curvature is so small that it can be neglected. Since the depth of the bottom is a constant, the velocity of wave propagation $c^2 = gh$ is also a constant. By definition, the wavelength is $\lambda = cT$

,where $T = 2\pi/\omega$ is the period of oscillations. The wave number k is defined as $k^2 = \omega^2/gh$. Then the wavelength is related to the wave number by the formula $\lambda = 2\pi/k$.

On the water surface, we introduce a Cartesian coordinate system such that the direction of the incident wave is aligned with the x_1 axis, as shown in Fig. 4.1. Then the positions of the barriers can be specified by their base segments $l_m = [a_m, b_m]$, $m = 1, .., N$, where $a_m = (a_1^m, a_2^m)$ and $b_m = (b_1^m, b_2^m)$.

Let L denote the composite line representing the union of the barrier segments: $L = \sum_{m=1}^{N} l_m$. The task is to find the wave pressure at an arbitrary point $x = (x_1, x_2)$ on the water surface. Let u_1 and u_2 denote the horizontal components of the velocity of particles at the point x, z be the depth below the free surface, and ξ denote the free surface elevation above the unperturbed level.

First, we consider a plane water layer of constant depth h (see [70]). On retaining the leading terms, the continuity equation for the fluid flow in a prismatic volume with the base given by the elementary rectangle $\delta x_1 \delta x_2$ can be written as

$$\frac{\partial}{\partial x_1}(u_1 h \delta x_2)\delta x_1 + \frac{\partial}{\partial x_2}(u_2 h \delta x_1)\delta x_2 = -\frac{\partial}{\partial t}\left\{(\xi + h)\delta x_1 \delta x_2\right\}, \tag{4.1}$$

whence

$$\frac{\partial \xi}{\partial t} = -h\left(\frac{\partial u_1}{\partial x_1} + \frac{\partial u_2}{\partial x_2}\right). \tag{4.2}$$

If there is no perturbing forces, the equations of motion have the form

$$\rho\frac{\partial u_1}{\partial t} = -\frac{\partial p}{\partial x_1}, \quad \rho\frac{\partial u_2}{\partial t} = -\frac{\partial p}{\partial x_2}. \tag{4.3}$$

If the vertical acceleration of the fluid particles is neglected, it is easy to show that the pressure at an arbitrary point x is approximately equal to the static pressure caused by the depth below the free surface (see [70]). As a

result, we have the equation

$$p - p_0 = g\rho(z_0 + \xi - z), \tag{4.4}$$

where z_0 is the ordinate of the free surface in the unperturbed state. This equation yields

$$\frac{\partial p}{\partial x_1} = g\rho\frac{\partial \xi}{\partial x_1}, \quad \frac{\partial p}{\partial x_2} = g\rho\frac{\partial \xi}{\partial x_2}, \quad \frac{\partial^2 p}{\partial t^2} = g\rho\frac{\partial^2 \xi}{\partial t^2} \tag{4.5}$$

From relations (4.2)–(4.5), it is easy to derive the wave equation

$$\frac{\partial^2 p}{\partial t^2} = c^2\left(\frac{\partial^2 p}{\partial x_1^2} + \frac{\partial^2 p}{\partial x_2^2}\right) \tag{4.6}$$

Assuming that the wave process is a harmonic one with the frequency ω and the time dependence given by the multiplier $exp(-i\omega t)$, Eq.(4.6) can be reduced to the Helmholtz equation

$$\frac{\partial^2 p}{\partial x_1^2} + \frac{\partial^2 p}{\partial x_2^2} + k^2 p = 0 \quad or \quad (\Delta + k^2)p = 0, \tag{4.7}$$

which describes harmonic oscillations of water on the sea surface.

The boundary condition on the boundary of the barriers has the form

$$\frac{\partial p}{\partial n_y}\Big|_L = 0, \tag{4.8}$$

where y is a point on the barrier surface and n_y is the normal vector to the barrier surface at this point.

The wave pressure is sought in the form of the sum of the incident plane wave and the wave p^{inc} scattered from the set of barriers p^{sc}:

$$p = p^{inc} + p^{sc}, \quad p^{inc} = e^{ikx_1}. \tag{4.9}$$

The boundary value problem (4.7) with boundary conditions (4.8) can be reduced to a system of BIEs on the considered array of barriers. Consider a

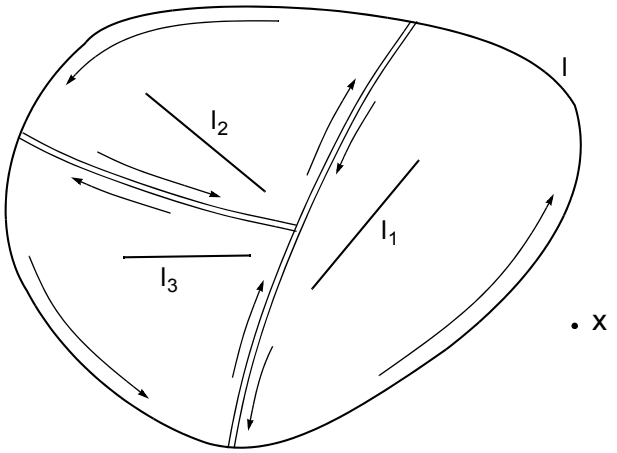

Figure 4.2: Set of contours for deriving the underlying BIE.

contour l enclosing all the obstacles under study, while the observation point x remains outside it (see Fig. 4.2).

For this contour, we have the standard integral representation (see [65])

$$p^{sc}(x) = \int_l \left(p(y) \frac{\partial \Phi}{\partial n_y} - \frac{\partial p(y)}{\partial n_y} \Phi \right) dl_y \tag{4.10}$$

where $\Phi = \Phi(r)$ is the Green's function and here, again, we use its two-dimensional representation as Hankel function $\Phi(r) = (i/4)H_0^{(1)}(r)$, $r = |y - x|$. The integration point y belongs to l.

It is easy to see that the contributions made by a pair of contours traversed along the same arc segment but in opposite directions cancel out, since the corresponding integrals involve the same functions with normal derivatives of opposite signs. This means that the integral over the original outer contour is equal to the sum of the integrals over three arcs, each enclosing its own barrier (for illustrative purposes, Fig. 4.2 depicts only three barriers, but they can be as many as desired).

Let each arc shrink to its barrier. Then the contour is replaced by the array of two-sided rectilinear arcs along the banks of the physical barriers. Each two-sided arc is represented as a pair of one-sided ones: l_m^+ and l_m^- , where m is the

index of the corresponding barrier. Here, l_m^+ is chosen so that the unit normal vector n_m^+ to it is directed to the right of the segment (a_m, b_m). Accordingly, the unit normal vector n_m^- to l_m^- is directed to the left of the segment (a_m, b_m).

The wave pressures on l_m^+ and l_m^- are denoted by p^+ and p^-, respectively. The point y_m belongs to l_m^+. Then, in view of boundary condition (4.8), representation (4.10) is rearranged into

$$p^{sc}(x) = \sum_{m=1}^{N} \left(\int_{l_m^+} \left(p^+(y) \frac{\partial \Phi}{\partial n_m^+} \right) dl_y^+ + \int_{l_m^-} \left(p_m^-(y) \frac{\partial \Phi}{\partial n_m^-} \right) dl_y^- \right) =$$

$$= \sum_{m=1}^{N} \int_{l_m^+} g(y) \frac{\partial \Phi}{\partial n_m^+}(k|y-x|) dl_y^+, \quad g(y) = p^+(y) - p^-(y), \quad y \in l_m, \quad (4.11)$$

where $g(y)$ is the jump in pressure in passing the corresponding barrier. Thus, if the pressure jump function is found, then the scattered field at an arbitrary point x on the fluid surface can be obtained using formula (4.11).

To derive BIEs, following the standard approach [9, 65], on the left-hand side of (4.11), we take into account that the scattered field is equal to the total field minus the scattered one. Then we send x in this relation to the boundary $(x \to y_j^0 \in L)$ and differentiate the resulting expression with respect to the normal n_j^+ at the point y_j^0:

$$\frac{\partial p(y_j^0)}{\partial n_j^+} = \frac{\partial p^{inc}(y_j^0)}{\partial n_j^+} + \sum_{m=1}^{N} \int_{l_m^+} g(y) \frac{\partial^2 \Phi}{\partial n_j^+ \partial n_m^+}(k|y-y_j^0|) dl_y^+. \quad (4.12)$$

Again using boundary conditions (4.8), from the last equality, we derive a system of BIEs for determining the jump in pressure:

$$\sum_{m=1}^{N} \int_{l_m^+} g(y) \frac{\partial^2 \Phi}{\partial n_j^+ \partial n_m^+}(k|y-y_j^0|) dl_y = -\frac{\partial p^{inc}(y_j^0)}{\partial n_j^+}. \quad (4.13)$$

Note that Eq. (4.13) in the more general case of curvilinear contours can be found in [71, 72]. Here, we only demonstrate the derivation procedure for a set of screens.

All the quantities involved in (4.13) can be written as closed form expressions. Specifically,

$$n_1^{m+} = \frac{b_2^m - a_2^m}{|b_m - a_m|}, \quad n_2^{m+} = -\frac{b_1^m - a_1^m}{|b_m - a_m|}, \quad \frac{\partial p^{inc}(y_j^0)}{\partial n_j^+} = ik\frac{b_2^j - a_2^j}{|b_j - a_j|}e^{iky_1^j}. \tag{4.14}$$

Moreover, in view of the recurrence expressions for Hankel functions, we have

$$\frac{\partial H_1^{(1)}}{\partial r} = \frac{H_0^{(1)}(r) - H_2^{(1)}(r)}{2}, \quad H_1^{(1)}(r) = \frac{r}{2}\left[H_0^{(1)}(r) - H_2^{(1)}(r)\right]. \tag{4.15}$$

Then, for $y \in l_m$, it is easy to obtain

$$\frac{\partial^2 \Phi}{\partial n_j^+ \partial n_m^+}(k|y - y_j^0|) =$$

$$= -\frac{ikH_1^{(1)}(k|y - y_j^0|)\left[(b_2^m - a_2^m)(b_2^j - a_2^j) + (b_1^m - a_1^m)(b_1^j - a_1^j)\right]}{4|b_m - a_m||b_j - a_j||y - y_j^0|}. \tag{4.16}$$

Moreover, system (4.13) becomes

$$\sum_m \int_{l_m^+} g(y)K(y, y_j^0)dl_y = 4|b_j^2 - a_j^2|e^{iky_1^j},$$

$$K(y, y_j^0) = \frac{H_1^{(1)}(k|y - y_j^0|)\left[(b_2^m - a_2^m)(b_2^j - a_2^j) + (b_1^m - a_1^m)(b_1^j - a_1^j)\right]}{|b_m - a_m||y - y_j^0|} \tag{4.17}$$

In the integrand, it is convenient to pass to dimensionless variables. For this purpose, we make the following substitutions ($0 \le t, \tau \le 1$):

$$y_1^m = a_1^m + (b_1^m - a_1^m)t_m, \quad y_1^j = a_1^j + (b_1^j - a_1^j)\tau_j, \tag{4.18}$$

$$y_2^m = a_2^m + (b_2^m - a_2^m)t_m, \quad y_2^j = a_2^j + (b_2^j - a_2^j)\tau_j, \quad dl_y^m = |b_m - a_m|dt_m, \quad (y \in l_m) \tag{4.19}$$

Then system (4.17) takes the form

$$\sum_m \int_0^1 g(t_m)K(t_m, \tau_j)dt_m = 4(b_j^2 - a_j^2)e^{iky_1^j(\tau_j)},$$

$$K(t_m,\tau_j)=\frac{H_1^{(1)}(k|y(t_m)-y(\tau_j)|)\left[(b_2^m-a_2^m)(b_2^j-a_2^j)+(b_1^m-a_1^m)(b_1^j-a_1^j)\right]}{|y(t_m)-y_j(\tau_j)|} \tag{4.20}$$

Note that the kernels of system (4.20) have a hypersingular singularity. If the points $y(t_m)$ and $y(\tau_j)$ lie on a single barrier (i.e., $m=j$), the kernels of system (4.20) become

$$\frac{H_1^{(1)}(k|y(t_m)-y(\tau_j)|)\left[(b_2^m-a_2^m)(b_2^j-a_2^j)+(b_1^m-a_1^m)(b_1^j-a_1^j)\right]}{|y(t_m)-y_j(\tau_j)|}=$$

$$=\frac{H_1^{(1)}(k|b_j-a_j||t_j-\tau_j|)|b_j-a_j|}{|t_j-\tau_j|}. \tag{4.21}$$

From the asymptotics of the Hankel function for small values of the argument, $H_1^{(1)}(x)\approx -2i/(\pi x)$, it follows that

$$\frac{H_1^{(1)}(k|b_j-a_j||t_j-\tau_j|)|b_j-a_j|}{|t_j-\tau_j|}\sim -\frac{2i}{\pi k(t_j-\tau_j)^2},\quad t_m\to\tau_j; \tag{4.22}$$

i.e., the kernel is hypersingular.

Extracting the singularity of the kernel in explicit form, we reduce system (4.20) to

$$\sum_m\int_0^1 g(t_m)K_{j,m}(t_m,\tau_j)dt_m=4(b_2^j-a_2^j)e^{iky_1^j(\tau_j)}, \tag{4.23}$$

where the kernel is given by

$$K_{j,m}(t_m,\tau_j)=\begin{cases}\frac{H_1^{(1)}(k|y(t_m)-y(\tau_j)|)\left[(b_2^m-a_2^m)(b_2^j-a_2^j)+(b_1^m-a_1^m)(b_1^j-a_1^j)\right]}{|y_m(t_m)-y_j(\tau_j)|}, & m\neq j,\\ -\frac{2i}{\pi k}\left[\frac{1}{(t_j-\tau_j)^2}+\frac{\pi ki|t_j-\tau_j|H_1^{(1)}(k|b_j-a_j||t_j-\tau_j|)|b_j-a_j|-2}{2|t_j-\tau_j|^2}\right], & m=j\end{cases} \tag{4.24}$$

Here, the hypersingular singularity of the kernel is extracted in explicit form.

4.1.1 Iteration algorithm and its discrete implementation using fast computational mathods

The idea of the proposed iteration method can be described as follows.

System (4.23), (4.24) is discretized using the Belotserkovskii-Lifanov method [71, 72]. Taking into account that, for each pair of barriers (m, j), the variables t_m and τ_j range within the interval $(0, 1)$, we introduce the following partition of the barriers with a discrete set of nodes chosen on them:

$$\tau_v^j = \frac{v - 0.5}{n_j},\ v = 1, 2, .., n_j; \quad t_u^m = \frac{u}{n_m},\ u = 1, 2, .., n_m, \tag{4.25}$$

where n_m and n_j are chosen so that the number of partition points in l_m and l_j for the wavelength λ is sufficiently large. Practical experience shows that the partition must be such that it ensures at least ten points per wavelength. Then, according to the Belotserkovskii-Lifanov method, system (4.23), (4.24) has the discrete analogue

$$\sum_{m=1}^{N} \sum_{u=1}^{n_m} g(t_u^m) K_{uv}^{mj} = 4(b_2^j - a_2^j) e^{iky_1^j(\tau_v^j)}, \tag{4.26}$$

where

$$K_{uv}^{mj} = \begin{cases} \frac{H_1^{(1)}(k|y(t_u^m) - y(\tau_v^j)|)\left[(b_2^m - a_2^m)(b_2^j - a_2^j) + (b_1^m - a_1^m)(b_1^j - a_1^j)\right]}{n_m |y(t_u^m) - y(\tau_v^j)|}, & m \neq j, \\ -\frac{2i}{\pi k}\left(\frac{1}{\tau_v^j - t_u^j} - \frac{1}{\tau_v^j - t_{u-1}^j}\right) + \frac{|b_j - a_j||t_v^j - \tau_u^j| H_1^{(1)}(k|b_j - a_j||\tau_v^j - t_u^j|) - 2}{n_j |\tau_v^j - t_u^j|^2}, & m = j \end{cases} \tag{4.27}$$

Note that the discretization of general hyper singular equations is also discussed in [71, 72].

It is easy to see that the dimension of LAS (4.26) is $D = \sum_{m=1}^{N} n_m$. If the incident waves are of high frequency, satisfactory accuracy can be achieved by using fine grids on the set of barriers. Then the resulting system is of high dimension and direct classical methods, such as Gaussian elimination, become ineffective, since their complexity is $O(D^3)$ (see [28]). With the aim of devising a faster solution method, we examine the structure of the matrix of system (4.26) in more detail.

Obviously, when $m = j$ (the points belong to a single barrier), the formula for finding the coefficients is a difference scheme with respect to the indices

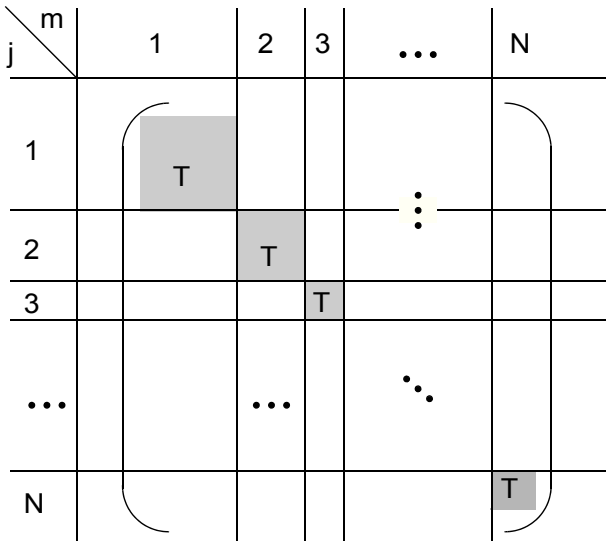

Figure 4.3: Structure of the matrix for the discretization of the problem for N barriers.

u and v. In this case, we obtain a symmetric Toeplitz matrix, which can be solved using fast methods described in previous chapters. Physically, the case $m = j$ determines the contribution made by scattering from a single barrier to the complete wave field. However, for $m \neq j$ (the points belong to different barriers), the matrix elements have no special form. Physically, this case describes the influence exerted on the general structure of the wave field by multiple reflections of a wave from various barriers.

The structure of the coefficient matrix is shown in Fig. 4.3. Here, T denotes the Toeplitz parts of the matrix. Based on this matrix representation, we construct an iteration algorithm in which N Toeplitz systems of equations order n_m are solved at every step.

At the zero step of the algorithm, the pressure on each barrier is determined regardless of the other barriers:

$$\sum_{u=1}^{n_j} g^0(t_u^j) K_{uv}^{jj} = 4(b_2^j - a_2^j) e^{iky_1(\tau_v^j)}, \quad j = 1, 2, .., N, \quad v = 1, 2, .., n_j. \quad (4.28)$$

At every new iteration step, the pressure is refined using the values obtained at the previous step:

$$\sum_{u=1}^{n_j} g^s(t_u^j) K_{uv}^{jj} = 4(b_2^j - a_2^j) e^{iky_1(\tau_v^j)} - \sum_{m=1, m\neq j}^{N} \sum_{u=1}^{n_j} g^{s-1}(t_u^m) K_{uv}^{mj}, \qquad (4.29)$$

where $j = 1, 2, .., N$, $v = 1, 2, .., n_j$. Obviously, several independent LAS (as many as the number of barriers) with Toeplitz matrices have to be solved at every step.

In our problem we have used the conjugate gradient method with circulant preconditioning (PCG) as in the previous chapters. The overall complexity of the this approach to the solution of a system with a Toeplitz matrix is $O[2N_{iter} n \log 2n]$, where the number N_{iter} of iterations is small. Based on this estimates for Toeplitz solvers, we can analyze the complexity of the fast method proposed for solving the problem of waves interacting with a set of thin screens. For convenience, the segments are assumed to have an identical length. Then the number of nodes for all the segments is identical as well and the size of system (4.26) is $D = \sum_{m=1}^{N} n = Nn$. As was noted above, the direct numerical solution of this system would require $O(D^3) = O(N^3 n^3)$ operations. Instead, the problem for each barrier is solved separately at each iteration step. Even without using fast methods, the complexity is then reduced to $O(Nn^3)$. If the number m_{iter} of iterations in the algorithm is small (which is confirmed by numerical experiments), this simple approach is superior for $m_{iter} Nn^3 < (Nn)^3$, i.e., if $m_{iter} < N^2$. The efficiency of this method can be further enhanced by applying superfast solvers for Toeplitz systems at each step of the algorithm. Then, as is easy to see, we obtain the estimate $O[2m_{iter} N_{iter} Nn \log 2n]$, where N_{iter} is the number of iterations in PCG method. This estimate is confirmed by numerical experiments.

The numerical results presented below were obtained using the iteration method described above. Within five significant digits, they coincide with

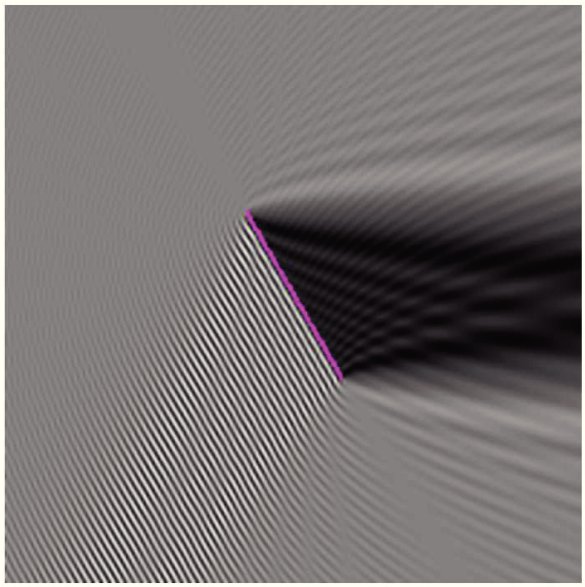

Figure 4.4: Scattering of a plane wave from a single barrier placed at an angle of 30°.

the solution of the corresponding Toeplitz-structured LAS based on Gaussian elimination. Moreover, with the use of the fast algorithm, the computations can be executed in real time.

The following examples were considered.

Example 1. Canonical case: a single barrier placed at an angle of 30° to the wavefront. The length of the barrier = 10 meters, and the wavelength = 0.628 m (wave number = 10 rad/m). Obviously, for a single barrier, there is no influence of neighboring barriers, so the iteration method immediately produces an exact result. The structure of the wave field is shown in Fig. 4.4.

As was expected, the method converged after two steps. Moreover, the second step was required only because the residual cannot be determined at the first step. At the first step, CG without preconditioning converged after 44 iterations. At the second step, CG immediately produced the exact result. The number of nodes was N = 256.

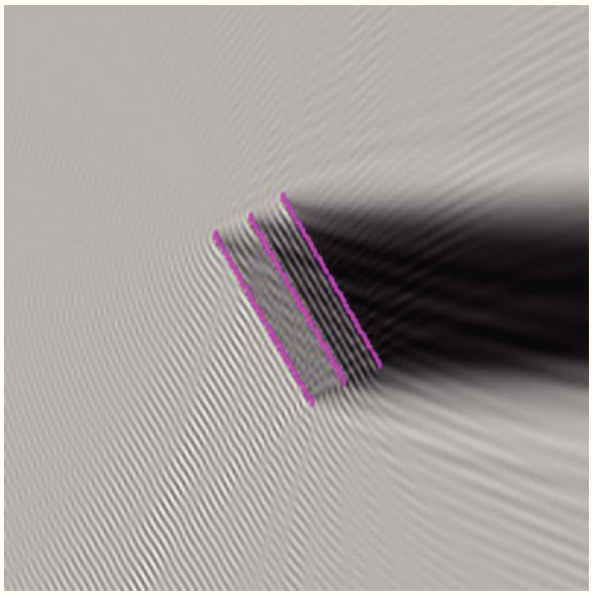

Figure 4.5: Scattering of a plane wave from a set of three parallel barriers placed at an angle of 30°.

Example 2. Another two barriers separated by a distance of 2 m are placed in parallel to the one considered in Example 1. The total number of nodes is $N = 3 * 256 = 768$.

The structure of the wave field is displayed in Fig. 4.5. This time the method converged after nine steps. The process of computations is described in Table 4.1.

Example 3. Two barriers make an angle of 90 degrees. The distance between their neighboring ends is $2.8\,m\,(\sqrt{2^2+2^2})$, $N = 2 * 256 = 512$. The other parameters are the same as in Example 4.1. The complete geometry is presented in Fig. 4.6.

As in Example 1, the method converged after two steps. This is a surprising result, since there must be multiple reflections of waves from the barriers. However, by varying the wave number, it becomes clear that the interaction

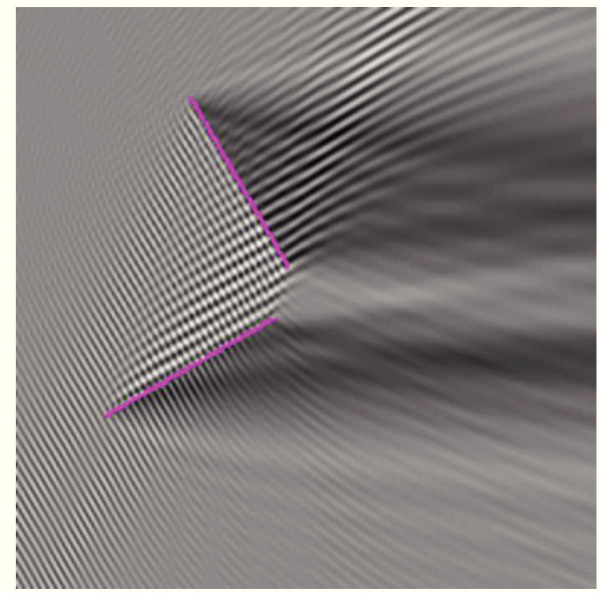

Figure 4.6: Scattering of a plane wave from two mutually orthogonal barriers.

of the barriers is weak in this case. Specifically, the method converges after three steps if the wavelength is doubled and after eight steps if the wavelength is three times as long.

Example 4. The same as in Example 3 but for two adjoining barriers (see Fig. 4.7). The wavelength is $1.884\,m$. This case required the largest number of iterations: $N = 2 * 128 = 256$. The method converged after five steps (see Fig. 4.7).

Example 5. The barriers form a square-like configuration. The distance between the ends of neighboring barriers is 2.8 meters ($\sqrt{2^2 + 2^2}$). The other parameters are the same as in Example 1 (see Fig. 4.8). The dimension of the system is $N = 4 * 256 = 1024$. The convergence process is described in Table 4.2.

Example 6. The same as in Example 5 but the barriers are adjoining, $N = 4 * 256 = 1024$ (see Fig. 4.9).

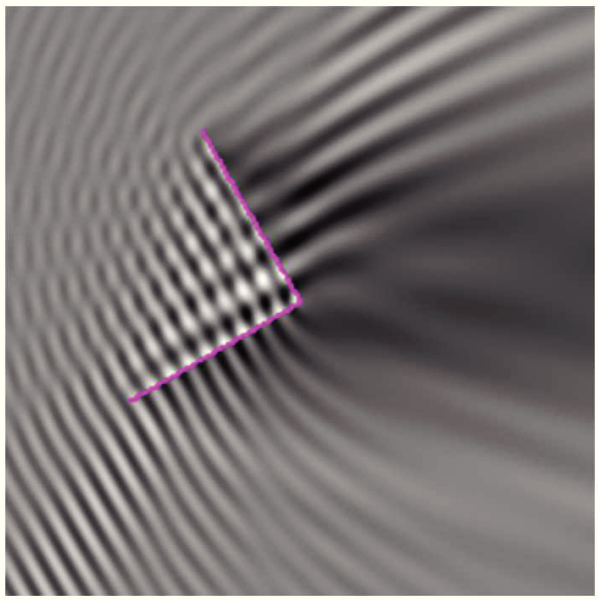

Figure 4.7: Scattering of a plane wave from two mutually orthogonal adjoining barriers.

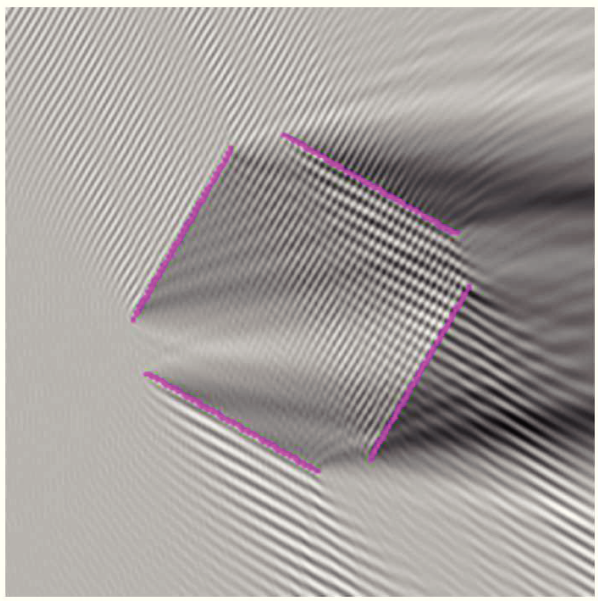

Figure 4.8: Scattering of a plane wave from four mutually orthogonal barriers.

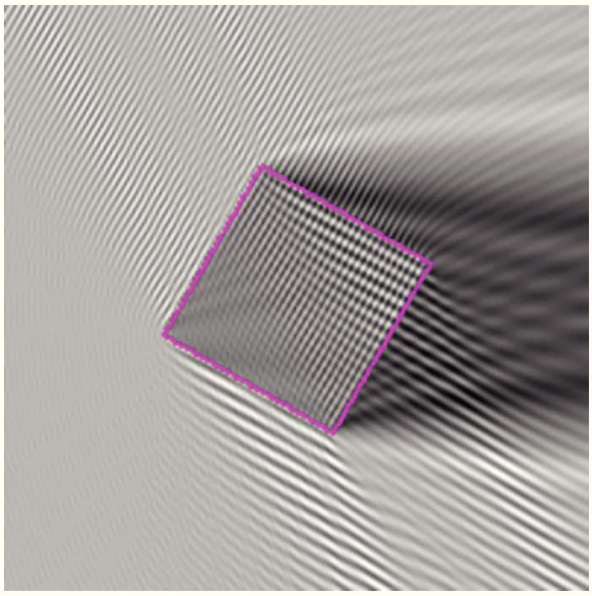

Figure 4.9: Scattering of a plane wave from four mutually orthogonal adjoining barriers.

In this case, the method converged after 41 steps. Curiously, no oscillations must be observed inside the square, since the wave process inside the square is fictitious. This is confirmed by the direct computation of the complete LAS based on Gaussian elimination, which produces the same wave pattern.

Note that the performance of the algorithm is demonstrated here for several screens. If the number of screens is increased considerably, the dimension of the LAS after the discretization can reach tens of thousands and more. It is in this case that the proposed algorithm becomes efficient.

Note also that the idea of using an iteration algorithm in which every step involves the inversion of matrices corresponding to scattering from a single screen can also be applied to curvilinear screens. However, the advantages of Toeplitz solvers fail to be used in that case.

Table 4.1: Number of iterations of the conjugate gradient method

Step	Norm of the error	barrier 1	barrier 2	barrier 3
1	-	44	44	44
2	2.566861	11	36	22
3	0.205326	9	3	4
4	0.010384	2	2	2
5	0.004213	1	3	1
6	0.003428	1	1	3
7	0.002215	1	1	1
8	0.001082	1	1	1
9	0.000850	1	1	1

Table 4.2: Number of iterations of the conjugate gradient method

Step	Norm of the error	barrier 1	barrier 2	barrier 3	barrier 4
1	-	44	49	44	49
2	0.098940	7	2	7	2
3	0.001390	1	1	1	1
4	0.001242	1	1	1	1
5	0.001627	1	1	1	1
6	0.003054	1	1	1	1
7	0.001458	1	1	1	1
8	0.001906	1	1	1	1
9	0.000829	1	1	1	1

4.2 General Conclusions

The current research concern a solving of fundamental problem about efficient numerical realization of integral expressions and boundary integral equations arising in wave dynamics, acoustics, and boundary-value problems of mechanics with mixed boundary conditions. This includes:

1) Development of an FFT-based method to accelerate numerical algorithms in diffraction problems. This is based on the reduction of integrand to a form suitable for application of the fast Fourier transform. Developed approach is applied to solve diffraction problem for plane rigid screen in high frequency range. Derivation of the diffraction integral is based on Kirchhoff's physical diffraction theory. After a special change of variables, based on a specific form of the phase function, with the use of some efficient semi-analytic realization of this change, the integral is reduced to a form permitting application of FFT. It is shown, that the developed method allow us to significantly reduce the time of computation, keeping the accuracy of direct numerical methods. An essential decreasing of necessary computer resources at the expense of high performance of the developed method permit the research wide range of physical parameters.

2) The fast numerical algorithm is also developed for solving wide range of problems in mechanics of continua. Integral equations in such problem often has difference kernel and in numerical form can be represented as discrete convolution. Application of the convolution theorem with the fast Fourier transform algorithm allows us to evaluate this integral fast and accurate.

The numerical solution to the static crack problem for linear cracks in the non-classical porous material of a Cowin-Nunziato type is constructed by fast iteration methods founded on Conjugate Gradient method with a preconditioning. It is shown, that arising integral equation, after discretization, may be

reduced to linear algebraic systems with matrix of Toepliz form. To accelerate CG method there can be applied FFT-methods. This leads to a quasi-linear numerical algorithm. There is presented a comparison between the classical direct Gauss elimination, iterative conjugate gradients method and fast versions of the CG method, such as preconditioned CG. We can conclude that fast PCG methods considerably accelerate numerical calculations, while the number of iterations is weakly sensitive to the number of nodes.

3) In the case when the diffraction is happen by a general-form object whose shape is neither linear nor circular, the problem can be reduced to an integral equation with a general-form kernel. There is developed a new approach, which operate on each iteration step with an integral equation, which has a convolution kernel. Different averaging procedures of changing the full kernel with convolution one are presented. Analytical approximation is applied to star-like obstacles for two-dimensional scattering by soft obstacles. Discrete numerical approximation is demonstrated on the problem of a flow around bodies placed in the incompressible inviscid fluid. With such a treatment, we approximate the exact matrix by a certain Toeplitz one and then apply a fast algorithm for this matrix, on each iteration step. This admits again a quasi-linear numerical algorithm. The practical convergence of the algorithm is demonstrated by examples for different geometries. We illustrate the convergence of this iteration scheme both for hard and soft boundary conditions. It appears that the method is highly efficient for hard boundaries, being much less efficient for soft boundaries.

4) In the present chapter we apply the same idea to wave processes with obstacles which represent an arbitrary set of linear rigid screen of finite length. The iteration process is proposed, when at each iteration step one needs only solution of the problem for every isolated single screen. All equations in this case are of convolution type, and they are reduced again to Toepliz-like matrix

equations in a discrete form. The algorithm developed shows fast convergence for respective second-kind Fredholm integral equation.

Bibliography

[1] Cooley J.W., Tukey J.W., An algorithm for the Machine Calculation of Complex Fourier Series, Math. Comp., 19, 297–301 (1965)

[2] Tyrtyshnikov E.E., Methods for Numerical Analysis. Akademiya, Moscow (2006) [in Russian]

[3] Van Loan C., Computational Frameworks for the Fast Fourier Transform. SIAM, Philadelphia (1992)

[4] Rokhlin V., Rapid solution of integral equation of classical potential theory, J. Comput. Physics., 60, 187–207 (1985)

[5] Greengard L., Rokhlin V., A fast algorithm for particle simulations, J. Comput. Physics., 73, 325–348 (1987)

[6] Rokhlin V., Rapid solution of integral equations of scattering theory in two dimensions, J. Comput. Physics., 86, 414–439 (1990)

[7] Williams E.G., Maynard J.D., Numerical evaluation of the Rayleigh integral for planar radiators using the FFT, JASA, 2020–2030 (1982)

[8] Williams E.G., Numerical evaluation of the radiation from unbaffled, finite plates using the FFT, JASA, 343–347 (1982)

[9] Sumbatyan M.A., Scalia A., Equations of Mathematical Diffraction Theory. CRC Press, Boca Raton, Florida (2005)

[10] Skudrzyk E., The Foundations of Acoustics, Basic Mathematics and Basic Acoustics. Springer-Verlag, Wien (1971)

[11] Honl H., Maue A.W., Westpfhal K., Theorie der Beugung, in Handbuch der Physik, Ed. by S. Flugge, 25(1). Springer-Verlag, Berlin (1961)

[12] Abramowitz M., Stegun I., Handbook of Mathematical Functions. Dover, New York (1965)

[13] Ifeachor E.C., Jervis B.W., Digital Signal Processing: A Practical Approach, 2nd Edition. Prentice Hall, Upper Saddle River, New Jersey (2002)

[14] Aizikovich S.M., Alexandrov V.M., Argatov I.I., et al., Mechanics of Contact Interactions, Ed. by I. I. Vorovich and V. M. Alexandrov. Fizmatlit, Moscow (2001) [in Russian]

[15] Press W.H., Teukolsky S.A., Vetterling W.T., Flannery B.P., Numerical Recipes: The Art of Scientific Computing, second ed.. Cambridge University Press, Cambridge (1992)

[16] Cowin S.C., Nunziato J.W., Linear elastic materials with voids, J. Elast., 13, 125–147 (1983)

[17] Puri P., Cowin S.C., Plane waves in linear elastic materials with voids, J. Elast., 15, 167–183 (1985)

[18] Scalia A., Sumbatyan M.A., Contact problem for porous elastic half-plane, J. Elast., 60, 91–102 (2000)

[19] Scalia A., Contact problem for porous elastic strip, Int. J. Eng. Sci., 40, 401–410 (2002)

[20] Atkin R.J., Cowin S.C., Fox N., On boundary conditions for polar materials, ZAMP, 28, 1017 (1977)

[21] Chandrasekharaiah D.S., Effects of surface stresses and voids on Rayleigh waves in an elastic solid, Int. J. Eng. Sci., 25, 205–211 (1987)

[22] Ciarletta M., Iovane G., Sumbatyan M. A., On stress analysis for cracks in elastic materials with voids, Int J Eng Sci, 41, 2447–2461 (2003)

[23] Gradshteyn I.S., Ryzhik I.M., Table of Integrals, Series, and Products. Academic Press, New York (2007)

[24] Lifanov I.K., Poltavskii L.N., Vainikko G.M., Hypersingular Integral Equations and Their Applications. CRC Press, Boca Raton, Florida (2004)

[25] Voevodin V. V., Tyrtyshnikov E. E., Numerical Processes with Toeplitz Matrices. Nauka, Moscow (1987) [in Russian]

[26] Stewart M., A superfast Toeplitz solver with improved numerical stability, SIAM J. Matrix Anal. Appl., 25, 669–693 (2003)

[27] Van Barel M., Heinig G., Kravanja P., A stabilized superfast solver for nonsymmetric Toeplitz systems, SIAM J. Matrix Anal. Appl, 23, 494–510 (2001)

[28] Golub G.H., Van Loan C.F., Matrix Computations, 3rd Edition. Johns Hopkins Univ. Press, Baltimore, Md. (1996)

[29] Levinson N., The Wiener RMS (Root-Mean-Square) error criterion in filter design and prediction, J. Math. and Phys., 25, 261–278 (1946)

[30] Trench W., An algorithm for the inversion of finite Toeplitz matrices, SIAM J. Appl. Math., 12, 512–522 (1964)

[31] de Hoog F., A new algorithm for solving Toeplitz systems of equations, Linear Algebra Appl., 88/89, 123–138 (1987)

[32] Ammar G., Gragg W., Superfast solution of real positive definite Toeplitz systems, SIAM J. Matrix Anal. Appl., 9, 61–76 (1988)

[33] Strang G., A proposal for Toeplitz matrix calculations, Studies Appl. Math., 84, 171–176 (1989)

[34] Chan T., An optimal circulant preconditioner for Toeplitz systems, SIAM J. Sci. Stat. Comput., 9, 766–771 (1988)

[35] Chan R.H., Ng M.K., Conjugate gradient methods for Toeplitz systems, SIAM Rev., 38, 427–482 (1996)

[36] Oseletets I. V., Tyrtyshnikov E. E., A unifying approach to the construction of circulant preconditioners, Linear Algebra Appl., 418 (2,3), 435–449 (2006)

[37] Colton D., Kress R., Integral Equation Methods in Scattering Theory. John Wiley, New York (1983)

[38] Hackbusch W., Novak Z.P., On the fast matrix multiplication in the boundary element method by panel clustering, Numer. Math., 54 (4), 463–491 (1989)

[39] Bebendorf M., Approximation of boundary element matrices, Numer. Math., 86, 565–589 (2000)

[40] Borm S., Grasedyck L., Huckbusch W., Introduction to hierarchical matrices with applications, Eng. Anal. Bound. Elem., 27, 405–422 (2003)

[41] Bebendorf M., Hierarchical Matrices. Springer, Berlin (2008)

[42] Borm S., Efficient Numerical Methods for Non-local Operators: H^2-Matrix Compression, Algorithms and Analysis. Ems Tracts in Mathematics, Zurich (2010)

[43] Tyrtyshnikov E., Incomplete cross approximation in the mosaic-skeleton method, Computing, 64, 367–380 (2000)

[44] Goreinov S.A., Tyrtyshnikov E.E., Zamarashkin N.L., A Theory of pseudo-skeleton approximations, Linear Algebra Appl., 261, 1–21 (1997)

[45] Nechepurenko Yu.M., Fast numerically stable algorithms for a wide class of linear descrete transformations, Preprint 92, Dpt. Comp. Math., Russian Academy Sci., (1985) [in Russian]

[46] Brandt A., Lubrecht A.A., Multilevel matrix multiplication and fast solution of integral equations, J. Comput. Physics., 90, 348–370 (1990)

[47] Harten A., Discrete multiresolution analysis and generalized wavelets, J. Appl. Numer. Math., 12, 153–193 (1993)

[48] Harten A., Adaptive multiresolution schemes for shock computations, UCLA CAM Report, 93–06 (1993)

[49] Beylkin G., Coifman R., Rokhlin V., Fast wavelet transform and numerical algorithms, Comm. Pure Appl. Math., 44, 141–183 (1991)

[50] Canning F.X., The impedance matrix localization (IML) method for moment-method calculations, IEEE Anten. Prop., 32, 18–30 (1990)

[51] Phillips J.R., White J.K., A precorrected-FFT method for electrostatic analysis of complicated 3-D structures, IEEE Trans. Comput. Aided Des. Integr. Circuits Syst., 16, 1059–1072 (1997)

[52] Fata S.N., Fast Galerkin BEM for 3D potential theory, Comput. Mech., 42, 417–429 (2008)

[53] Hu F.Q., A spectral boundary integral equation method for the 2D Helmholtz equation, J. Comp. Phys., 120, 340–347 (1995)

[54] Liu J., Liu Q.H., A spectral integral method (SIM) for periodic and non-periodic structures, IEEE Microwave Wireless Compon. Lett., 14 (3) 97–99 (2004)

[55] Martinsson P.G., Rokhlin V., An accelerated kernel-independent fast multipole method in one dimension, SIAM J. Sci. Comp., 29(3), 1160–1178 (2007)

[56] http://www.hlibpro.com.

[57] Bojars N.N., Scattering by a cylinder: A fast exact numerical solution, JASA, 75(2), 320–323, 1984.

[58] Kantorovich L.V., Akilov G.P., Functional Analysis. Pergamon Press, New York (1982)

[59] Banerjee P.K., Butterfield R., Boundary Element Methods in Engineering Science. McGraw Hill, London (1981)

[60] Bonnet M., Boundary Integral Equations Methods for Solids and Fluids. John Wiley, NY (1999)

[61] Prudnikov A.P., Brychkov Y.A., Marichev O.I., Integrals and Series (vol.1). Gordon and Breach, Amsterdam (1986)

[62] Horn R.A., Johnson C.R., Matrix Analysis. Cambridge University Press, Cambridge (1985)

[63] Bowman J.J., Senior T.B.A., Uslenghi P.L.E., Electromagnetic and Acoustic Scattering by Simple Shapes. North-Holland, Amsterdam (1969)

[64] Shenderov E.L., Wave Problems in Underwater Acoustics. Defense Technical Information Center (1974)

[65] Brebbia C.A., Telles J.C.F., Wrobel L.C., Boundary Element Techniques: Theory and Applications in Engineering. Springer-Verlag, Berlin (1984)

[66] Scarpetta E., Sumbatyan M.A., On the oblique wave penetration in elastic solids with a doubly periodic array of cracks, Quart. Appl. Math., 58, 239–250 (2000)

[67] Linton C.M., McIver P., Handbook of Mathematical Techniques for Wave/Structure Interactions. CRC, Boca Raton, Florida (2001)

[68] Porter R., Evans D.V., Wave scattering by periodic arrays of breakwaters, Wave Motion, 23, 95–120 (1996)

[69] Lim R., Hackman R.H., A formulation of multiple scattering by many bounded obstacles using a multi-centered T supermatrix, J. Acoust. Soc. Am., 91, 613–638 (1992)

[70] Lamb H., Hydrodynamics. Dover, New York (1945)

[71] Vainikko G.M., Lifanov I.K., Poltavskii L.N., Numerical Methods in Hypersingular Integral Equations and Their Applications. Yanus-K, Moscow (2001) [in Russian]

[72] Lifanov I.K., The Method of Singular Integral Equations and Numerical Experiment. Yanus, Moscow (1995) [in Russian]

Publications concerning PhD thesis:

[73] Sumbatyan M.A., Popuzin V.V., Application of FFT to the short wavelength diffraction by a plane hard screen, Proc. XII Intern. Conf. Modern problems in mechanics of continua, 1–5 Dec. 2008, Rostov-on-Don: TsVVR, 199–202 (2008) [in Russian]

[74] Popuzin V.V., Application of the FFT to solve integral equations in mechanics of continua, Proc. of international school-conference of young scientists "Mechanics 2009", 28 Sep – 1 Oct 2009, Aghavnadzor, Armenia: EGUAS, 292–296 (2009) [in Russian]

[75] Sumbatyan M.A., Popuzin V.V., An efficient numerical algorithm for one-dimensional diffraction integral, Izvestiya Vuzov. Severo-Kavkazskii Region. Natural sciences series. Special edition., ISSN 0324–3005, 207–210 (2009) [in Russian]

[76] Scalia A., Popuzin V., Pennisi M., Fast iteration algorithm for integral equations of the first kind arising in 2d diffraction by soft obstacles, J. Comput. Acoust., 21(3), 1350007-1–1350007-10 (2013)

[77] Scalia A., Sumbatyan M.A., Popuzin V., A fast BIE iteration method for an arbitrary body in a flow of incompressible inviscid fluid, J. Comput. Applied Math., 237(1), 508–519 (2013)

[78] Popuzin V.V., Sumbatyan M.A., Tanyushin R.A., Fast iteration method in the problem of waves interacting with a set of thin screens, Comput. Math. Math. Phys., 53, 1195–1206 (2013)

[79] Popuzin V.V., An explicit-form representation for the kernel of integral equation in the crack problem for a porous elastic material, Proc. of international school-conference of young scientists "Mechanics 2013", 204–208 (2013) [in Russian]